UNIVERSITY OF CALIFORNIA, SAN DIEGO

Baseline Effects in Functional Magnetic Resonance Imaging

A Dissertation submitted in partial satisfaction of the
Requirements for the degree Doctor of Philosophy

in

Bioengineering

by

Joy Liau

Committee in charge:

Professor Thomas T. Liu, Chair
Professor Gabriel Silva, Co-Chair
Professor Richard Buxton
Professor Marcos Intaglietta
Professor Eric Wong

2008

The Dissertation of Joy Liau is approved, and it is acceptable in quality and form for publication on microfilm and electronically:

Co-chair

Chair

University of California, San Diego

2008

TABLE OF CONTENTS

LIST OF FIGURES

LIST OF TABLES

ACKNOWLEDGEMENTS

I would like to acknowledge Professor Thomas T. Liu for his support as the chair of my committee. His work with the many paper drafts and discussions of the results have been immensely helpful.

I would like to thank Professor Gabriel Silva for generously serving as the co-chair of my committee. I would also like to thank Professors Richard Buxton, Marcos Intaglietta, Eric Wong, and Beau Ances for their service on my committee.

Finally, I would like to acknowledge the students and staff of the Center for Functional Magnetic Resonance Imaging, whose support and encouragement have been invaluable.

Chapter 1, in full, is a reprint of the material as it appears in Neuroimage 2008. Liau, Joy; Perthen Joanna E.; Liu Thomas T. The dissertation author was the primary investigator and author of this paper.

Chapter 2, in full, has been submitted for publication of the material as it may appear in Neuroimage 2008. Liau, Joy; Liu Thomas T. The dissertation author was the primary investigator and author of this paper.

VITA

2002	Bachelor of Science, University of North Carolina, Chapel Hill
2001-2003	Research Assistant, University of North Carolina, Chapel Hill
2003	Master of Science, University of North Carolina, Chapel Hill
2006-2008	Teaching Assistant, Department of Bioengineering, University of California, San Diego
2005-2008	Research Assistant, University of California, San Diego
2008	Doctor of Philosophy, University of California, San Diego

PUBLICATIONS

"Cardiac Optical Mapping Under a Translucent Stimulation Electrode" Annals of Biomedical Engineering, vol. 32, pp. 1202-1210, September 2005.

"Caffeine reduces the activation extent and contrast-to-noise ratio of the functional cerebral blood flow response but not the BOLD response" Neuroimage, vol. 42, pp. 296-305, August 2008.

FIELDS OF STUDY

Major Field: Bioengineering

Studies in Cardiac Electrophysiology
Professor Stephen B. Knisley

Studies in Functional Magnetic Resonance Imaging
Professor Thomas T. Liu

ABSTRACT OF THE DISSERTATION

Baseline Effects in Functional Magnetic Resonance Imaging

by

Joy Liau

Doctor of Philosophy

University of California, San Diego, 2008

Professor Thomas T. Liu, Chair
Professor Gabriel Silva, Co-Chair

The interpretation of functional MRI (fMRI) signals is complicated by the indirect relation of the signals to neural activity. Prior work has shown that significant variability in fMRI signals may be due to non-neural factors. Normalization methods that reduce fMRI signal variability due to non-neural factors and yield measures more

closely related to neural activity are desirable to the fMRI community. In this work, we measured cerebral blood flow (CBF) using arterial spin labeling fMRI, the blood oxygenation level dependent (BOLD) signal using BOLD fMRI, and venous oxygenation ($\%O_{2,v}$) using T2-Relaxation-Under-Spin-Tagging MRI. We used these measurements to assess the effect of non-neural factors on fMRI signals and to evaluate existing normalization methods. In the first study, we used a caffeine dose (200 mg) to decrease baseline CBF (CBF_0) and found significant ($p<0.05$) reductions in both the CBF activation extent and contrast-to-noise ratio (CNR) but no significant changes in the BOLD activation extent and CNR. The decreases in the CBF activation extent and CNR were consistent with a significant caffeine-induced decrease in the absolute CBF change accompanied by no significant change in the residual noise. In the second study, we found that the functional and hypercapnic BOLD and CBF responses all exhibited a significant inverse dependence on CBF_0. Hypercapnic normalization increased inter-subject variability in the normalized responses as compared to the original responses, reflecting the presence of a systematic bias term that was inversely dependent on the hypercapnic BOLD response. In contrast, normalized responses obtained by using the hypercapnic BOLD response as a covariate were unaffected by the systematic bias and exhibited reduced inter-subject variability. In the third study, we found that both $\%O_{2,v}$ and baseline CBF had a significant inverse dependence on the BOLD response in brain regions with both BOLD and CBF activation. Furthermore, $\%O_{2,v}$ was significantly correlated to CBF_0. However, CBF_0 measures were uncorrelated to $\%O_{2,v}$ or the BOLD response in brain regions with only BOLD activation. In these regions, localization of CBF_0 measures

to capillaries produced significant correlations between the CBF_0 and both $\%O_{2,v}$ and the BOLD response.

INTRODUCTION

In the past decade, functional magnetic resonance imaging (fMRI) has revolutionized studies of the working human brain. Functional MRI is a specialized application of conventional MRI. While conventional MRI is designed to measure anatomy, fMRI measures dynamic changes in brain function. In a typical fMRI experiment, a subject inside the MRI scanner is presented with a stimulus (e.g. visual, motor, sensory) while low spatial resolution images are recorded at a high time resolution. Changes in the MRI signal that are correlated with the stimulus presentation over time are then interpreted as neural responses.

fMRI Methods

There are two major types of fMRI methods used to measure brain function: 1) blood oxygenation level dependent (BOLD) fMRI, and 2) arterial spin labeling (ASL) fMRI. Since deoxyhemoglobin (dHb) is paramagnetic and oxyhemoglobin is diamagnetic, changes in dHb content and concentration produce changes in the transverse relaxation rate and measured MRI signal amplitude. This signal is referred to as the BOLD signal. BOLD fMRI is widely used due to its high signal-to-noise ratio and ease of implementation. Although the BOLD signal is generally interpreted as a measure of neural activity, it is linked to neural activity through a host of physiological variables. As shown in Figure I.1, increases in neural activity cause increases in both cerebral oxygen metabolism ($CMRO_2$) and cerebral blood flow (CBF). Increases in $CMRO_2$ increase the dHb concentration while increases in CBF

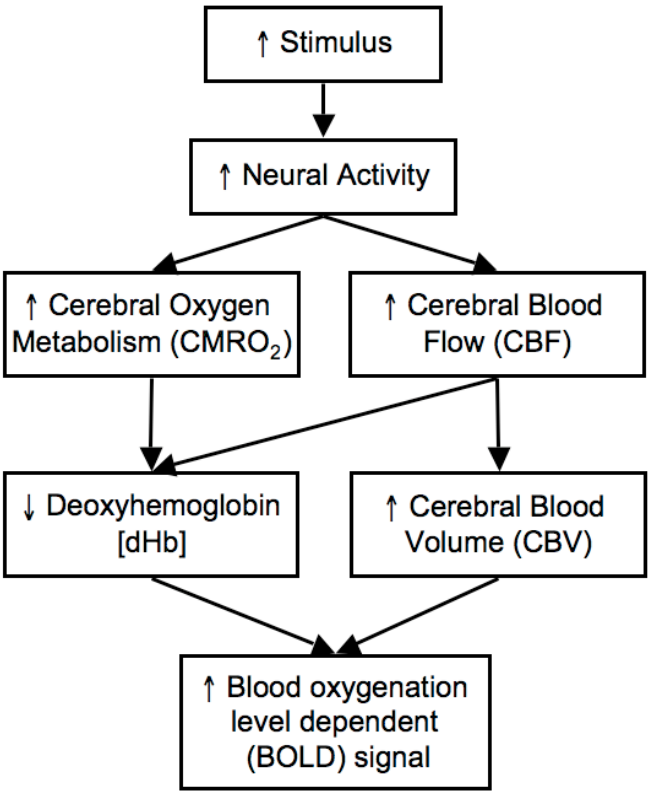

Figure I.1: Schematic of BOLD signal origins.

decrease the dHb concentration. These two effects generally combine to produce a net decrease in the dHb concentration. Also, increases in CBF result in increases in the cerebral blood volume (CBV). Finally, the dHb concentration and CBV determine the BOLD signal. Due to its complex origins, the BOLD signal cannot be directly interpreted as a measure of neural activity. In addition, dHb is carried downstream of the site of neural activity by flowing blood, so the BOLD signal and the site of neural activity are displaced in space.

The second major fMRI method is ASL. In contrast to BOLD fMRI's dependence on dHb, ASL directly measures CBF. In a typical ASL fMRI experiment, blood is magnetically inverted below the imaging plane. After waiting a period of time for the inverted blood to flow into the imaging plane, the "tag" image is acquired. A "control" image is also acquired where blood is not magnetically inverted. Subtracting the tag image from the control image cancels out the static tissue component while retaining the component reflecting inflowing blood. ASL fMRI is analogous to prior methods using contrast agents, where tagged blood acts as an endogeneous contrast agent. ASL fMRI is advantageous to BOLD fMRI because it is a direct measure of a single physiological variable (i.e. CBF), and the signal may be spatially located near the site of neural activity (Luh et al. 2000). However, ASL has a low signal-to-noise ratio since the fraction of the imaging voxel comprised of inflowing blood is around 1%. Also, ASL fMRI is more technically challenging to implement than BOLD fMRI due to its specialized pulse sequence and need for bolus width control for CBF quantification (Buxton 2002).

The non-invasive and repeatable nature of fMRI has made it a powerful research tool for the neuroscience community. The applications of fMRI to neuroscience have been diverse, ranging from studies of diseases like autism (Williams and Minshew 2007), schizophrenia (Ragland et al. 2007), and Parkinson's disease (Dagher and Nagano-Saito 2007), to studies of normal changes in brain function with age (Handwerker et al. 2007) and reorganization of brain function with disability (Amedi et al. 2003). Great potential also exists for clinical application of fMRI. Mapping of activation extent has been used to delineate functional regions for pre-surgical planning (Haberg et al. 2004), and measurement of response amplitudes has been used to evaluate the effectiveness of drug treatment (Davis et al. 2005). However, use of fMRI in clinical applications has been limited by the fMRI signal's indirect relation to neural activity.

fMRI Signal Variability

Since the BOLD signal is indirectly related to neural activity (see Figure I.1), factors that are unrelated to neural activity also contribute to BOLD signal variability. High BOLD signal variability has been reported across subjects (Aguirre et al. 1998) and in the same subject across scan sessions (McGonigle et al. 2000). One non-neural factor that contributes to BOLD variability is cerebral vascular reactivity. Development of arteriosclerosis with normal aging leads to decreased cerebral vascular reactivity, with effects varying by brain region (D'Esposito et al. 2003). Consistent with age-related decreases in cerebral vascular reactivity, (Handwerker et al. 2007) found that older subjects had smaller BOLD responses than younger subjects

in the frontal and supplementary eye fields and primary visual cortex, but not the primary motor cortex. Another non-neural factor that contributes to BOLD variability is the baseline CBF. Prior work found that increased baseline CBF from inhalation of carbon dioxide caused decreases in the BOLD response amplitude (Bandettini and Wong 1997; Cohen et al. 2002; Stefanovic et al. 2006). Consistent with the carbon dioxide studies, (Mulderink et al. 2002) used a caffeine dose to decrease baseline CBF and found increased BOLD responses. However, another research group found that a caffeine dose did not change the BOLD response (Liu et al. 2004a). These differences in findings on caffeine's effect on the BOLD response may be due to the different withdrawal states and caffeine consumption levels of the subject groups (Yang et al. 2007). A third non-neural factor that affects the BOLD signal is blood hematocrit, where increases in the blood hematocrit have been found to increase the BOLD response (Gustard et al. 2003). Development of a method to reduce the influence of non-neural factors on the BOLD signal would allow BOLD fMRI measures to be more directly interpreted as neural activity and would reduce BOLD variability.

Although CBF measurements in ASL fMRI are more closely related to neural activity than the BOLD signal (Figure I.1), non-neural factors are also thought to contribute to CBF response variability. One notable factor is the baseline CBF. Two competing models have been proposed for the relation between CBF responses and baseline CBF: 1) an additive model, and 2) a proportional model. In the additive model, the percent functional CBF response is inversely dependent on baseline CBF while the absolute functional CBF response is constant. Two ASL studies provide evidence for the additive model, one with subjects breathing room air (Kastrup et al.

1999), and another using breath-hold to induce hypercapnia and increase baseline CBF (Li et al. 2000). In the proportional model, the absolute functional CBF response is directly dependent on baseline CBF, and the percent functional CBF response is constant. This model is supported by a PET study using hypercapnia and hypocapnia to modulate baseline CBF (Shimosegawa et al. 1995). However, evidence from other studies suggest that neither model provides a complete description of the relation of the CBF response to baseline CBF. In a PET study that controlled end-tidal CO_2 levels (Kemna et al. 2001) and a pulsed ASL study that used indomethacin to reduce baseline CBF (St Lawrence et al. 2002), decreases in baseline CBF were accompanied by reductions in both the percent functional CBF response and absolute functional CBF response.

fMRI Normalization Methods

The prior work reviewed indicates that significant portions of BOLD and CBF signal variability may be unrelated to neural activity. Furthermore, the relation between the non-neural factors and fMRI signal variability is not well understood, as highlighted by the conflicting results on the relation of baseline CBF and both the BOLD and CBF signals. A better understanding of how non-neural factors contribute to fMRI signal variability would aid development of methods to reduce this variability. Reduction of variability due to non-neural factors would increase the statistical power of experiments, reducing the necessary sample size and accompanying cost. Also, reduction of non-neural variability would allow differences

in subject groups to be attributed to differences in neural activity versus group differences in the non-neural factors.

Methods to obtain measurements that are more closely related to neural activity from BOLD or combined BOLD/CBF signals have been of great interest to the fMRI community. Three of these methods are: 1) calibrated BOLD, 2) hypercapnic normalization, and 3) T2-Relaxation-Under-Spin-Tagging (TRUST) fMRI.

Calibrated BOLD is a method proposed by (Davis et al. 1998) that allows fMRI signals to be more directly interpreted as neural activity. This method relies on the use of mild hypercapnia to increase CBF while not changing cerebral $CMRO_2$ or neural activity (Jones et al. 2005; Sicard and Duong 2005; Zappe et al. 2008). By measuring BOLD and CBF measures to both the hypercapnic stimuli and a functional task, the $CMRO_2$ response and the $CBF/CMRO_2$ coupling ratio may be estimated. Calibrated BOLD has recently been applied to studies of metabolism and $CBF/CMRO_2$ coupling ratio changes due to aging (Ances et al. 2008) and drug effects (Chen and Parrish 2008; Perthen et al. 2008). However, the application of calibrated BOLD has been limited by its reliance on CBF measures, which are not widely available, have low signal-to-noise, and may be difficult to obtain in some brain regions.

Hypercapnic normalization is another method to obtain fMRI measures that are more directly related to neural activity. It refers to the division of the functional BOLD fMRI response by the BOLD response to a mild hypercapnic task (Bandettini and Wong 1997). As non-neural factors are either similar or identical for the

functional and hypercapnic responses, division of the two responses can reduce the variability due to these factors. (Bandettini and Wong 1997) first showed that hypercapnic normalization of a motor task by the response to inhaled 5% CO_2 reduced differences in the resting cerebral blood volume across the brain. (Cohen et al. 2004) used a similar procedure with subjects scanned with different protocols (i.e. pulse sequences and magnetic field strengths) and found that hypercapnic normalization reduced BOLD signal sensitivity to different scan protocols. Although (Cohen et al. 2004) found that hypercapnic normalization reduced differences related to the scan protocol, it also increased inter-subject variability. Another study found that hypercapnic normalization of a visuosaccade task by a breath-hold task reduced age-related differences in two brain regions (frontal and supplementary eye fields) (Handwerker et al. 2007). These reductions in inter-group differences were accompanied by increased inter-subject variability in the older subject group. In two recent studies, hypercapnic normalization of a working memory task (Thomason et al. 2007) and a motor task (Biswal et al. 2007) by breath-hold tasks reduced inter-subject variability. These conflicting results of prior studies clearly indicate a need for a better understanding of hypercapnic normalization's effect on inter-subject variability.

A third method to improve fMRI signal interpretation as neural activity is T2-Relaxation-Under-Spin-Tagging (TRUST) fMRI. In TRUST fMRI, estimates of whole brain venous oxygenation are obtained by measures of the transverse relaxation time constant of blood in the sagittal sinus (Lu and Ge 2008). TRUST fMRI venous oxygenation measures were found to be inversely dependent on the BOLD response amplitude and were used to reduce inter-subject BOLD signal variability (Lu et al.

2008b). This method also has been applied to increase the statistical power of a study comparing the BOLD responses to 8Hz and 4Hz flashing checkerboard visual stimuli (Lu et al. 2008a). TRUST fMRI's lack of dependence on the CBF signal and hypercapnic task makes it a promising method to reduce BOLD variability and improve interpretation of the BOLD response as neural activity. However, the TRUST fMRI pulse sequence is not widely available, and the physiological relationship between venous oxygenation and the BOLD signal is not well understood.

Outline of Thesis Work

In this work, we developed a better understanding of how non-neural factors influence the BOLD and CBF signals. We also used that information to validate and propose improvements to an existing normalization method that allows a more direct interpretation of the BOLD fMRI response as neural activity. Specifically, we: 1) showed that reductions in the baseline CBF reduced the contrast-to-noise ratio in the CBF response but not the BOLD response, 2) determined the effect of hypercapnic normalization on inter-subject variability of the BOLD fMRI response, and 3) assessed whether measures of baseline CBF and venous oxygenation account for inter-subject variability in the BOLD fMRI response.

In the first part of this work, we sought to determine whether the spatial extents of functional activation maps based on the CBF and BOLD responses were changed by the baseline CBF. Measures of the spatial extent of functional activation are important for a number of fMRI applications, such as pre-surgical planning (Haberg et al. 2004) and longitudinal tracking of changes in brain activation with disease

progression and drug treatment (Davis et al. 2005). Prior studies have shown that modulation of the baseline CBF can directly alter the functional CBF and BOLD responses, suggesting that the spatial extents of the functional activation maps based on these signals may also depend on baseline CBF (Kastrup et al. 1999; Cohen et al. 2002). In this study, we use a 200 mg caffeine dose to decrease the baseline CBF and measure the contrast-to-noise ratio and resulting spatial extents of the BOLD and CBF responses. Furthermore, we measure the components of the contrast-to-noise ratio (signal noise, baseline signal, absolute and percent signal changes) before and after the caffeine dose to determine the signal components leading to the observed contrast-to-noise ratio change.

In the second part of this work, we use measures of the baseline CBF and the BOLD and CBF responses to both visual and hypercapnic stimuli to assess the effect of hypercapnic normalization on inter-subject variability. We show that division of the functional BOLD response by the hypercapnic BOLD response can lead to a systematic bias that increases inter-subject variability. The systematic bias results from a positive intercept in the linear relationship between the functional and hypercapnic BOLD responses. We then use a mathematical model of the BOLD signal in combination with the measured CBF responses to show how this positive intercept term depends on the relation between functional and hypercapnic CBF responses. In addition, we demonstrate that use of the hypercapnic BOLD response as a covariate for the functional BOLD response can generate normalized responses without systematic bias and with reduced inter-subject variability.

In the third part of this work, we use measures of the baseline CBF, venous oxygenation, and the BOLD and CBF responses to both visual stimulus and hypercapnia to better understand the relation between both baseline CBF and venous oxygenation and the BOLD response. We show that baseline CBF is well correlated with both venous oxygenation and the BOLD response when measured in a region of interest based on both BOLD and CBF activation. We then show that baseline CBF measured in a region of interest based only on BOLD activation is complicated by the presence of draining veins.

CHAPTER 1:

CAFFEINE REDUCES THE ACTIVATION EXTENT AND CONTRAST-TO-NOISE RATIO OF THE FUNCTIONAL CEREBRAL BLOOD FLOW RESPONSE BUT NOT THE BOLD RESPONSE

1.1 ABSTRACT

Measures of the spatial extent of functional activation are important for a number of functional magnetic resonance imaging (fMRI) applications, such as pre-surgical planning and longitudinal tracking of changes in brain activation with disease progression and drug treatment. The interpretation of the data from these applications can be complicated by inter-subject or inter-session variability in the measured fMRI signals. Prior studies have shown that modulation of baseline cerebral blood flow (CBF) can directly alter the functional CBF and blood oxygenation level dependent (BOLD) responses, suggesting that the spatial extents of functional activation maps based on these signals may also depend on baseline CBF. In this study, we used a caffeine dose (200 mg) to decrease baseline CBF and found significant ($p<0.05$) reductions in both the CBF activation extent and contrast-to-noise ratio (CNR) but no significant changes in the BOLD activation extent and CNR. In contrast, caffeine significantly changed the temporal dynamics of the BOLD response but not the CBF response. The decreases in the CBF activation extent and CNR were consistent with a significant caffeine-induced decrease in the absolute CBF change accompanied by no significant change in the residual noise. Measures of baseline CBF also accounted for a significant portion of the inter-subject variability in the CBF activation map area and CNR. Factors that can modulate baseline CBF, such as age, medication, and disease, should therefore be carefully considered in the interpretation of studies that use functional CBF activation maps.

1.2 INTRODUCTION

Measures of the spatial extent of functional activation are important for a number of clinical functional MRI (fMRI) applications, such as longitudinal tracking of changes in brain activation with disease progression and medical treatment (Davis et al. 2005) and pre-surgical planning (Haberg et al. 2004). However, interpretation of activation maps based on the blood oxygenation level dependent (BOLD) signal can be complicated by the BOLD signal's complex dependence on a number of physiological variables. Furthermore, the BOLD signal has been found to vary significantly across subjects and imaging sessions (Aguirre et al. 1998).

As an alternative, functional perfusion or CBF activation maps obtained with arterial spin labeling (ASL) reflect the response of a single physiological variable. Because ASL CBF measures reflect delivery of blood to the capillary bed, it has been suggested that these measures may be better localized to the sites of neural activity than the BOLD signal, which is biased toward large draining veins (Luh et al. 2000). Also, studies have suggested that CBF measurements may be less susceptible to intra-subject and inter-subject variability as compared to BOLD (Aguirre et al. 2002; Tjandra et al. 2005) and have more robust behavior in the presence of baseline signal drifts (Wang et al. 2003; Olson et al. 2006).

These potential advantages of ASL CBF over BOLD fMRI make CBF activation maps a desirable candidate for clinical fMRI applications. However, it is also important to consider how differences in baseline CBF may affect CBF and BOLD activation maps since baseline CBF can be significantly altered by age, disease, and medical treatment (Lassen 1959; Melamed et al. 1980). Prior studies

have shown that the BOLD signal amplitude may be inversely proportional to baseline CBF (Cohen et al. 2002), while the functional absolute CBF change may be either directly proportional to (Shimosegawa et al. 1995) or independent of (Kastrup et al. 1999) baseline CBF. These prior findings suggest that modulation of the baseline CBF may alter the spatial extents of functional activation maps. In this study, we directly assess the dependence of both functional CBF and BOLD activation maps on baseline CBF.

1.3 THEORY

In this section we review the general linear model that is used to generate statistical measures for both CBF and BOLD contrast from ASL data. We also present expressions that are useful for understanding the factors that can affect the contrast-to-noise ratio.

General Linear Model

The general linear model (GLM) for ASL data can be written as:

$$\mathbf{p} = \kappa\left(\mathbf{X}\mathbf{h}_{\mathbf{BOLD}} + \mathbf{M}\left(\mathbf{X}\mathbf{h}_{\mathbf{CBF}} + \mathbf{1}_N b\right) + \mathbf{S}\mathbf{d} + \mathbf{P}\mathbf{c} + \mathbf{n}\right) \qquad [1.1]$$

where $\mathbf{p}$ is a $N \times 1$ vector that represents the raw measured data consisting of alternating tag and control images (Mumford et al. 2006; Restom et al. 2006) and κ is a scaling term that is described in more detail below. In general, $\mathbf{X}$ is an $N \times k$ design matrix, $\mathbf{h}_{\mathbf{BOLD}}$ is a $k \times 1$ vector of BOLD hemodynamic parameters, $\mathbf{M}$ is a $N \times N$ diagonal matrix consisting of alternating –1s and 1s for the tag and control images, respectively, $\mathbf{h}_{\mathbf{CBF}}$ is a $k \times 1$ vector of CBF hemodynamic parameters, $\mathbf{1}_N$ is a $N \times 1$ column vector of 1s, and b is a scalar representing the baseline CBF value. In this paper, we construct $\mathbf{X}$ as the $N \times 1$ vector obtained from the convolution of a block design stimulus pattern with a gamma density function (Boynton et al. 1996). The peak-to-peak amplitude of $\mathbf{X}$ is normalized to unity, so that the parameter weights $\mathbf{h}_{\mathbf{BOLD}}$ and $\mathbf{h}_{\mathbf{CBF}}$ represent the amplitudes of the BOLD and CBF responses, respectively. The term $\mathbf{Sd}$ represents nuisance components, where $\mathbf{S}$ is a $N \times 2$ matrix composed of constant and linear terms, and $\mathbf{d}$ is a 2×1 vector of scalar weights. The

constant term is a vector of 1's so that the first element of **d** represents the amplitude of the constant component. The term **Pc** represents physiological noise components, where **P** is a $N \times m$ matrix of physiological noise regressors and **c** is a $m \times 1$ vector of regressor weights. Finally, **n** is a $N \times 1$ vector that represents additive Gaussian noise with covariance matrix $\sigma^2\mathbf{C}$.

In this paper, we define the scaling term as $\kappa = M_{0B}(TI_1)e^{-TI_2/T_{1B}}e^{-TE_1/T_{2B}^*}$, where M_{0B} is the equilibrium magnetization of the arterial blood, TI_1 is the specified bolus width of the tag, TI_2 is the inversion time, T_{1B} denotes the longitudinal relaxation time constant of arterial blood, TE_1 is the echo time of the first echo (see Methods), and T_{2B}^* is the transverse relaxation time constant of arterial blood. An estimate of M_{0B} in measured signal units can be obtained with the use of additional calibration scans (Wang et al. 2005), as described in the Methods section. We assume that T_{1B} and T_{2B}^* are equal to 1664 and 106 ms, respectively (Lu et al. 2004; St Lawrence and Wang 2005) . Note that because of the short echo time used in this study (2.9ms, see Methods), the definition of the scaling constant is fairly insensitive to variations in T_{2B}^*. With the scaling term defined as above, the CBF response amplitude $\mathbf{h_{CBF}}$ and the baseline CBF value b are in physiological units of mL/(100g-min) (Wong et al. 1998). Furthermore, the use of the estimate of M_{0B} accounts for differences in scanner gains between scan sessions, facilitating the inter-session comparison of the BOLD amplitude $\mathbf{h_{BOLD}}$ and the constant term.

Since test statistics formed from the GLM are invariant with respect to κ, it is convenient to define a normalized GLM of the form:

$$\tilde{\mathbf{p}} = \mathbf{X}\mathbf{h}_{\mathbf{BOLD}} + \mathbf{M}\left(\mathbf{X}\mathbf{h}_{\mathbf{CBF}} + \mathbf{1}_N \mathrm{b}\right) + \mathbf{S}\mathbf{d} + \mathbf{P}\mathbf{c} + \mathbf{n} \qquad [1.2]$$

where $\tilde{\mathbf{p}} = \mathbf{p}/\kappa$. We use this normalized GLM for the remainder of the paper.

For statistical tests, it is helpful to rewrite the GLM in the following form:

$$\tilde{\mathbf{p}} = \mathbf{Z}\beta + \mathbf{n} \qquad [1.3]$$

where $\mathbf{Z} = \begin{bmatrix} \mathbf{X} & \mathbf{MX} & \mathbf{M1}_N & \mathbf{S} & \mathbf{P} \end{bmatrix}$ and $\boldsymbol{\beta} = \begin{bmatrix} \mathbf{h}_{\mathbf{BOLD}}^T & \mathbf{h}_{\mathbf{CBF}}^T & \mathrm{b}^T & \mathbf{d}^T & \mathbf{c}^T \end{bmatrix}^T$. The F-statistic to test the contrast $\mathbf{A}\hat{\boldsymbol{\beta}} = \mathbf{0}$ can be written as

$$F = \frac{N-r}{s} \frac{\left(\mathbf{A}\hat{\boldsymbol{\beta}}\right)^T \left[\mathbf{A}\left(\mathbf{Z}^T\mathbf{Z}\right)^{-1}\mathbf{A}^T\right]^{-1}\left(\mathbf{A}\hat{\boldsymbol{\beta}}\right)}{RSS} \qquad [1.4]$$

where $\mathbf{A}$ is a $s \times r$ contrast matrix, $\hat{\boldsymbol{\beta}} = \left(\mathbf{Z}^T\mathbf{Z}\right)^{-1}\mathbf{Z}^T\tilde{\mathbf{p}}$, RSS is the residual sum of squares, r is the total number of regressors, and s is the number of tested contrasts (Seber and Lee 2003). As described in further detail under Methods, the current study employs a dual echo acquisition sequence in which the first and second echoes are used for the estimation of CBF and BOLD activation, respectively. Since the data acquired in each echo exhibits both CBF and BOLD-weighted components, the form of the GLM presented above applies to both sets of data. To assess the significance of the CBF activation we compute the F-statistic with $\mathbf{A} = \begin{bmatrix} 0 & 1 & \mathbf{0} \end{bmatrix}$ where $\mathbf{0}$ is a $1 \times (r-2)$ row vector of zeros. Similarly, we test the significance of the BOLD activation by defining $\mathbf{A} = \begin{bmatrix} 1 & 0 & \mathbf{0} \end{bmatrix}$.

Expressions for Contrast-to-Noise Ratio

The F-statistic has the form of a squared contrast-to-noise ratio in which the numerator is an estimate of the energy in the contrast of interest (after nuisance terms have been removed) and the denominator is the estimate of the noise variance (Liu et al. 2001). The square root of the F-statistic thus has the form of a contrast-to-noise ratio. Indeed, in the absence of nuisance terms and with the assumption of uncorrelated noise, the square root of the F-statistic for the BOLD contrast can be written as $\sqrt{F_{BOLD}} = \|\mathbf{X}\|_2 \frac{\hat{h}_{BOLD}}{\hat{\sigma}_{n,BOLD}}$ where $\hat{h}_{BOLD}$ is the estimate of the BOLD response amplitude (normalized as described above to account for differences in inter-session gains), $\hat{\sigma}_{n,BOLD}$ is the estimate of the noise standard deviation for the BOLD-weighted data, and $\|\mathbf{X}\|_2$ denotes the norm of the design matrix, which for this paper is simply a vector norm. When nuisance terms and correlated noise are considered, the general form of the statistic is

$$\sqrt{F_{BOLD}} = \eta_{BOLD} \frac{\hat{h}_{BOLD}}{\hat{\sigma}_{n,BOLD}} \qquad [1.5]$$

where $\eta_{BOLD} = \sqrt{\mathbf{X}^T \left(\mathbf{C}^{-1/2}\right)^T \left(\mathbf{I} - \mathbf{P}_{NW}\right) \mathbf{C}^{-1/2} \mathbf{X}}$, and $\mathbf{P}_{NW} = \mathbf{C}^{-1/2}\mathbf{N}\left(\mathbf{N}^T\mathbf{C}^{-1}\mathbf{N}\right)^{-1}\mathbf{N}^T\left(\mathbf{C}^{-1/2}\right)^T$ is a projection matrix that projects onto the subspace spanned by the whitened nuisance regressors (Liu et al. 2001), where $\mathbf{N} = [\mathbf{MX} \quad \mathbf{M1}_N \quad \mathbf{S} \quad \mathbf{P}]$ are the nuisance regressors for the BOLD-weighted data. Note that the square root operation is well-defined because we have assumed that $\mathbf{X}$ is a vector. Also, since the peak-to-peak amplitude of $\mathbf{X}$ is normalized to unity in this study, η_{BOLD} is greater than one (mean = 4.2, standard deviation = 0.65, with the actual value depending on the subspace spanned by the whitened nuisance regressors), making $\sqrt{F_{BOLD}}$ larger than

$\left(\hat{h}_{BOLD}/\hat{\sigma}_{n,BOLD}\right)$ by a factor of η_{BOLD}. Equation 1.5 indicates that, to first order, changes in $\sqrt{F_{BOLD}}$ across conditions can be attributed to changes in $\hat{h}_{BOLD}$ and $\hat{\sigma}_{n,BOLD}$. In addition, there will be a second order effect on the magnitude of η_{BOLD} due to inter-session differences in the structure of the covariance matrix and the space spanned by the physiological noise regressors that make up a portion of the nuisance subspace. Since the BOLD signal is typically expressed in terms of percent change, it is helpful to rewrite Equation 1.5 as

$$\begin{aligned}\sqrt{F_{BOLD}} &= \eta_{BOLD}\frac{\hat{h}_{BOLD}}{BOLD_0}\frac{BOLD_0}{\hat{\sigma}_{n,BOLD}} \\ &= \eta_{BOLD}\cdot\frac{\%\Delta BOLD}{100}\cdot SNR_{BOLD}\end{aligned} \qquad [1.6]$$

where $\%\Delta BOLD$ denotes the percent change in the BOLD signal, $BOLD_0 = \mathbf{c}^T\hat{\mathbf{d}}$ denotes the baseline BOLD signal (i.e constant term) with $\mathbf{c}^T = \begin{bmatrix}1 & 0\end{bmatrix}$, and the signal-to-noise ratio SNR_{BOLD} is the baseline signal divided by the standard deviation of the noise.

Similar to the expressions presented above for the BOLD estimates, the square-root of the F-statistic for the CBF estimate has the form

$$\sqrt{F_{CBF}} = \eta_{CBF}\frac{\hat{h}_{CBF}}{\hat{\sigma}_{n,CBF}} \qquad [1.7]$$

where $\hat{h}_{CBF}$ denotes the estimate of the CBF response amplitude, $\hat{\sigma}_{n,CBF}$ is the estimate of the noise standard deviation, both in physiological units of mL/(100g-min), and $\eta_{CBF} = \sqrt{\mathbf{X}^T\mathbf{M}^T\left(\mathbf{C}^{-1/2}\right)^T\left(\mathbf{I}-\mathbf{P}_{NW}\right)\mathbf{C}^{-1/2}\mathbf{M}\mathbf{X}}$ where $\mathbf{P}_{NW}$ is the previously

defined projection matrix with $\mathbf{N} = [\mathbf{X} \quad \mathbf{M1}_N \quad \mathbf{S} \quad \mathbf{P}]$ as the nuisance regressors for the CBF-weighted data. Equation 1.7 can be rewritten as

$$\begin{aligned} \sqrt{F_{CBF}} &= \eta_{CBF} \frac{\hat{h}_{CBF}}{\hat{b}} \frac{\hat{b}}{\hat{\sigma}_{n,CBF}} \\ &= \eta_{CBF} \cdot \frac{\%\Delta CBF}{100} \cdot SNR_{CBF} \end{aligned} \qquad [1.8]$$

where $\%\Delta CBF$ denotes the percent change in the CBF signal, $\hat{b}$ is the estimate of the baseline CBF signal in physiological units, and SNR_{CBF} is the baseline CBF signal divided by the standard deviation of the noise.

In the Methods and Results sections, we make use of Equations 1.5 through 1.8 to better understand how changes in $\sqrt{F_{CBF}}$ depend on changes in $\hat{h}_{CBF}$, $\hat{\sigma}_{n,CBF}$, $\%\Delta CBF$, and SNR_{CBF}; and similarly, how changes in $\sqrt{F_{BOLD}}$ depend on changes in $\hat{h}_{BOLD}$, $\hat{\sigma}_{n,BOLD}$, $\%\Delta BOLD$, and SNR_{BOLD}.

1.4 METHODS

Experimental Protocol

Data presented here were also used for a separate analysis examining the metabolic effects of a caffeine dose (Perthen et al. 2008), and the experimental protocol is repeated here for convenience. Ten healthy adult subjects (5 males, mean age 33 years, standard deviation 7 years) participated in the study after giving informed consent. Subjects were instructed to refrain from ingesting caffeine for twelve hours prior to the study. The estimated daily caffeine usage of each subject based on self-report of coffee, tea, and caffeinated soda consumption is shown in Table 1.1. Each experiment consisted of a pre-dose and a post-dose imaging session. In between the sessions, the subjects ingested a 200 mg caffeine pill and rested outside of the magnet for 30 minutes, similar to previous protocols using caffeine (Liu et al. 2004b; Behzadi and Liu 2006). A total of 45 minutes elapsed between ingestion of the caffeine pill and the first functional scan in the post-dose session to allow for proper absorption of caffeine from the gastrointestinal tract (Fredholm et al. 1999).

Each imaging session consisted of the following resting-state and functional scans: 1) a resting-state scan (8 min 20s of the off condition) and 2) two block design scans (6 min 50s each scan, consisting of 60s initial off period, 4 cycles of 20s on/60s off, then 30s final off period). The on periods of the functional task consisted of a full-contrast full-field black and white checkerboard pattern flashing at 8 Hz. In the center of the screen was a small white square with the numbers (2-4-3-5) appearing sequentially at 2 Hz. The off periods were of equal luminance to the on periods and consisted of a gray background with a white square in the middle. Subjects were

instructed to fixate on the center white square at all times and press buttons on a 4-button response box in accordance to the numbers, where each number corresponded to the index through pinky fingers of the right hand. The flashing checkerboard was intended to activate the visual cortex while the motor task maintained subject attention. In the pre-dose session only, subjects had two hypercapnia scans at the end of the study where they received a 5% CO_2 gas mixture through a non-rebreathing mask. The hypercapnia and the resting state scans were used for a related study (Perthen et al. 2008).

A high-resolution anatomical scan was done at the beginning of each session to facilitate the alignment of post-dose and pre-dose data. Also, after the resting-state scan, minimum contrast and cerebrospinal fluid (CSF) scans were acquired to facilitate quantification of CBF.

Image Acquisition

Imaging data were acquired on a GE Signa Excite 3 Tesla whole body system with a body transmit coil and an eight channel receive head coil. Laser alignment was used to landmark the subjects and minimize differences in head position between pre-dose and post-dose sessions.

The resting-state and functional scans were acquired with a PICORE QUIPSS II (Wong et al. 1998) ASL sequence (TR = 2.5 s, TI1/TI2 = 600/1500 ms) with a dual echo spiral readout (TE1/TE2 = 2.9/24 ms, FOV = 24 cm, 64 x 64 matrix, and a flip angle of 90^{o}). Six oblique axial 5-mm slices were prescribed about the calcarine sulcus for all functional runs.

The calibration scans for CBF quantification used the same in-plane parameters as the functional scans, but the number of slices was increased to ensure coverage of the lateral ventricles. The CSF reference scan consisted of a single-echo, single repetition scan acquired at full relaxation at an echo time of 2.9 ms, while the minimum contrast scan was acquired with TR = 2 s and TE = 11 ms. The high-resolution anatomical scan was acquired with a magnetization prepared 3D fast spoiled gradient echo (FSPGR) sequence (TI = 450 ms, TR = 7.9 ms, TE = 3.1 ms, 12^{o} flip angle, FOV 25 cm, matrix 256 x 256 x 256).

Cardiac pulse and respiratory effort data were monitored using a pulse oximeter (InVivo) and a respiratory effort transducer (BIOPAC), respectively. The pulse oximeter was placed on the subject's left index finger, and the respiratory effort belt was placed around the subject's abdomen. Physiological data were sampled at 40 samples per second using a multi-channel data acquisition board (National Instruments).

Data Preprocessing and General Linear Model Analysis

All images were coregistered using AFNI software (Cox 1996). The structural scan from each post-dose session was aligned to the structural scan of its respective pre-dose session, and the rotation and shift matrix used for this alignment was then applied to the post-dose images (Liu et al. 2004b). Data from the first ten seconds of each functional scan were discarded to allow magnetization to reach a steady state.

A general linear model (GLM) analysis (see Theory) was performed on the block design functional runs to determine statistical significance of the responses.

For each scanner session, data from the two functional runs were concatenated for GLM analysis (Restom et al. 2006). Pre-whitening was performed using an autoregressive AR(1) model (Woolrich et al. 2001). The measured cardiac and respiratory data were included as regressors in the GLM to account for the influence of physiological fluctuations on the measurements (Restom et al. 2006). F statistic and p value maps indicating significance of CBF functional activation were obtained from the GLM analysis of the first echo data. Analysis of the second echo data yielded similar maps for the BOLD functional activation.

For each voxel, values of $\sqrt{F_{CBF}}$, $\hat{h}_{CBF}$, $\hat{\sigma}_{n,CBF}$, and $\hat{b}$ were calculated directly from the GLM analysis of the first echo data. Per voxel values of $\%\Delta CBF$ and SNR_{CBF} were calculated from the per voxel $\hat{h}_{CBF}$, $\hat{\sigma}_{n,CBF}$, and $\hat{b}$ values using Equation 1.8. Also for each voxel, a CBF time series was computed from the running subtraction of the first echo data after detrending and removal of BOLD-weighted components (Liu and Wong 2005). Similarly, per voxel values of $\sqrt{F_{BOLD}}$, $\hat{h}_{BOLD}$, $\hat{\sigma}_{n,BOLD}$, and $BOLD_0$ were calculated from the GLM analysis of the second echo data, and per-voxel values of $\%\Delta BOLD$, and SNR_{BOLD} were obtained using Equation 1.6. The per voxel BOLD time series were obtained from the running average of the second echo data after detrending and removal of CBF-weighted components.

Defining Regions-of-Interest, Average Parameter Values, and Average Time Series

Figure 1.1 shows an example of region-of-interest (ROI) formation for the most inferior functional slice from Subject 8. ROIs were defined using a combination

of the following masks: 1) a visual cortex anatomical mask, 2) a volume overlap mask, and 3) a mask based on functional activation. The visual cortex anatomical mask was defined as the posterior third of the brain in each functional slice to include visual areas while excluding motor areas. With the slice coverage used in this protocol, the acquired slices did not include visual areas of the temporal lobe. After registration of the post-dose functional volume to the pre-dose volume, some voxels (especially those in the outer two slices) had only minimal overlap between the two sessions. To identify areas with sufficient overlap between the pre-dose and post-dose sessions, a volume overlap mask was defined to include voxels in the brain with over 90% volume overlap between the pre-dose and post-dose sessions. Initial CBF functional activation maps were defined from voxels that exhibited functional CBF activation at an overall significance level of $p<0.05$, with correction for multiple comparisons using the AFNI AlphaSim program (Cox 1996). The intersection of the visual cortex anatomical mask, the volume overlap mask, and the initial CBF functional activation maps from the pre-dose and post sessions defined the pre-dose and post-dose CBF activation maps, respectively. The binary version of these maps (e.g 1 assigned to non-zero values of the maps) constituted the CBF activation masks. For each subject, a CBF intersection ROI was formed from the intersection of the pre-dose and post-dose CBF activation masks to select the same volume of activation between sessions for pairwise comparison. In addition, a CBF union ROI was also formed for each subject

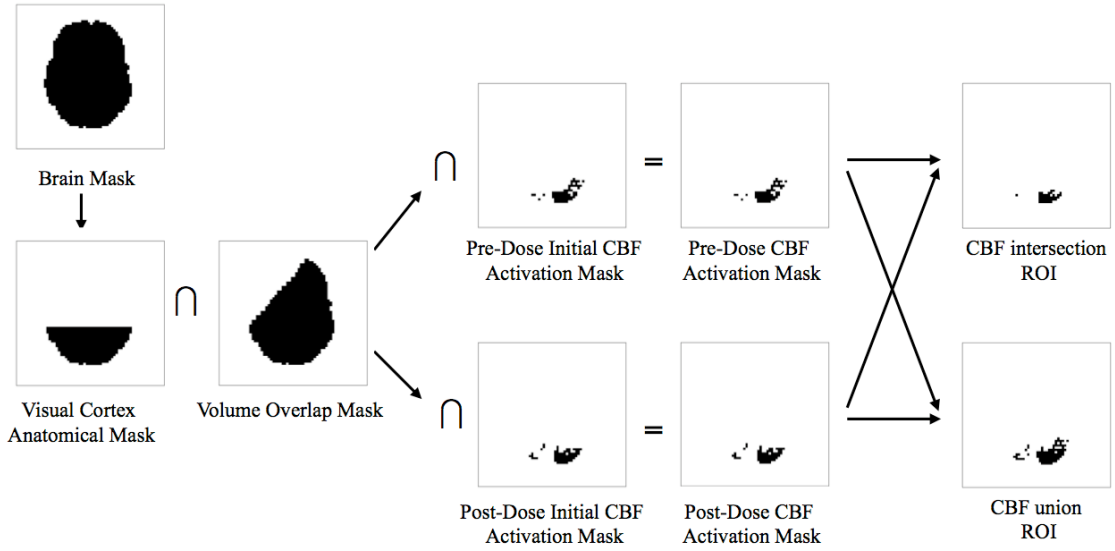

Figure 1.1: Example of region-of-interest (ROI) formation for the most inferior functional slice from subject 8. As seen in the volume overlap mask, the left anterior portion of the brain in this slice had less than 90% volume overlap between the pre-dose and post-dose sessions. For this example, the initial CBF activation masks are identical to the CBF activation masks because this slice did not include areas of motor activity.

by taking the union of the pre-dose and post-dose CBF activation masks. This process was repeated with the BOLD data (overall significance level $p<0.05$) to create pre-dose and post-dose BOLD functional activation maps, and BOLD intersection and union ROIs.

For each metric and ROI, a per-subject average value was obtained by averaging the metric across all voxels within the ROI. The per voxel ΔCBF time series were defined as the per voxel CBF time series after subtraction of the per voxel baseline CBF ($\hat{b}$). Division of the per voxel ΔCBF time series by $\hat{b}$ produced the per voxel %ΔCBF time series. The per voxel ΔCBF and %ΔCBF time series were averaged over voxels within each ROI to form the per subject ΔCBF and %ΔCBF time series. The per subject ΔCBF and %ΔCBF time series were averaged over cycles to form the per subject ΔCBF and %ΔCBF block responses, which were then averaged over subjects to form the group average ΔCBF and %ΔCBF block responses, respectively. Similarly, per voxel %ΔBOLD time series, per subject %ΔBOLD time series, and the per subject and group average %ΔBOLD block responses were computed.

To assess the temporal dynamics of the CBF and BOLD responses, we interpolated each subject's ΔCBF and %ΔBOLD block responses to a time resolution of 0.25s and computed the following timing parameters: 1) time to reach 50% of the peak response (T_{50}), 2) time after the peak to return to 50% of the peak response (TA_{50}), and 3) the full-width half-maximum (FWHM = $TA_{50} - T_{50}$).

Statistical Tests

We used two-tailed paired t-tests to compare pre-dose and post-dose parameter estimates. For both the CBF and BOLD data, we compared the pre-dose and post-dose values of the number of functionally active voxels (using the pre-dose and post-dose activation maps) and the contrast-to-noise ratio estimates $\sqrt{F_{CBF}}$ and $\sqrt{F_{BOLD}}$ (with separate tests for the intersection and union ROIs). In addition, to better understand the factors that alter the contrast-to-noise ratio, we also performed pre-dose versus post-dose comparisons of the amplitude estimates $\hat{h}_{CBF}$ and $\hat{h}_{BOLD}$, the noise estimates $\hat{\sigma}_{n,CBF}$ and $\hat{\sigma}_{n,BOLD}$, the baseline estimates $\hat{b}$ and $BOLD_0$, the percent change estimates $\%\Delta CBF$ and $\%\Delta BOLD$, and the signal-to-noise ratio estimates SNR_{CBF} and SNR_{BOLD}.

To further assess the dependence of the number of active voxels, the contrast-to-noise ratio, and the functional response amplitude on baseline CBF, we computed the correlation between the number of active voxels (CBF or BOLD) and the per subject baseline CBF estimate $\hat{b}$, the correlation between the CNR estimates ($\sqrt{F_{CBF}}$ or $\sqrt{F_{BOLD}}$) and $\hat{b}$, and also the correlation between the absolute functional amplitudes ($\hat{h}_{CBF}$ and $\hat{h}_{BOLD}$) and $\hat{b}$. To account for the effect of activation extent size on the measurement of response amplitude (Laurienti et al. 2002), we also computed the correlation between $\hat{b}$ and the CBF total response magnitude (defined as the product of $\hat{h}_{CBF}$ and the number of active CBF voxels) and the correlation between $\hat{b}$ and the BOLD total response magnitude (defined as the product of $\hat{h}_{BOLD}$ and the number of active BOLD voxels). These correlations were computed using data from

the pre-dose session only, the post-dose session only, and the union of the pre-dose and post-dose sessions.

To assess caffeine's effect on CBF and BOLD temporal dynamics, we used paired two-tailed t-tests to compare the pre-dose and post-dose timing parameters (T_{50}, TA_{50}, and FWHM) across subjects. In addition, to examine whether possible changes in the shape of the curve affected correlation of the responses with the GLM reference function ($\mathbf{X}$), we computed the correlation between the reference function and the per subject ΔCBF and %ΔBOLD time series. Paired two-tailed t-tests were then used to compare the pre-dose and post-dose correlation values across subjects.

1.5 RESULTS

Figure 1.2 shows example pre-dose and post-dose activation maps from Subject 1 for the CBF data (top two rows) and BOLD data (bottom two rows). The post-dose CBF activation map (second row) exhibits fewer active voxels than the pre-dose CBF activation map (top row). In contrast, there is not a clear difference between the number of active voxels in the pre-dose (third row) and post-dose (last row) BOLD activation maps. Figure 1.3 shows example pre-dose and post-dose activation maps for the third or fourth most inferior slice from each subject for the CBF data (top two rows) and BOLD data (bottom two rows). Consistent with the trend found in Subject 1's data in Figure 1.2, the post-dose CBF activation maps (second row) exhibit fewer active voxels than the pre-dose CBF activation maps (top row) for all subjects. Also in agreement with Figure 1.2, the number of active voxels in the pre-dose (third row) and the post-dose (last row) BOLD activation maps appear to be similar. For the CBF data, Table 1.1 shows per subject and average metric values and two-tailed paired t-test results for comparisons of: 1) the number of active voxels in the pre-dose versus post-dose activation maps, and 2) the metrics in the intersection ROI. Table 1.2 shows the same information for the BOLD data. In agreement with the results of Figures 1.2 and 1.3, we found that the caffeine dose significantly reduced the number of voxels across subjects in the post-dose as compared to the pre-dose CBF activation maps (22.8% reduction, $p = 0.0031$, $t = -3.99$), but did not find a significant difference in the number of voxels in the pre-dose versus post-dose BOLD activation maps ($p = 0.69$, $t = 0.41$).

Table 1.1:
Per subject and average values of the estimated daily caffeine usage, number of active voxels in CBF activation maps, and CBF data metrics in the CBF intersection ROI.

	Estimated daily caffeine usage	CBF # active voxels		$\sqrt{F_{CBF}}$		$\hat{h}_{CBF}$ (mL/(100g-min))		$\hat{\sigma}_{CBF}$		$\hat{b}$;Baseline CBF (mL/(100g-min))		$\%\Delta CBF$		SNR_{CBF}	
Subject	(mg/d)	Pre	Post	Pre	Post	Pre	Post	Pre	Post	Pre	Post	Pre	Post	Pre	Post
1	187.5	503	326	5.07	3.81	36.2	30.6	28.1	32.1	84.6	72.2	44.0	44.4	3.15	2.35
2	250.0	313	188	3.70	3.37	44.6	47.0	55.8	64.6	56.2	30.6	92.1	192.9	1.08	0.59
3	175.0	185	115	3.50	2.87	40.8	32.1	43.2	40.9	59.7	25.7	75.3	163.4	1.39	0.66
4	180.0	262	221	2.98	3.44	39.3	37.7	51.7	49.4	56.0	43.7	98.0	111.9	1.20	0.98
5	140.0	512	368	5.18	3.71	49.9	34.5	36.4	36.2	72.6	41.8	109.6	86.6	2.13	1.20
6	150.0	544	448	3.94	4.29	38.2	34.8	45.0	36.3	92.3	57.4	42.7	64.8	2.22	1.71
7	145.0	323	270	3.98	4.03	54.9	40.5	54.4	37.3	87.8	50.4	66.0	93.5	1.75	1.40
8	113.0	385	430	4.80	4.08	48.0	33.6	38.8	34.0	88.1	46.5	57.1	81.2	2.54	1.50
9	138.0	294	250	4.07	3.34	39.1	30.3	35.9	37.8	81.8	59.7	49.6	57.1	2.35	1.69
10	85.0	549	371	5.45	4.09	41.8	31.9	31.3	29.7	83.2	47.8	52.3	93.5	2.87	1.68
mean	156.4	387.0	298.7	4.27	3.70	43.3	35.3	42.1	39.8	76.2	47.6	68.7	98.9	2.07	1.38
std	42.9	124.4	102.7	0.77	0.42	5.7	4.9	9.1	9.7	13.3	12.9	22.8	44.2	0.67	0.51
t-test		0.003;		0.030;		0.002;		0.347;		<0.001;		0.033;		<0.001;	
(p;t)	-	-3.99		-2.58		-4.24		-0.99		-8.85		2.51		-7.10	

Table 1.2:
Per subject and average values of the number of active voxels in BOLD activation maps and BOLD data metrics in the BOLD intersection ROI.

	BOLD # active voxels		$\sqrt{F_{BOLD}}$		$\hat{h}_{BOLD}$		$\hat{\sigma}_{n,BOLD}$		$BOLD_0$		$\%\Delta BOLD$		SNR_{BOLD}	
Subject	Pre	Post	Pre	Post	Pre	Post	Pre	Post	Pre	Post	Pre	Post	Pre	Post
1	735	726	7.95	7.20	61.3	66.7	32.7	36.1	5864.8	5853.0	1.07	1.21	200.1	178.4
2	780	924	5.58	4.92	77.0	68.0	49.8	52.8	5508.6	5605.4	1.47	1.26	123.0	116.9
3	982	911	5.93	6.16	61.0	55.9	44.1	40.2	5643.6	5161.1	1.11	1.13	135.2	136.7
4	832	658	5.62	4.84	76.3	64.4	51.9	48.6	5387.3	5482.8	1.50	1.24	121.3	128.7
5	1399	1273	8.32	7.95	76.5	67.4	38.7	35.5	6150.9	5561.1	1.34	1.35	182.2	173.9
6	865	981	4.18	6.11	64.5	72.0	52.7	39.1	5865.2	5822.8	1.17	1.32	136.3	171.5
7	689	953	5.78	9.19	70.4	70.7	47.6	34.3	6247.2	5678.7	1.16	1.28	143.0	174.0
8	1035	1084	5.94	6.82	64.2	66.3	43.5	39.2	6154.5	5637.4	1.09	1.24	164.0	159.8
9	734	665	6.27	5.75	53.6	53.3	37.2	36.8	5746.9	5545.3	0.98	1.03	164.4	162.5
10	763	811	7.07	6.88	52.9	50.7	31.5	31.0	6054.3	5878.9	0.90	0.89	207.7	207.5
mean	881.4	898.6	6.26	6.58	65.8	63.5	43.0	39.4	5862.3	5622.7	1.18	1.20	157.7	161.0
std	202.2	183.0	1.16	1.27	8.6	7.1	7.3	6.3	276.7	201.2	0.19	0.13	29.5	25.5
t-test	0.694;		0.484;		0.301;		0.083;		0.023;		0.734;		0.570;	
(p;t)	0.41		0.73		-1.10		-1.95		-2.74		0.35		0.59	

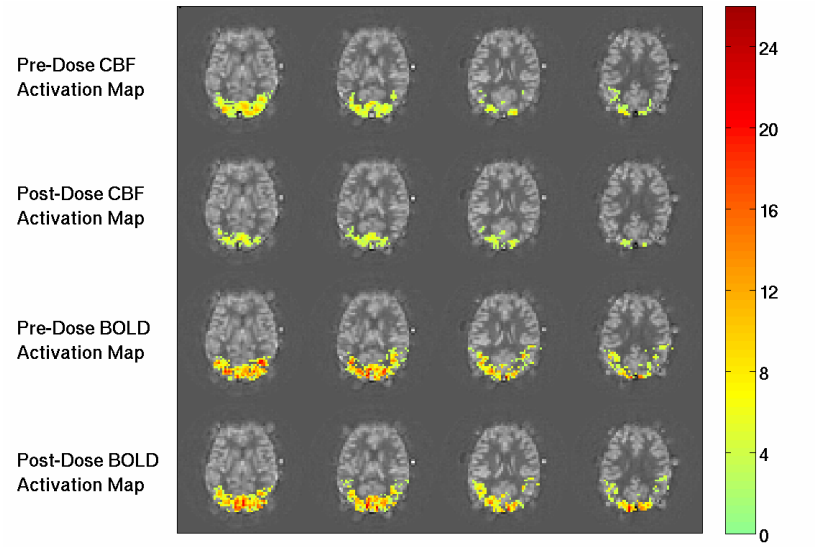

Figure 1.2: Example functional activation maps from Subject 1. The CNR values for activated regions are overlaid on baseline CBF maps. Top and second rows show the pre-dose and post-dose CBF activation maps, respectively. The number of voxels is visibly decreased from the pre-dose to the post-dose conditions. The third and fourth rows show the pre-dose and post-dose BOLD activation maps, respectively. There is no apparent difference in the number of active BOLD voxels between the two conditions. The colorbar shows CNR ($\sqrt{F_{CBF}}$ and $\sqrt{F_{BOLD}}$) values.

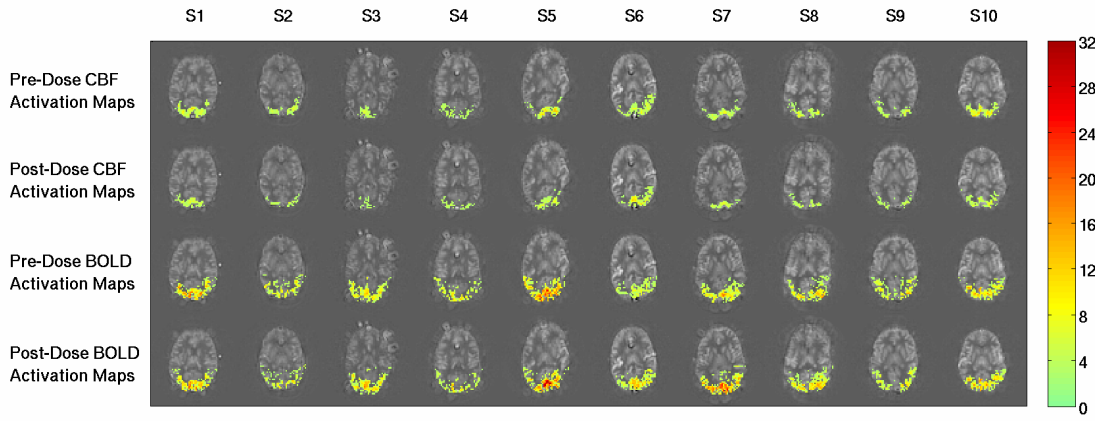

Figure 1.3: Example functional activation maps for the third or fourth most inferior slice from each subject. Each column shows data from a single subject (denoted S1 to S10), and CNR values for activated regions are overlaid on baseline CBF maps. Top and second rows show the pre-dose and post-dose CBF activation maps, respectively. The number of active CBF voxels is visibly decreased from the pre-dose to the post-dose conditions for all subjects. The third and fourth rows show the pre-dose and post-dose BOLD activation maps, respectively. The number of active BOLD voxels in the two conditions appear to be similar. The colorbar shows CNR ($\sqrt{F_{CBF}}$ and $\sqrt{F_{BOLD}}$) values.

Consistent with the observed reduction in the number of functionally active CBF voxels, the caffeine dose significantly reduced $\sqrt{F_{CBF}}$ in the CBF intersection ROI (13.4% reduction, p = 0.030, t = -2.58). The reduction in $\sqrt{F_{CBF}}$ was consistent with a significant decrease in $\hat{h}_{CBF}$ (18.4% reduction, p = 0.002, t = -4.24) and a lack of a significant change in $\hat{\sigma}_{n,CBF}$(p = 0.35, t = -0.99) (see also Equation 1.7). The caffeine dose significantly increased $\%\Delta CBF$ (43.5% increase, p = 0.033, t = 2.51) and significantly reduced SNR_{CBF} (33.3% decrease, p < 0.001, t = -7.10). Note that the product of these average relative changes $(1.435 \cdot 0.667 = 0.957)$ shows an overall decrease roughly consistent with the reduction in $\sqrt{F_{CBF}}$ (see Equation 1.8). There is not exact agreement because the per subject average $\sqrt{F_{CBF}}$ does not equal the product of the per subject average values of $\%\Delta CBF$ and SNR_{CBF}, reflecting the fact that the product of two average quantities does not in general equal the average of the product. In agreement with the findings of our previous studies (Liu et al. 2004b; Behzadi and Liu 2006), the caffeine dose significantly reduced the baseline CBF estimate $\hat{b}$ across subjects (37.6% reduction, p < 0.001 , t = -8.85). When considered together with the lack of a significant change in $\hat{\sigma}_{n,CBF}$ the decrease in $\hat{b}$ is consistent with the observed decrease in SNR_{CBF}. Consistent with the results obtained with the CBF intersection ROI, the caffeine dose significantly decreased $\sqrt{F_{CBF}}$ (p=0.008, t=-3.43), $\hat{h}_{CBF}$ (p<0.001 t=-6.80), SNR_{CBF} (p<0.001, t=-6.89), and $\hat{b}$ (p<0.001, t=-8.94), significantly increased $\%\Delta CBF$ (p=0.01, t=3.24), and did not significantly change $\hat{\sigma}_{n,CBF}$ (p=0.18, t=-1.47) in the CBF union ROI.

In agreement with the lack of a significant difference in the number of functionally active BOLD voxels between the pre-dose and post-dose conditions, the caffeine dose did not significantly change $\sqrt{F_{BOLD}}$ (p = 0.48, t = 0.73) for the intersection ROI. Consistent with the lack of a significant change in $\sqrt{F_{BOLD}}$, we found that the caffeine dose did not have a significant effect on either $\hat{h}_{BOLD}$ (p = 0.30, t = -1.10) or $\hat{\sigma}_{n,BOLD}$ (p = 0.083, t = -1.95) (see Equation 1.5). In addition caffeine did not lead to a significant change in either SNR_{BOLD} (p = 0.57, t = 0.59) or $\%\Delta BOLD$ (p = 0.73, t = 0.35) (see Equation 1.6). We found that the caffeine dose significantly decreased $BOLD_0$ (4.0% reduction, p = 0.023, t = -2.74). Although there were not significant changes in either SNR_{BOLD} or $\hat{\sigma}_{n,BOLD}$, the average percent changes in these quantities (2.1% increase and 8.4% decrease, respectively), are roughly consistent with the observed decrease in $BOLD_0$. Consistent with the results obtained with the BOLD intersection ROI, the caffeine dose did not significantly change $\sqrt{F_{BOLD}}$ (p=0.44, t=0.81), $\hat{h}_{BOLD}$ (p=0.74, t=-0.34), $\hat{\sigma}_{n,BOLD}$ (p=0.08, t=-1.96), SNR_{BOLD} (p=0.50, t=0.70), or $\%\Delta BOLD$ (p=0.51, t=0.68), but significantly decreased $BOLD_0$ (p=0.02, t=-2.92) in the BOLD union ROI. The similarity of the paired t-test results of metrics in the intersection and union ROIs for both the CBF and BOLD data indicate that pairwise comparisons of pre-dose and post-dose data were not sensitive to the choice of ROI.

Figure 1.4 shows scatter plots of (a) the number of functionally active CBF voxels versus the baseline CBF estimate $\hat{b}$ and (b) $\sqrt{F_{CBF}}$ versus $\hat{b}$ across subjects for data from both the pre-dose (blue solid circles) and post-dose (red crosses) sessions.

We found that $\hat{b}$ was significantly correlated to the number of active CBF voxels in the pre-dose condition (r = 0.76, p = 0.011), the post-dose condition (r = 0.65, p = 0.042), and the union of the pre-dose and post-dose conditions (r = 0.72, p <0.001). Similarly, $\hat{b}$ was significantly correlated with $\sqrt{F_{CBF}}$ in the pre-dose condition (r = 0.65, p = 0.043), the post-dose condition (r = 0.71, p = 0.022) and the union of the pre-dose and post-dose conditions (r = 0.66, p = 0.0014). Although $\hat{b}$ was not significantly correlated with $\hat{h}_{CBF}$ (pre-dose only: p = 0.97; post-dose only: p = 0.09; pre-dose and post-dose: p = 0.99), it was significantly correlated with the CBF total response magnitude in the pre-dose condition (r = 0.71, p = 0.023) and the union of the pre-dose and post-dose conditions (r = 0.73, p < 0.001) but not the post-dose condition (r = 0.56, p = 0.096). In contrast, $\hat{b}$ was not significantly correlated with the number of active BOLD voxels (pre-dose only: p = 0.610; post-dose only: p = 0.452; pre-dose and post-dose: p = 0.439) or $\sqrt{F_{BOLD}}$ (pre-dose only: p = 0.497; post-dose only: p = 0.359; pre-dose and post-dose: p = 0.702). Also, $\hat{b}$ was not significantly correlated with $\hat{h}_{BOLD}$ (pre-dose only: p = 0.49; post-dose only: p = 0.33; pre-dose and post-dose: p = 0.35) or the BOLD total response magnitude (pre-dose only: p = 0.56; post-dose only: p = 0.82; pre-dose and post-dose: p = 0.95).

Figure 1.5 shows the pre-dose (blue lines) and post-dose (red lines) group average (a) %ΔBOLD, (b) %ΔCBF, and (c) ΔCBF block responses. Consistent with previous findings from our group (Liu et al. 2004b), the caffeine dose visibly accelerated the temporal dynamics of the BOLD block response and significantly decreased T_{50} (22.5% decrease, p<0.001, t=-4.87) and TA_{50} (6.4% decrease, p=0.002,

t=-4.31) but did not change the FWHM (p=0.81, t=-0.24). Caffeine had a less visible effect on the CBF block response, with no significant effect on T_{50} (p=0.23, t=-1.28) or FWHM (p=0.22, t=-1.32) and an almost significant reduction in TA_{50} (p=0.07, t=-2.09). The correlations between the reference function and the per subject %ΔBOLD time series were not significantly changed by caffeine (p=0.49, t=-0.73). Consistent with the relative lack of caffeine-induced change in the temporal dynamics of the CBF response, we also found no significant caffeine-induced change in the correlations between the reference function and the per subject ΔCBF time series (p=0.30, t=1.09).

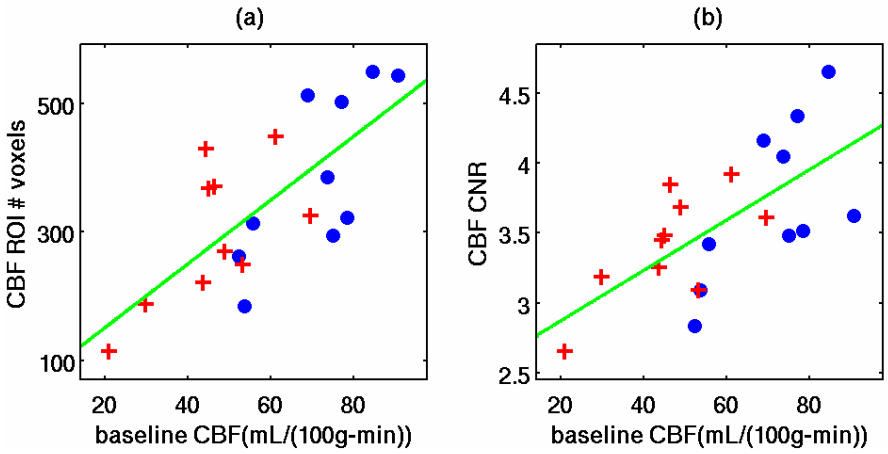

Figure 1.4: Scatter plots of (a) the number of voxels in the CBF activation maps versus baseline CBF (pre-dose only: r = 0.76, p = 0.011; post-dose only: r = 0.65, p = 0.042; pre-dose and post-dose: r = 0.72, p <0.001) and (b) CBF CNR versus baseline CBF (pre-dose only: r = 0.65, p = 0.043; post-dose only: r = 0.71, p = 0.022; pre-dose and post-dose: r = 0.66, p = 0.0014). Data are from the pre-dose (blue solid circles) and post-dose (red crosses) sessions. As discussed in the text, no significant correlations were found with similar analyses of baseline CBF versus the number of voxels in the BOLD activation maps, the BOLD CNR, $\hat{h}_{BOLD}$, or $\hat{h}_{CBF}$ (p>0.09).

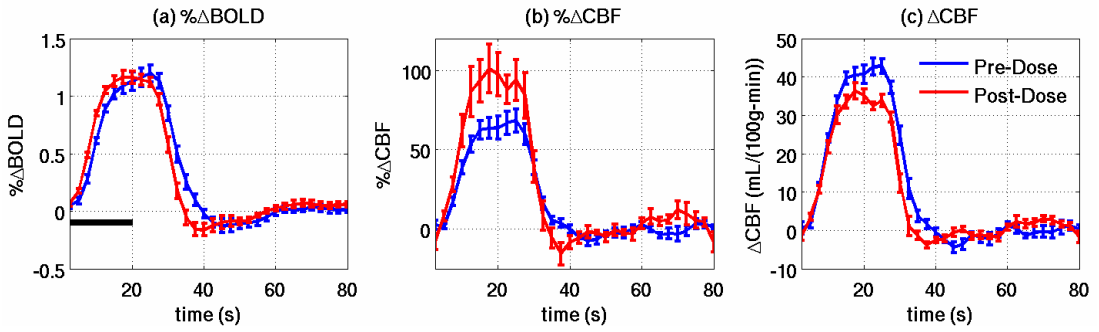

Figure 1.5: Pre-dose (blue lines) and post-dose (red lines) group average responses for (a) %ΔBOLD, (b) %ΔCBF, and (c) ΔCBF. Vertical bars show standard error, and the horizontal black bar indicates the visual stimulus.

1.6 DISCUSSION

The caffeine dose significantly decreased the number of functionally active voxels in the CBF activation maps but not the BOLD activation maps. The decrease in the number of active CBF voxels was consistent with a significant decrease in $\sqrt{F_{CBF}}$. This reduction was in turn found to reflect a reduction in the functional response amplitude $\hat{h}_{CBF}$ without a concomitant drop in the noise standard deviation $\hat{\sigma}_{n,CBF}$. Alternatively, we could also view the drop in $\sqrt{F_{CBF}}$ as due to a significant drop in SNR_{CBF} that is partially offset by an increase in $\%\Delta CBF$. Note that the decrease in SNR_{CBF} is a direct consequence of the caffeine-induced reduction of baseline CBF coupled with a lack of change in the noise term $\hat{\sigma}_{n,CBF}$ (see Equation 1.8).

Several prior studies have provided support for two competing models describing the dependence of the functional CBF response on baseline CBF: an additive model and a proportional model. In the additive model, $\%\Delta CBF$ is inversely related to baseline CBF while the absolute functional CBF change ($\hat{h}_{CBF}$ in this study) is constant. This model is supported by two arterial spin labeling studies, one with subjects breathing room air (Kastrup et al. 1999), and another using breathhold-induced hypercapnia to increase baseline CBF (Li et al. 2000). In the proportional model, $\hat{h}_{CBF}$ is proportional to baseline CBF, and $\%\Delta CBF$ is constant, as supported by the results of a PET study using hypercapnia and hypocapnia to modulate baseline CBF (Shimosegawa et al. 1995). However, there is also evidence indicating that

neither model provides an adequate description. In a PET study that controlled end-tidal CO_2 levels (Kemna et al. 2001) and a pulsed arterial spin labeling study that used indomethacin to reduce baseline CBF (St Lawrence et al. 2003), decreases in baseline CBF produced reductions in both $\%\Delta CBF$ and the absolute functional CBF change. In this work, we found a significant caffeine-induced reduction in $\hat{h}_{CBF}$ and a significant increase in $\%\Delta CBF$, which is not consistent with either the additive or the proportional model. Discrepancies between study findings may be related to the different measurement techniques and methods of baseline CBF manipulation. Further work is clearly needed to elucidate the neurovascular mechanisms relating changes in both $\%\Delta CBF$ and $\hat{h}_{CBF}$ to changes in baseline CBF.

The dependence of functional CBF contrast on baseline CBF was further demonstrated by the correlation analyses presented in Figure 1.4, where it was shown that both $\sqrt{F_{CBF}}$ and the number of activated voxels in the CBF activation maps were significantly correlated with baseline CBF. The observed correlations were significant whether considering the pre-dose data only, the post-dose data only, or the union of the pre-dose and post-dose data. This finding indicates that the effect of baseline CBF on functional CBF contrast is a critical factor that should be considered in the analysis of functional CBF maps. In agreement with (Kastrup et al. 1999), we did not find a significant correlation between $\hat{h}_{CBF}$ and baseline CBF. Note that the observed decrease in $\hat{h}_{CBF}$ with the caffeine-related decrease in baseline CBF might have suggested the presence of a positive correlation between $\hat{h}_{CBF}$ and baseline CBF. However, the decreases in $\hat{h}_{CBF}$ were observed by comparing each subject's pre-dose

and post-dose values across a common region-of-interest, which was specific to each subject. In examining the correlation of $\hat{h}_{CBF}$ and baseline CBF across subjects, we computed these metrics using all voxels showing significant functional CBF activation. As shown in Figure 1.4a, the number of activated voxels varied across subjects and showed a positive correlation with baseline CBF. The increase in the number of voxels in subjects with higher baseline CBF values tended to lower the average $\hat{h}_{CBF}$ measured across the activated region, offsetting any trend towards an increase in $\hat{h}_{CBF}$ and contributing to a lack of correlation between $\hat{h}_{CBF}$ and baseline CBF. The correlation between the CBF activation extent and baseline CBF and the lack of correlation between $\hat{h}_{CBF}$ and baseline CBF suggests that the product of $\hat{h}_{CBF}$ and the number of active CBF voxels should be correlated with baseline CBF. Indeed, we found significant positive correlations between the CBF total response magnitude and baseline CBF for the pre-dose data and for the union of the pre-dose and post-dose data.

In agreement with the findings of the current study, previous studies have shown that caffeine reduces the baseline BOLD-weighted signal $BOLD_0$ (Haacke et al. 2003; Perthen et al. 2008), most likely reflecting an increase in deoxyhemoglobin content that accompanies the caffeine-induced reduction in baseline CBF. Our finding that $\%\Delta BOLD$ was not significantly affected by caffeine agrees with the findings of our previous studies (Liu et al. 2004b; Behzadi and Liu 2006) but not others (Mulderink et al. 2002; Chen and Parrish 2007). As noted by (Laurienti et al. 2002), differences in chronic caffeine usage and the duration of withdrawal between these studies may account for the differences in the modulation of the BOLD signal

amplitude. In their study, (Laurienti et al. 2002) found that a caffeine dose tended to increase BOLD magnitude in high (>300mg/day) caffeine users and decrease BOLD magnitude in low (<120mg/day) caffeine users when both groups began from a withdrawal state. A more recent study by the same group found that a caffeine dose tended to decrease BOLD magnitude in both high (>600mg/day) and low (<200mg/day) caffeine users when both groups began from a native state (Yang et al. 2007). The results in the withdrawal state (30 hours) of caffeine were consistent with their previous study, with an increase in the BOLD signal in the high users and a decrease in the low users.

Consistent with previous results from our group (Liu et al. 2004b), we found that the caffeine dose accelerated the temporal dynamics of the BOLD response. However, we also found that the caffeine dose did not significantly change the temporal dynamics of the CBF response. The difference in the temporal dynamics of the CBF and BOLD responses may reflect the different physiological origins of the two responses, where the CBF response reflects the change in a single physiological variable while the BOLD response exhibits a complex dependence on changes in cerebral blood flow, cerebral blood volume and oxygen metabolism (Buxton et al. 2004). An additional potential factor is the relative difference in the dynamics of the vasculature associated with the two responses, with the CBF response depending primarily on the dynamics of the arterioles and capillaries and the BOLD response being weighted towards the dynamics of the venules and veins (Luh et al. 2000). The different vascular weighting of the CBF and BOLD responses is also reflected in differences in the spatial patterns of activation shown in Figures 1.2 and 1.3.

In this study, we used a fixed caffeine dose to decrease baseline CBF in a group of subjects that had similar self-reported daily caffeine usage levels. However, it is important to note that differences in daily caffeine usage level and subject-dependent changes in blood caffeine concentration levels from the pre-dose to post-dose sessions may also affect functional CBF and BOLD responses. For future studies, accounting for these factors by inclusion of plasma or saliva caffeine concentration measurements would help to further our understanding of the correlation between baseline CBF and the CNR and activation extent of the CBF response.

A key assumption in this study is that the performance of the motor and visual tasks are equivalent in the pre-dose and post-dose sessions. While the presented stimuli are identical between sessions, it is possible that subjects became more vigilant to the motor task after a caffeine dose, reducing attention to the visual stimulus. However, the relatively undemanding task of pressing buttons with one hand at 2 Hz was easily performed by our subjects, so was unlikely to require disproportionate amounts of attention in the pre-dose and post-dose sessions. In addition, our findings of a significant caffeine-induced increase in $\%\Delta CBF$ and no significant change in $\%\Delta BOLD$ do not appear to be consistent with decreased visual activity after caffeine. Furthermore, a previous study by our group (Liu et al. 2004b) that used only a visual stimulus also found no change in $\%\Delta BOLD$ with a caffeine dose, further suggesting that performance on the motor task had a negligible effect on the visual response in the present study.

We also consider whether the results of this study are due to brain physiology or technical limitations in measurement methods. The caffeine-induced reduction of CBF CNR and activation extent appears to be a product of both factors. Use of

arterial spin labeling to measure baseline CBF produced a caffeine-induced decrease in SNR from reduction of the perfusion signal. Also, the caffeine-induced physiological reduction in the absolute functional CBF response ($\hat{h}_{CBF}$) prevented $\%\Delta CBF$ from compensating for the SNR reduction, leading to the overall CNR decrease. In contrast, we found the BOLD response is less sensitive to caffeine-induced reductions in baseline CBF. It is possible that the observed lack of change in the BOLD response may be due to BOLD SNR limitations at 3 Tesla. A previous study at 7 Tesla found an increase in $\%\Delta BOLD$ with a hypocapnia-induced decrease in baseline CBF (Cohen et al. 2002). However, one study at 1.5 Tesla found a general caffeine-related increase in the BOLD response (Mulderink et al. 2002), while two other studies at 1.5 Tesla found that caffeine's effect on the BOLD response depended on the daily caffeine usage levels of the subject groups (Laurienti et al. 2002; Yang et al. 2007). These findings suggest that BOLD SNR limitations at 3T are not a main factor in the observed lack of a caffeine-induced change in the BOLD response and that the discrepancy between our findings and those of (Cohen et al. 2002) is most likely due to other differences in the experimental protocols.

A possible confound in this study was the use of hypercapnia at the end of the pre-dose session. BOLD and CBF signals are expected to be close to a physiological steady-state 30 to 60 seconds after a hypercapnic stimulus (Stefanovic et al. 2006). As the first functional scan of the post-dose session took place at least 45 minutes after the last hypercapnia run, confounds due to the hypercapnia are expected to be negligible.

In summary, our results show that caffeine significantly reduces the CNR and activation extent of the functional CBF response. Furthermore, we found that measures of baseline CBF could explain a significant portion of the inter-subject variability in the number of activated CBF voxels and the CNR of the CBF data. Taken together, these observations suggest that additional factors that can modulate baseline CBF, such as disease, normal aging, and the use of vasoactive medications, such as statins, are also likely to have an effect on functional CBF maps. Consideration of these factors and measures of baseline CBF should therefore be integrated into the analysis and interpretation of studies that utilize functional CBF maps obtained with arterial spin labeling.

1.7: APPENDIX A.1

USE OF GENERAL LINEAR MODEL REGRESSOR WEIGHTS AS CEREBRAL BLOOD FLOW MEASUREMENTS

To understand how general linear model (GLM) regressor weights may be used as direct measurements of cerebral blood flow (CBF), we first write the components of the control and tag images of the arterial spin labeling signal (ignoring physiological and thermal noise terms):

$$y_{con} = \exp\left(-TE/T_2^*\right)\left(s_m M_0 + M_{0b} \cdot TI_1 \cdot CBF\right) \qquad \text{[A.1.1]}$$

$$y_{tag} = \exp\left(-TE/T_2^*\right)\left(s_m M_0 + M_{0b} \cdot TI_1 \cdot CBF\left(1 - 2\alpha\exp\left(-TI/T_{1B}\right)\right)\right) \qquad \text{[A.1.2]}$$

where $s_M = 1 - \beta e^{-TI_p/T_1}$ and α denotes inversion efficiency. We then consider an example with just 4 images, and with F and B denoting the flow and BOLD (i.e. the T2* term) time series respectively.

$$\begin{bmatrix} y_{tag,1} \\ y_{con,1} \\ y_{tag,2} \\ y_{con,2} \end{bmatrix} = s_m M_0 \begin{bmatrix} B[1] \\ B[2] \\ B[3] \\ B[4] \end{bmatrix} + M_{0,b} TI_1 \begin{bmatrix} \left(1 - 2\alpha\exp\left(-TI/T_{1B}\right)\right)F[1]B[1] \\ F[2]B[2] \\ \left(1 - 2\alpha\exp\left(-TI/T_{1B}\right)\right)F[3]B[3] \\ F[4]B[4] \end{bmatrix} \qquad \text{[A.1.3]}$$

We then separate the right-hand most term into a component that is modulated by the tag and control conditions and one that is not:

$$\begin{aligned} \begin{bmatrix} y_{tag,1} \\ y_{con,1} \\ y_{tag,2} \\ y_{con,2} \end{bmatrix} &= s_m M_0 \begin{bmatrix} B[1] \\ B[2] \\ B[3] \\ B[4] \end{bmatrix} + M_{0,b} TI_1 \left(1 - \alpha\exp\left(-TI/T_{1B}\right)\right) \begin{bmatrix} F[1]B[1] \\ F[2]B[2] \\ F[3]B[3] \\ F[4]B[4] \end{bmatrix} + M_{0,b} TI_1 \cdot \alpha\exp\left(-TI/T_{1B}\right) \begin{bmatrix} -F[1]B[1] \\ F[2]B[2] \\ -F[3]B[3] \\ F[4]B[4] \end{bmatrix} \qquad \text{[A.1.4]} \\ &= s_m M_0 \begin{bmatrix} B[1] \\ B[2] \\ B[3] \\ B[4] \end{bmatrix} + M_{0,b} TI_1 \left(1 - \alpha\exp\left(-TI/T_{1B}\right)\right) \begin{bmatrix} F[1]B[1] \\ F[2]B[2] \\ F[3]B[3] \\ F[4]B[4] \end{bmatrix} + M_{0,b} TI_1 \cdot \alpha\exp\left(-TI/T_{1B}\right)\mathbf{M} \begin{bmatrix} F[1]B[1] \\ F[2]B[2] \\ F[3]B[3] \\ F[4]B[4] \end{bmatrix} \end{aligned}$$

where **M** is the modulation matrix with -1s and 1s along the diagonal. Assuming the functional BOLD-weighting of the flow terms is negligible:

$$\begin{aligned}\begin{bmatrix} y_{tag,1} \\ y_{con,1} \\ y_{tag,2} \\ y_{con,2} \end{bmatrix} &\approx s_m M_0 \left(\begin{bmatrix} 1 \\ 1 \\ 1 \\ 1 \end{bmatrix} B_0 + \begin{bmatrix} \Delta B[1] \\ \Delta B[2] \\ \Delta B[3] \\ \Delta B[4] \end{bmatrix} \right) + M_{0,b} TI_1 s_q B_0 \left(\begin{bmatrix} 1 \\ 1 \\ 1 \\ 1 \end{bmatrix} F_0 + \begin{bmatrix} \Delta F[1] \\ \Delta F[2] \\ \Delta F[3] \\ \Delta F[4] \end{bmatrix} \right) + M_{0,b} TI_1 \cdot \alpha \exp\left(-TI/T_{1B}\right) B_0 \mathbf{M} \left(\begin{bmatrix} 1 \\ 1 \\ 1 \\ 1 \end{bmatrix} F_0 + \begin{bmatrix} \Delta F[1] \\ \Delta F[2] \\ \Delta F[3] \\ \Delta F[4] \end{bmatrix} \right) \\ &= s_m M_0 \left(\mathbf{1}_\mathbf{N} B_0 + \mathbf{X}\mathbf{h}'_{BOLD} \right) + \frac{\kappa s_q}{\alpha \exp\left(-TI/T_{1B}\right)} \left(\mathbf{1}_\mathbf{N} F_0 + \mathbf{X}\mathbf{h}_{perf} \right) + \kappa \mathbf{M} \left(\mathbf{1}_\mathbf{N} F_0 + \mathbf{X}\mathbf{h}_{perf} \right) \end{aligned} \quad [A.1.5]$$

where $\kappa = M_{0b} \cdot TI_1 \cdot \alpha \exp\left(-TI/T_{1B}\right) \cdot B_0$, B_0 is the baseline BOLD weighting (which is small for short TE), F_0 is baseline blood flow, and $\mathbf{h}'_{BOLD}$ is the regressor weight for the static tissue BOLD component. Note that $s_m M_0 \left(\mathbf{1}_\mathbf{N} B_0 + \mathbf{X}\mathbf{h}'_{BOLD} \right)$ is the static tissue signal, $\frac{\kappa s_q}{\alpha \exp\left(-TI/T_{1B}\right)} \left(\mathbf{1}_\mathbf{N} F_0 + \mathbf{X}\mathbf{h}_{perf} \right)$ is the blood signal component that is not modulated by the tag and control, and $\kappa \mathbf{M} \left(\mathbf{1}_\mathbf{N} F_0 + \mathbf{X}\mathbf{h}_{perf} \right)$ is the blood signal component that is modulated by the tag and control. Equation A.1.5 can be rewritten as:

$$\begin{aligned} \mathbf{y} &= \mathbf{1}_\mathbf{N} \left(s_m M_0 B_0 + \frac{\kappa s_q}{\alpha \exp\left(-TI/T_{1B}\right)} F_0 \right) + \left(s_m M_0 \mathbf{X}\mathbf{h}'_{BOLD} + \frac{\kappa s_q}{\alpha \exp\left(-TI/T_{1B}\right)} \mathbf{X}\mathbf{h}_{perf} \right) + \kappa \mathbf{M} \left(\mathbf{1}_\mathbf{N} F_0 + \mathbf{X}\mathbf{h}_{perf} \right) \\ &= \kappa \mathbf{1}_\mathbf{N} \left(\frac{s_m}{\kappa} M_0 B_0 + \frac{s_q}{\alpha \exp\left(-TI/T_{1B}\right)} F_0 \right) + \kappa \left(\frac{s_m}{\kappa} M_0 \mathbf{X}\mathbf{h}'_{BOLD} + \frac{s_q}{\alpha \exp\left(-TI/T_{1B}\right)} \mathbf{X}\mathbf{h}_{perf} \right) + \kappa \mathbf{M} \left(\mathbf{1}_\mathbf{N} F_0 + \mathbf{X}\mathbf{h}_{perf} \right) \\ &\approx \kappa \left(\mathbf{X}\mathbf{h}_{BOLD} + \mathbf{1}_\mathbf{N} d + \mathbf{M} \left(\mathbf{1}_\mathbf{N} F_0 + \mathbf{X}\mathbf{h}_{perf} \right) \right) \end{aligned} \quad [A.1.6]$$

Note that the baseline BOLD and functional BOLD terms have a perfusion-dependent term that we have assumed is negligible. To determine if this is a good approximation, we can consider some typical parameters. For the baseline BOLD term we take the ratio of:

$$\frac{\frac{s_m}{\kappa} M_0 B_0}{\frac{s_q}{\alpha \exp\left(-TI/T_{1B}\right)} F_0} = \frac{s_m M_0}{s_q M_{0b} TI_1 F_0}$$
$$\approx \frac{1}{TI_1 F_0} \qquad [A.1.7]$$
$$\approx \frac{1}{(0.6s)(0.01/s)}$$
$$\approx 167$$

Therefore for baseline magnetization, the flow term in the delivered blood is less than 1% of the tissue component. Although we neglect this component here, we should keep in mind that it may have a slight effect when analyzing data across subjects and conditions. Therefore by using a GLM including the term κ:

$$\mathbf{p} = \kappa\left(\mathbf{X}\mathbf{h}_{\mathbf{BOLD}} + \mathbf{1}_N \mathrm{d} + \mathbf{M}\left(\mathbf{X}\mathbf{h}_{\mathbf{CBF}} + \mathbf{1}_N \mathrm{b}\right)\right) \qquad [A.1.8]$$

the amplitudes of the baseline CBF and functional CBF response may be taken directly from the regressor weights b and $\mathbf{h}_{\mathbf{CBF}}$, respectively.

1.8: APPENDIX A.2

SQUARE ROOT OF THE F-STATISTIC AS AN ESTIMATE OF THE CONTRAST-TO-NOISE RATIO

In this section, we show that the square root of the F-statistic ($\sqrt{F}$) may be used as an estimate of the contrast-to-noise ratio, which is defined as (functional signal change)/(noise standard deviation). For this proof, we consider four cases of the general linear model (GLM), which have: (Case 1) no nuisance terms and no accounting for correlated noise, (Case 2) use of nuisance terms but no accounting for correlated noise, (Case 3) no nuisance terms, but with accounting for correlated noise, and (Case 4) use of nuisance terms and accounting for correlated noise.

In the first case of the GLM, which has no nuisance terms and no accounting for correlated noise, the GLM in Equation 1.3 may be defined using $\mathbf{Z} = [\mathbf{X}]$ and $\boldsymbol{\beta} = [\mathrm{h}]$, where we assume that $\mathbf{X}$ is a vector so its norms and square roots are well defined. Using Equation 1.4 with $\mathbf{A} = [1]$, the numerator of $\sqrt{F}$ may then be written as $\sqrt{\hat{\mathrm{h}}^{\mathrm{T}} \mathbf{X}^{\mathrm{T}} \mathbf{X} \hat{\mathrm{h}}}$, which produces the overall relationship $\sqrt{F} = \|\mathbf{X}\|_2 \frac{\hat{h}}{\hat{\sigma}_n}$, where $\|\mathbf{X}\|_2$ is the vector norm of $\mathbf{X}$. Note that this takes the general form:

$$\sqrt{F} = \eta \frac{\hat{h}}{\hat{\sigma}_n} \qquad \text{[A.2.1]}$$

where $\eta = \sqrt{\left[\mathbf{A}\left(\mathbf{Z}^{\mathrm{T}}\mathbf{Z}\right)^{-1}\mathbf{A}^{\mathrm{T}}\right]^{1}}$, and $\sqrt{F}$ is directly proportional to the contrast-to-noise ratio, which is defined as $\left(\hat{h}/\hat{\sigma}_{n}\right)$ in GLM notation. Therefore, in the first case of the GLM, which has no nuisance terms and no accounting for correlated noise, $\eta = \|\mathbf{X}\|_{2}$.

In the second case of the GLM, which has nuisance terms but no accounting of correlated noise, the model presented in Equation 1.3 is defined using $\mathbf{Z} = \begin{bmatrix}\mathbf{X} & \mathbf{S}\end{bmatrix}$ and $\boldsymbol{\beta} = \begin{bmatrix}\mathrm{h}^{\mathrm{T}} & \mathbf{d}^{\mathrm{T}}\end{bmatrix}$. In this case, $\mathbf{A} = \begin{bmatrix}1 & \mathbf{0}\end{bmatrix}$, where $\mathbf{0}$ is a $1 \times l$ row vector of zeros, and l is the number of nuisance regressors. To find η, we first compute:

$$\mathbf{Z}^{\mathrm{T}}\mathbf{Z} = \begin{bmatrix}\mathbf{X}^{\mathrm{T}} \\ \mathbf{S}^{\mathrm{T}}\end{bmatrix}\begin{bmatrix}\mathbf{X} & \mathbf{S}\end{bmatrix} = \begin{bmatrix}\mathbf{X}^{\mathrm{T}}\mathbf{X} & \mathbf{X}^{\mathrm{T}}\mathbf{S} \\ \mathbf{S}^{\mathrm{T}}\mathbf{X} & \mathbf{S}^{\mathrm{T}}\mathbf{S}\end{bmatrix} \qquad [A.2.2]$$

Since $\mathbf{A}$ is set to select only the upper left-hand element of $\left(\mathbf{Z}^{\mathrm{T}}\mathbf{Z}\right)^{-1}$, it is only necessary to compute that element of the block inverse. To do this, we use the following block matrix inverse formula:

$$\begin{bmatrix}\mathbf{A} & \mathbf{D} \\ \mathbf{C} & \mathbf{B}\end{bmatrix}^{-1} = \begin{bmatrix}\left(\mathbf{A} - \mathbf{D}\mathbf{B}^{-1}\mathbf{C}\right)^{-1} & -\mathbf{E}\Delta^{-1} \\ \Delta^{-1}\mathbf{F} & \Delta^{-1}\end{bmatrix} \qquad [A.2.3]$$

where $\Delta = \mathbf{B} - \mathbf{C}\mathbf{A}^{-1}\mathbf{D}$, $\mathbf{E} = \mathbf{A}^{-1}\mathbf{D}$, and $\mathbf{F} = \mathbf{C}\mathbf{A}^{-1}$. Using this formula with Equation A.2.2, we obtain:

$$\left(\mathbf{Z}^{\mathrm{T}}\mathbf{Z}\right)^{-1} = \begin{bmatrix}\left(\mathbf{X}^{\mathrm{T}}\mathbf{X} - \mathbf{X}^{\mathrm{T}}\mathbf{S}\left(\mathbf{S}^{\mathrm{T}}\mathbf{S}\right)^{-1}\mathbf{S}^{\mathrm{T}}\mathbf{X}\right)^{-1} & \ldots \\ \ldots & \ldots\end{bmatrix} \qquad [A.2.4]$$

Taking the calculation for η further produces:

$$\left[\mathbf{A}\left(\mathbf{Z}^{\mathrm{T}}\mathbf{Z}\right)^{-1}\mathbf{A}^{\mathrm{T}}\right]^{1} = \mathbf{X}^{\mathrm{T}}\mathbf{X} - \mathbf{X}^{\mathrm{T}}\mathbf{S}\left(\mathbf{S}^{\mathrm{T}}\mathbf{S}\right)^{-1}\mathbf{S}^{\mathrm{T}}\mathbf{X} \qquad [A.2.5]$$

This can also be expressed as $\left[\mathbf{A}\left(\mathbf{Z}^{\mathrm{T}}\mathbf{Z}\right)^{-1}\mathbf{A}^{\mathrm{T}}\right]^{1} = \mathbf{X}^{\mathrm{T}}\left(\mathbf{I}-\mathbf{P}_{\mathbf{S}}\right)\mathbf{X}$, where $\mathbf{P}_{\mathbf{S}}$ indicates the projection onto the subspace spanned by **S**. Therefore, in the second case of the GLM, which includes nuisance terms but assumes uncorrelated noise:

$$\eta = \sqrt{\mathbf{X}^{\mathrm{T}}\left(\mathbf{I}-\mathbf{P}_{\mathbf{S}}\right)\mathbf{X}} \qquad \text{[A.2.6]}$$

In the third case of the GLM, where correlated noise is accounted for, but no nuisance terms are included, a pre-whitened GLM is used:

$$\mathbf{C}^{-1/2}\tilde{\mathbf{p}} = \mathbf{Z}\beta + \mathbf{n} \qquad \text{[A.2.7]}$$

where **C** is the covariance matrix, $\mathbf{C} = \mathbf{C}^{1/2}\left(\mathbf{C}^{1/2}\right)^{\mathrm{T}}$, $\mathbf{Z} = \left[\mathbf{C}^{-1/2}\mathbf{X}\right]$, $\boldsymbol{\beta} = [\mathrm{h}]$, and $\mathbf{A} = [1]$. Then:

$$\left[\mathbf{A}\left(\mathbf{Z}^{\mathrm{T}}\mathbf{Z}\right)^{-1}\mathbf{A}^{\mathrm{T}}\right]^{1} = \left(\mathbf{C}^{-1/2}\mathbf{X}\right)^{\mathrm{T}}\mathbf{C}^{-1/2}\mathbf{X} \qquad \text{[A.2.8]}$$

The square root of A.2.8 produces η for the third case of the GLM:

$$\eta = \sqrt{\mathbf{X}^{\mathrm{T}}\mathbf{C}^{-1}\mathbf{X}} \qquad \text{[A.2.9]}$$

In the fourth case of the GLM, where both nuisance terms and correlated noise are accounted for, the pre-whitened GLM in Equation A.2.7 is used where $\mathbf{Z} = \left[\mathbf{C}^{-1/2}\mathbf{X} \quad \mathbf{C}^{-1/2}\mathbf{S}\right]$, $\boldsymbol{\beta} = \left[\mathrm{h}^{\mathrm{T}} \quad \mathbf{d}^{\mathrm{T}}\right]$, $\mathbf{A} = \left[1 \quad \mathbf{0}\right]$, and **0** is a $1 \times l$ row vector of zeros. To find η for this case, we first compute:

$$\mathbf{Z}^{\mathrm{T}}\mathbf{Z} = \begin{bmatrix}\left(\mathbf{C}^{-1/2}\mathbf{X}\right)^{\mathrm{T}} \\ \left(\mathbf{C}^{-1/2}\mathbf{S}\right)^{\mathrm{T}}\end{bmatrix}\left[\mathbf{C}^{-1/2}\mathbf{X} \quad \mathbf{C}^{-1/2}\mathbf{S}\right] = \begin{bmatrix}\mathbf{X}^{\mathrm{T}}\mathbf{C}^{-1}\mathbf{X} & \mathbf{X}^{\mathrm{T}}\mathbf{C}^{-1}\mathbf{S} \\ \mathbf{S}^{\mathrm{T}}\mathbf{C}^{-1}\mathbf{X} & \mathbf{S}^{\mathrm{T}}\mathbf{C}^{-1}\mathbf{S}\end{bmatrix} \qquad \text{[A.2.10]}$$

As before, we take the inverse of the upper left-hand element:

$$\left(\mathbf{Z}^{\mathrm{T}}\mathbf{Z}\right)^{-1} = \begin{bmatrix} \left(\mathbf{X}^{\mathrm{T}}\mathbf{C}^{-1}\mathbf{X} - \mathbf{X}^{\mathrm{T}}\mathbf{C}^{-1}\mathbf{S}\left(\mathbf{S}^{\mathrm{T}}\mathbf{C}^{-1}\mathbf{S}\right)^{-1}\mathbf{S}^{\mathrm{T}}\mathbf{C}^{-1}\mathbf{X}\right)^{-1} & \cdots \\ \cdots & \cdots \end{bmatrix} \qquad \text{[A.2.11]}$$

Taking the calculation of η one step further produces:

$$\begin{aligned} \left[\mathbf{A}\left(\mathbf{Z}^{\mathrm{T}}\mathbf{Z}\right)^{-1}\mathbf{A}^{\mathrm{T}}\right]^{1} &= \mathbf{X}^{\mathrm{T}}\mathbf{C}^{-1}\mathbf{X} - \mathbf{X}^{\mathrm{T}}\left(\mathbf{C}^{-1/2}\right)^{\mathrm{T}}\mathbf{C}^{-1/2}\mathbf{S}\left(\mathbf{S}^{\mathrm{T}}\mathbf{C}^{-1}\mathbf{S}\right)^{-1}\mathbf{S}^{\mathrm{T}}\left(\mathbf{C}^{-1/2}\right)^{\mathrm{T}}\mathbf{C}^{-1/2}\mathbf{X} \\ &= \mathbf{X}^{\mathrm{T}}\left(\mathbf{C}^{-1} - \mathbf{C}^{-1}\mathbf{S}\left(\mathbf{S}^{\mathrm{T}}\mathbf{C}^{-1}\mathbf{S}\right)^{-1}\mathbf{S}^{\mathrm{T}}\mathbf{C}^{-1}\right)\mathbf{X} \end{aligned} \qquad \text{[A.2.12]}$$

To reduce this expression, we derive the formula for the projection onto the pre-whitened nuisance subspace ($\mathbf{P}_{\tilde{\mathbf{S}}}$), where the pre-whitened nuisance subspace is $\tilde{\mathbf{S}} = \mathbf{C}^{-1/2}\mathbf{S}$. From the definition of the projection matrix:

$$\begin{aligned} \mathbf{P}_{\tilde{\mathbf{S}}} &= \tilde{\mathbf{S}}\left(\tilde{\mathbf{S}}^{\mathrm{T}}\tilde{\mathbf{S}}\right)^{-1}\tilde{\mathbf{S}}^{\mathrm{T}} \\ &= \mathbf{C}^{-1/2}\mathbf{S}\left(\left(\mathbf{C}^{-1/2}\mathbf{S}\right)^{\mathrm{T}}\mathbf{C}^{-1/2}\mathbf{S}\right)^{-1}\left(\mathbf{C}^{-1/2}\mathbf{S}\right)^{\mathrm{T}} \\ &= \mathbf{C}^{-1/2}\mathbf{S}\left(\mathbf{S}^{\mathrm{T}}\mathbf{C}^{-1}\mathbf{S}\right)^{-1}\mathbf{S}^{\mathrm{T}}\left(\mathbf{C}^{-1/2}\right)^{\mathrm{T}} \end{aligned} \qquad \text{[A.2.13]}$$

Combining this with Equation A.2.12 produces:

$$\begin{aligned} \left[\mathbf{A}\left(\mathbf{Z}^{\mathrm{T}}\mathbf{Z}\right)^{-1}\mathbf{A}^{\mathrm{T}}\right]^{1} &= \mathbf{X}^{\mathrm{T}}\left(\mathbf{C}^{-1} - \left(\mathbf{C}^{-1/2}\right)^{\mathrm{T}}\mathbf{P}_{\tilde{\mathbf{S}}}\mathbf{C}^{-1/2}\right)\mathbf{X} \\ &= \mathbf{X}^{\mathrm{T}}\left(\mathbf{C}^{-1/2}\right)^{\mathrm{T}}\left(\mathbf{I} - \mathbf{P}_{\tilde{\mathbf{S}}}\right)\mathbf{C}^{-1/2}\mathbf{X} \end{aligned} \qquad \text{[A.2.14]}$$

Therefore, for the fourth case of the GLM, which includes nuisance terms and accounts for correlated noise, the formula for η is:

$$\eta = \sqrt{\mathbf{X}^{\mathrm{T}}\left(\mathbf{C}^{-1/2}\right)^{\mathrm{T}}\left(\mathbf{I} - \mathbf{P}_{\tilde{\mathbf{S}}}\right)\mathbf{C}^{-1/2}\mathbf{X}}\,. \qquad \text{[A.2.15]}$$

Comparison of Equation A.2.15 to Equations A.2.6 and A.2.9 emphasizes the contributions of nuisance terms and pre-whitening, respectively, to η.

Also, η may be computed without use of the **A** matrix by recognizing that η is the energy of the model function of interest. In the fourth case of the GLM, which

accounts for correlated noise and includes nuisance terms, the model function of interest is a pre-whitened reference function with pre-whitened nuisance components removed:

$$\mathbf{C}^{-1/2}\mathbf{X} - \mathbf{P}_{\mathbf{S}}\mathbf{C}^{-1/2}\mathbf{X} = \left(\mathbf{1} - \mathbf{P}_{\mathbf{S}}\right)\mathbf{C}^{-1/2}\mathbf{X} \qquad \text{[A.2.16]}$$

Then, η is computed by taking the norm of Equation A.2.16. Note that the norm of A.2.16 is equivalent to A.2.15, so this method provides another interpretation of A.2.15.

The fourth case of the GLM is a representative model of typical functional magnetic resonance imaging data. In this case, Equations A.2.1 and A.2.15 indicate that, on a first order, $\sqrt{F}$ is directly proportional to the contrast-to-noise ratio $\left(\hat{h}/\hat{\sigma}_n\right)$. In support of this, Figure 1.6 shows scatter plots of the per voxel (a) $\sqrt{F_{CBF}}$ (y-axis) versus $\hat{h}_{CBF}/\hat{\sigma}_{n,CBF}$ (x-axis) and (b) $\sqrt{F_{BOLD}}$ (y-axis) versus $\hat{h}_{BOLD}/\hat{\sigma}_{n,BOLD}$ (x-axis) for Subject 1. $\sqrt{F_{CBF}}$ was significantly correlated to $\hat{h}_{CBF}/\hat{\sigma}_{n,CBF}$ ($r = 0.98$, $p < 0.001$), and $\sqrt{F_{BOLD}}$ was significantly correlated to $\hat{h}_{BOLD}/\hat{\sigma}_{n,BOLD}$ ($r = 0.97$, $p < 0.001$). These results indicate that inter-voxel differences in the covariance matrix and space spanned by the physiological noise regressors have a minimal effect on the relationship between $\sqrt{F}$ and $\left(\hat{h}/\hat{\sigma}_n\right)$. Results for other subjects were similar and are not shown.

Acknowledgements

This work was supported in part by a grant from the National Institutes of Health (ROINS051661). The authors thank Joanna Perthen, Richard Buxton, and

Amy Lansing for their assistance and for kindly sharing the experimental data used for this study.

Chapter 1, in full, is a reprint of the material as it appears in Neuroimage 2008. Liau, Joy; Perthen Joanna E.; Liu Thomas T. The dissertation author was the primary investigator and author of this paper.

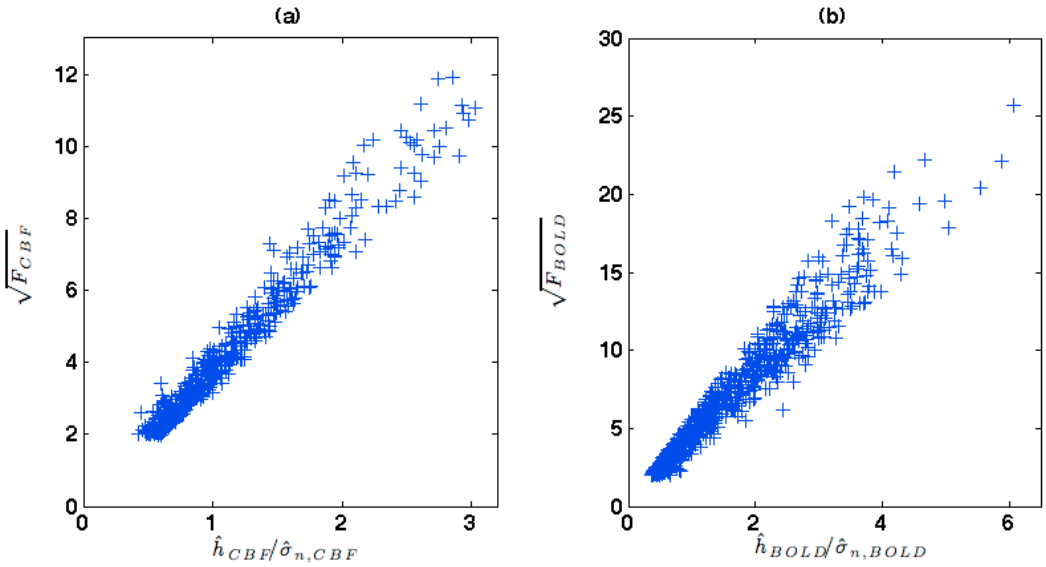

Figure 1.6: Scatter plots of per voxel (a) $\sqrt{F_{CBF}}$ versus $\hat{h}_{CBF}/\hat{\sigma}_{n,CBF}$ (r=0.98, p<0.001) and (b) $\sqrt{F_{BOLD}}$ versus $\hat{h}_{BOLD}/\hat{\sigma}_{n,BOLD}$ (r=0.97, p<0.001) for Subject 1.

CHAPTER 2:

INTER-SUBJECT VARIABILITY IN HYPERCAPNIC NORMALIZATION OF THE BOLD FMRI RESPONSE

2.1 ABSTRACT

In the application of hypercapnic normalization to functional magnetic resonance imaging (fMRI) studies, the blood oxygenation level dependent (BOLD) response to a functional stimulus is typically divided by the BOLD response to a hypercapnic challenge. While some prior studies have shown that hypercapnic normalization can reduce inter-subject BOLD variability, other studies have found an increase in inter-subject variability. In this study we used measures of baseline cerebral blood flow (CBF) and the functional BOLD and CBF responses to both visual stimuli and hypercapnia to assess the effect of hypercapnic normalization on inter-subject variability. We found that the functional and hypercapnic BOLD and CBF responses all exhibited a significant inverse dependence on baseline CBF. In contrast, the maximum BOLD response was independent of baseline CBF and was not a major source of inter-subject BOLD variability. Division of the functional BOLD response by the hypercapnic BOLD response increased inter-subject variability in the normalized responses as compared to the original responses, reflecting the presence of a systematic bias term that was inversely dependent on the hypercapnic BOLD response. This systematic bias resulted from a positive intercept term in the linear relationship between the functional and hypercapnic BOLD responses. This positive intercept term reflected a steeper inverse dependence of the hypercapnic CBF response on baseline CBF, as compared to the functional CBF response. In contrast to the results obtained with normalization based on division, normalized responses obtained by using the hypercapnic BOLD response as a covariate were unaffected by the

systematic bias and exhibited reduced inter-subject variability. The findings of this study indicate that the positive intercept in the linear relationship between functional and hypercapnic BOLD responses should be carefully considered in the hypercapnic normalization of BOLD fMRI data.

2.2 INTRODUCTION

Over the past decade, blood oxygenation level dependent (BOLD) functional MRI (fMRI) has become a powerful tool for non-invasive studies of the working human brain. Although the BOLD signal is widely regarded as a measure of neural activity, it reflects changes in a number of physiological variables, namely cerebral blood volume (CBV), cerebral blood flow, and cerebral oxygen metabolism (Buxton 2002). As a result, differences in factors unrelated to neural activity, such as vascular reactivity or hematocrit levels, can lead to significant variability in the BOLD response (D'Esposito et al. 2003; Gustard et al. 2003; Handwerker et al. 2007). The increased variability due to these factors can reduce the statistical power of fMRI studies, necessitating larger sample sizes with accompanying increased cost. Therefore, a method that reduces BOLD inter-subject variability due to non-neural factors would be of great use.

Hypercapnic normalization refers to the division of the functional BOLD response by the BOLD response to mild hypercapnia in each voxel, where hypercapnia is induced by either the administration of carbon dioxide or a voluntary breathhold (Bandettini and Wong 1997). It is generally assumed that the mild hypercapnic stimuli has a minimal effect on neural activity and oxygen metabolism (Jones et al. 2005; Sicard and Duong 2005; Zappe et al. 2008), so that the hypercapnic BOLD response primarily reflects changes in cerebral blood flow, as well as other factors such as magnetic field strength and baseline cerebral blood volume. As these non-neural factors are either similar or identical for the functional and hypercapnic

BOLD responses, division of the two responses can reduce the variability due to these factors. (Bandettini and Wong 1997) first used hypercapnic normalization to reduce BOLD variability associated with differences in resting cerebral blood volume across the brain. (Cohen et al. 2004) performed a similar procedure using subjects scanned with several protocols (i.e. different pulse sequences and magnetic field strengths) and found that hypercapnic normalization reduced the sensitivity to different scan protocols and magnetic field strengths. However, the results of that study showed that hypercapnic normalization increased inter-subject variability of the BOLD responses. In a study of aging, (Handwerker et al. 2007) demonstrated that hypercapnic normalization of a visuomotor saccade task by a breath-hold task removed significant age-related differences in two brain regions (frontal and supplementary eye fields). These reductions in inter-group differences were accompanied by increased inter-subject variability in the older subject group. In contrast, two recent studies have reported a decrease in inter-subject variability after hypercapnic normalization using a breath-hold challenge that was applied to the functional responses to a working memory task (Thomason et al. 2007) and a motor task (Biswal et al. 2007). The mixed results of these prior studies indicate the need for a better understanding of hypercapnic normalization's effect on inter-subject variability.

In this paper, we use measures of the baseline CBF and the BOLD and CBF responses to both visual stimulus and hypercapnia to better understand the effect of hypercapnic normalization on inter-subject variability. We show that division of the functional BOLD response by the hypercapnic BOLD response can lead to a systematic bias that increases inter-subject variability. The systematic bias results

from a positive intercept in the linear relationship between the functional and hypercapnic BOLD responses. We then use a mathematical model of the BOLD signal in combination with the measured CBF responses to show how this positive intercept term depends on the relation between the functional and hypercapnic CBF responses. In addition, we demonstrate that use of the hypercapnic BOLD response as a covariate for the functional BOLD response can generate normalized responses without systematic bias and with reduced inter-subject variability.

2.3 THEORY

In this section, we first show that the presence of a non-zero intercept in the linear relation between the functional and hypercapnic BOLD responses results in a systematic bias term in the normalized responses. We then show that normalized responses computed by division on a per-voxel basis or on a per-subject basis are similar. We conclude by using a BOLD signal model to determine the physical meaning of the normalized responses.

The Intercept in the Relation Between Functional and Hypercapnic BOLD Responses Results in a Systematic Bias Term in the Normalized Responses

Prior studies have noted a linear relation between the average functional BOLD responses B_i and the hypercapnic BOLD responses $B_{H,i}$ observed across a sample of healthy subjects (Handwerker et al. 2007; Thomason et al. 2007) of the form:

$$B_i = A \cdot B_{H,i} + G + E_i \qquad [2.1]$$

where A is the group slope, G is the group intercept, E_i is the residual to the linear fit, and the subscript i indicates the i^{th} subject. Examples of this relation are shown in Figure 2.1 (panels c and d). Normalizing by the subject average hypercapnic responses produces the normalized response for each subject of the form:

$$\hat{B}_i = \frac{B_i}{B_{H,i}} = A + \frac{G}{B_{H,i}} + \frac{E_i}{B_{H,i}} \quad , \qquad [2.2]$$

which is the sum of (a) the slope A between the functional and hypercapnic responses, (b) a systematic bias term $G/B_{H,i}$ that is inversely proportional to $B_{H,i}$, and (c) a residual term $E_i/B_{H,i}$. Note that the bias term $G/B_{H,i}$ represents systematic variability that is not eliminated by the hypercapnic normalization process. Examples of this systematic bias in the normalized response are shown in Figure 2.3 (panels b and f).

Hypercapnic Normalization on a Per-voxel Basis versus a Per-subject Basis

In the previous section, we showed that normalization using the subject average hypercapnic BOLD responses $B_{H,i}$ can result in a systematic bias term $G/B_{H,i}$ in the normalized response $\hat{B}_i$ when the normalization is performed on a per-subject basis. To date, most normalization approaches have divided the functional BOLD response $b_{i,j}$ in each voxel by the corresponding hypercapnic response $b_{H,i,j}$ in that voxel, where the subscripts i and j denote the i^{th} subject and j^{th} voxel, respectively (Bandettini and Wong 1997; Cohen et al. 2004; Biswal et al. 2007; Handwerker et al. 2007; Thomason et al. 2007). Averaging the per-voxel normalized responses $b_{i,j}/b_{H,i,j}$ across a region-of-interest (ROI) yields an average response B_i'' for each subject of the form:

$$B_i'' = \frac{1}{N_i}\sum_{j=1}^{N_i}\frac{b_{i,j}}{b_{H,i,j}} \qquad [2.3]$$

where N_i is the number of voxels in the ROI. In other words, B_i'' represents the average subject response obtained when normalization is performed on a per-voxel

basis prior to averaging over the ROI, while $\hat{B}_i$ in Eqn. 2.2 is the average response obtained when averaging of the functional and hypercapnic responses over the ROI is performed prior to normalization, which is then done a per-subject basis.

To determine the relation between the two types of normalized responses ($\hat{B}_i$ and B_i''), we make use of the linear relationship between $b_{i,j}$ and $b_{H,i,j}$ that has been demonstrated in previous studies (Bandettini and Wong 1997; Cohen et al. 2004; Biswal et al. 2007; Handwerker et al. 2007; Thomason et al. 2007). The relation has the form:

$$b_{i,j} = a_i \cdot b_{H,i,j} + g_i + e_{i,j} \qquad [2.4]$$

where a_i is the subject slope, g_i is the subject intercept, and $e_{i,j}$ is the residual to the linear fit. Examples of this relation are shown in Figure 2.1 (panels a and b). We show in Appendix B.1 that the linear relation in Eqn. 2.4 yields the following relation between B_i'' and $\hat{B}_i$:

$$B_i'' = \hat{B}_i + g_i\left(\frac{1}{N_i}\sum_{j=1}^{N_i}\frac{1}{b_{H,i,j}} - \left(\frac{1}{N_i}\sum_{j=1}^{N_i} b_{H,i,j}\right)^{-1}\right) \qquad [2.5]$$

The two normalized responses differ only by the subject dependent term $g_i\left(\frac{1}{N_i}\sum_{j=1}^{N_i}\frac{1}{b_{H,i,j}} - \left(\frac{1}{N_i}\sum_{j=1}^{N_i} b_{H,i,j}\right)^{-1}\right)$. We find empirically that this subject dependent term is positive and is about 25% of the average per-voxel normalized response B'' and 33% of the average per-subject normalized response $\hat{B}$ as shown in the Results and Figure 2.2. This reflects the empirical findings that the intercept g_i is approximately equal to 1 across subjects and the difference between the two summation terms is positive and

less than one, where $\frac{1}{N_i}\sum_{j=1}^{N_i}\frac{1}{b_{H,i,j}}$ is about twice as large as $\left(\frac{1}{N_i}\sum_{j=1}^{N_i}b_{H,i,j}\right)^{-1}$ (See also Results). For the remaining theoretical development, we will adopt the subject average form $\hat{B}_i$ because its usage simplifies the presentation for studies of inter-subject variability. Note however, that as expected from Eqn. 2.5, the experimental results obtained using both forms are similar, as shown in Figures 2.2 and 2.3 of the Results section.

Physical Meanings of Normalized Response Components

As shown in Eqn. 2.2, the presence of a non-zero intercept term *G* gives rise to a systematic bias term $G/B_{H,i}$. In this section, we use the BOLD signal model introduced by (Davis et al. 1998) to show that the intercept term *G* depends on the relation between the functional and hypercapnic CBF responses. We also show that the empirically observed linear relation between B_i and $B_{H,i}$ (Eqn. 2.1) is consistent with the Davis Model. The Davis Model can be written as:

$$B_i = M_i\left(1-\left(\frac{F_i}{100}+1\right)^{\alpha-\beta}\left(\frac{m_i}{100}+1\right)^{\beta}\right) \qquad [2.6]$$

where $M_i = TE\cdot P_i\cdot CBV_{0,i}\cdot\left[dHb_i\right]_{v_0}^{\beta}$ is the maximum attainable percent BOLD response, *TE* is the echo time, P_i is a scan dependent scaling term, $CBV_{0,i}$ is the resting cerebral blood volume, and $\left[dHb_i\right]_{v_0}$ is the venous deoxyhemoglobin concentration. In addition, F_i is the percent CBF response to a functional task, m_i is the percent cerebral oxygen metabolism response ($CMRO_2$) to a functional task, α is Grubb's exponent

(Grubb et al. 1974), and β is an exponent that depends primarily on vessel size and magnetic field strength (Davis et al. 1998). With hypercapnia, it is typically assumed that m_i = 0 (Davis et al. 1998; Hoge et al. 1999), so that the hypercapnic BOLD response is modeled as:

$$B_{H,i} = M_i\left(1-\left(\frac{F_{H,i}}{100}+1\right)^{\alpha-\beta}\right) \qquad [2.7]$$

where the subscript *H* denotes the hypercapnic condition. From Eqns. 2.6 and 2.7, we can see that the relation between B_i and $B_{H,i}$ will depend on the relation between the functional and hypercapnic CBF responses, F_i and $F_{H,i}$, and also the coupling between F_i and m_i.

To proceed, we make use of the following experimental observations obtained for a sample of healthy young subjects (see Results and Figures 2.4 and 2.5): 1) the maximum BOLD response M_i is relatively constant across subjects, 2) the CBF/$CMRO_2$ coupling ratio $n = F_i/m_i$ is relatively constant across subjects, and 3) the functional CBF response F_i is linearly related to the hypercapnic CBF response $F_{H,i}$, that is $F_i = c_1 \cdot F_{H,i} + c_2$, where c_1 is the group slope and c_2 is the group intercept. Combining these observations with Eqns. 2.6 and 2.7, we show in Appendix B.2 that the intercept term in the Eqn. 2.2 is given by:

$$G = M\left(1-\left(\frac{c_2}{100}+1\right)^{\alpha-\beta}\left(\frac{c_2}{n\cdot 100}+1\right)^{\beta}\right) \qquad [2.8]$$

and the slope is:

$$A = \frac{\left(\frac{c_2}{100}+1\right)^{\alpha-\beta}\left(\frac{c_2}{n\cdot 100}+1\right)^{\beta} - \left(\frac{c_1\cdot F_{HM}+c_2}{100}+1\right)^{\alpha-\beta}\left(\frac{c_1\cdot F_{HM}+c_2}{n\cdot 100}+1\right)^{\beta}}{1-\left(\frac{F_{HM}}{100}+1\right)^{\alpha-\beta}} \qquad [2.9]$$

where F_{HM} is the maximum hypercapnic CBF response observed across the group. As shown in Appendix B.2 and Figure 2.6, the nonlinear relation between B_i and $B_{H,i}$ is fairly well approximated by a linear relation (Eqn. 2.1) with intercept G and approximate slope A as defined in Eqns 2.8 and 2.9.

From Eqn. 2.8, we can see that the intercept G is non-zero whenever c_2 is not equal to zero. In other words, a non-zero intercept G in the B_i vs. $B_{H,i}$ relation reflects the presence of a non-zero intercept in the F_i vs. $F_{H,i}$ relation (see Discussion section).

2.4 METHODS

Experimental Protocol

Data presented here were also used for separate analyses examining a caffeine dose's effect on metabolism (Perthen et al. 2008) and functional activation extents (Liau et al. 2008), and the experimental protocol is repeated here for convenience. Ten healthy adult subjects (5 males, mean age 33±7 years) participated in the study after giving informed consent. During each imaging session, subjects were presented with a stimulus consisting of "on" periods of an 8Hz full-field, full-contrast flashing checkerboard pattern with a small white square in the center. Inside the square, the numbers (2-4-3-5) appeared sequentially at 2Hz. The "off" periods were of equal luminance to the on periods and consisted of a gray background with a white square in the middle. Subjects were instructed to fixate on the white square at all times and press buttons on a 4-button response box with their right hand in accordance to the numbers. The flashing checkerboard was intended to activate the visual cortex while the motor task maintained subject attention. Each session consisted of the following arterial spin labeling (ASL) scans: 1) a resting-state scan (8 min 20 s off), 2) two block design functional scans (60 s off, 4 x (20 s on/60 s off), 30 s off), and 3) two hypercapnia scans where subjects inhaled a 5% CO_2 gas mixture through a non-rebreathing face mask (off condition for the scan; 2 min room air, 3 min 5% CO_2, 2 min room air). A high-resolution anatomical scan was collected at the beginning of each session, and CBF calibration scans were acquired after the resting-state scan. Data were also acquired using the same protocol without the hypercapnia runs after

subjects ingested a caffeine dose. These data were collected for related studies (Liau et al. 2008; Perthen et al. 2008) and are not included here.

Imaging Protocol

Imaging data were acquired on a GE Signa Excite 3 Tesla whole body system with a body transmit coil and an eight channel receive head coil. The ASL scans were acquired with a PICORE QUIPSS II (Wong et al. 1998) ASL sequence (TR=2.5 s, TI1/TI2=600/1500 ms) with a spiral readout (TE1/TE2=2.9/24ms, FOV=24cm, 64x64 matrix, 90^{o} flip angle). Six oblique axial 5-mm slices were prescribed about the calcarine sulcus for all ASL scans.

The calibration scans for CBF quantification used the same in-plane parameters as the ASL scans, but the number of slices was increased to ensure coverage of the lateral ventricles. The calibration scans consisted of a CSF reference scan acquired at full relaxation (TE=2.9 ms) and a minimum contrast scan (TR=2 s, TE=11 ms). The high-resolution anatomical scan was acquired with a magnetization prepared 3D fast spoiled gradient echo (FSPGR) sequence (TI=450ms, TR=7.9ms, TE=3.1 ms, 12^{o} flip angle, FOV 25 cm, matrix 256x256x256).

Cardiac pulse and respiratory effort data were monitored using a pulse oximeter (InVivo) and a respiratory effort transducer (BIOPAC), respectively. The pulse oximeter was placed on the subject's left index finger, and the respiratory effort belt was placed around the subject's abdomen. Physiological data were sampled at 40 samples per second using a multi-channel data acquisition board (National Instruments).

Data Preprocessing and General Linear Model Analyses

All images were coregistered using AFNI software (Cox 1996). Data from the first 10 s of each ASL scan were discarded to allow magnetization to reach a steady state.

General linear model (GLM) analyses were used to determine the statistical significance of the responses. Pre-whitening was performed using an autoregressive AR(1) model (Woolrich et al. 2001). Data from the two functional runs were concatenated, measured cardiac and respiratory data were included as regressors, and a reference function based on the block design task was used in an unfiltered GLM (Mumford et al. 2006; Restom et al. 2006). GLM analysis of the first echo data produced p-value maps indicating the statistical significance of the functional CBF response, and analysis of the second echo data produced statistical maps of the functional BOLD response. This process was repeated with the first echo hypercapnia data and a reference function based on the CO_2 administration to produce p-value maps of the hypercapnic CBF response. Also, analysis of the second echo hypercapnia data produced statistical maps of the hypercapnic BOLD response.

For each subject, a mean ASL image was formed from the average difference of the control and tag images from the first echo of the ASL resting-state scan data (Liu and Wong 2005). This mean ASL image was corrected for coil inhomogeneities using the minimum contrast image (Wang et al. 2005) and converted to physiological units using the CSF image as a reference signal (Chalela et al. 2000) to produce per-voxel baseline CBF values.

Regions-of-Interest Definitions

Two regions-of-interest (ROIs) were used for data analyses: 1) a BOLD ROI based on functional and hypercapnic BOLD activation, and 2) a BOLD+CBF ROI that had additional inclusion criteria based on functional and hypercapnic CBF activation. As analyses using the Davis Model require reliable CBF and BOLD measures, these analyses used the BOLD+CBF ROI. The BOLD ROI was formed by the intersection of: 1) voxels containing significant functional BOLD responses ($p<0.01$), 2) voxels containing significant hypercapnic BOLD responses ($p<0.01$), and 3) a visual cortex anatomical mask defined as the posterior third of the brain to include visual areas while excluding motor areas. The BOLD+CBF ROI was formed by the intersection of: 1) the BOLD ROI, 2) voxels containing significant functional CBF responses ($p<0.01$), and 3) voxels containing significant hypercapnic CBF responses ($p<0.01$).

Functional and Hypercapnic Response Amplitudes

To reduce sensitivity to functional changes in cerebral blood volume, we used BOLD measurements based on the transverse relaxation rate R_2^* (Woolrich et al. 2006). After removal of physiological noise components and linear trends, the running average of the first and second echoes of the functional runs were taken to produce dual-echo functional BOLD data (Liu and Wong 2005). The dual-echo functional BOLD data were converted to R_2^* measurements by $R_2^* = \ln(S_1/S_2)/\Delta TE$, where S_1 and S_2 are the data from the first and second echoes, respectively, and (ΔTE=21.1ms) is the difference in the echo times. The R_2^* measurements were then

converted to R_2^* functional BOLD data by $e^{-TE_2 \cdot R_2^*}$, where (TE_2=24ms) is the second echo time used in this study. This process was repeated with the dual-echo hypercapnia BOLD data to form R_2^* hypercapnia BOLD data.

For computation of the functional response amplitudes, block design cycles with excessive head motion (evaluated by AFNI 3dvolreg (Cox 1996), rotation velocity>0.05deg/s, translation velocity>0.2mm/s) were excluded. The functional response amplitude was then defined as the percent increase of the response, using the mean signal from both runs in the active state (last 10 s of each on condition) and the mean signal from both runs in the baseline state (initial off condition). The per-voxel functional BOLD response amplitudes b were computed from the R_2^* functional BOLD data for each voxel, and the per-subject functional BOLD response amplitudes B were computed from the R_2^* functional BOLD data averaged over voxels in each ROI. The per-subject functional CBF response amplitudes F were computed from the first echo functional data after taking the running difference (Liu and Wong 2005) and averaging over voxels in each ROI.

For computation of the hypercapnic response amplitudes, data were averaged over runs, and the hypercapnic response amplitude was defined as the percent increase of the response, using the mean signal in the active state (last 1.5 min of the 5% CO_2 condition) and the mean signal in the baseline state (first air condition and last 30 s of the second air condition). The per-voxel hypercapnic BOLD response amplitudes b_H were computed from the per-voxel R_2^* hypercapnic BOLD data averaged over runs, and the per-subject hypercapnic BOLD response amplitudes B_H were computed from

the R_2^* hypercapnic BOLD data averaged over runs and voxels in each ROI. The per-subject hypercapnic CBF response amplitudes F_H were computed from the first echo hypercapnic data after taking the running difference (Liu and Wong 2005) and averaging over runs and voxels in each ROI.

Hypercapnic Normalization

For each ROI, we used two methods of normalization by division: 1) normalization on a per-voxel basis for comparison with prior work (Bandettini and Wong 1997; Cohen et al. 2004; Biswal et al. 2007; Handwerker et al. 2007; Thomason et al. 2007), and 2) normalization on a per-subject basis to facilitate the study of inter-subject variability (see Theory section). In the first method, the functional BOLD response b for each voxel was divided by the corresponding hypercapnic BOLD response b_H, and the normalized responses were averaged over each ROI to produce a per-voxel normalized response B'' for each subject (Eqn. 2.3). In the second method, the average BOLD response B for each subject was divided by the corresponding average hypercapnic BOLD response B_H to produce a per-subject normalized response $\hat{B}$ for each subject (Eqn. 2.2). As an alternative to normalization by division, we also used B_H as a covariate for B across subjects, where removal of linear trends in B explained by B_H produced per-subject covariate normalized responses $\hat{B}_{\text{cov}}$.

Davis Model and Baseline CBF Calculations

The Davis model signal components of the functional BOLD response were estimated using data from the BOLD+CBF ROI. The per-subject percent maximum

BOLD responses M were computed from B_H and F_H using Eqn. 2.7 and parameter values of α=0.38 (Grubb et al. 1974) and β=1.5 (Davis et al. 1998). The per-subject percent cerebral oxygen metabolism responses m were then computed from M, B, and F (Eqn. 2.6). Also, the per-voxel baseline CBF values were averaged over voxels in the BOLD+CBF ROI to produce the per-subject baseline CBF values.

Statistical Tests

Relations between measured values were assessed by correlation analyses, two-tailed paired t-tests, two-tailed one-sample t-tests, and linear fits. For example, the relations between B'' and $\hat{B}$ in each ROI were determined by correlation analyses and linear fits. Two-tailed one-sample t-tests were used to assess whether the regression coefficients from the linear fit were significantly different from zero. Also, the means of B'' and $\hat{B}$ in each ROI were compared by two-tailed paired t-tests. In addition, measures of the coefficient of variation of the functional and normalized responses ($B, \hat{B}, B'', \hat{B}_{\mathrm{cov}}$) were computed by dividing the standard deviation of each response by its mean.

2.5 RESULTS

The top row of Figure 2.1 shows scatter plots of the per-voxel functional BOLD responses b versus the hypercapnic BOLD responses b_H in the BOLD ROI (left column) and BOLD+CBF ROI (right column) for a representative subject. The green lines indicate linear fits. Consistent with prior work (Bandettini and Wong 1997; Cohen et al. 2004; Biswal et al. 2007; Handwerker et al. 2007; Thomason et al. 2007), significant correlations between the per-voxel functional and hypercapnic BOLD responses were found in each ROI for this representative subject (BOLD: r=0.68, p<0.001; BOLD+CBF: r=0.69, p<0.001). In addition, these correlations were found to be positive and significant for all subjects in the BOLD ROI (p<0.001) and for eight out of ten subjects in the BOLD+CBF ROI (p<0.008), with positive (but not significant) correlations for the remaining two subjects (r=0.31, p=0.087; r=0.22, p=0.352) for this ROI.

Consistent with a previous study (Handwerker et al. 2007), the linear relationships between the per-voxel functional BOLD responses b and hypercapnic BOLD responses b_H had significant positive intercepts g in each ROI (BOLD: g=0.62, t=9.04, p<0.001; BOLD+CBF: g=0.46, t=3.97, p<0.001) and significant positive slopes a in each ROI (BOLD: a=0.52, t=16.71, p<0.001; BOLD+CBF: a=0.74, t=7.02, p<0.001) for the representative subject. When examined across the study group, the intercepts g and slopes a were positive in both the BOLD ROI ($\bar{g}$=1.07±0.68, t=4.94, p<0.001; $\bar{a}$=0.21±0.13, t=5.13, p<0.001) and in the BOLD+CBF ROI ($\bar{g}$=0.95±0.35, t=8.57, p<0.001; $\bar{a}$=0.25±0.19, t=4.10, p=0.003). In the Theory section and Appendix

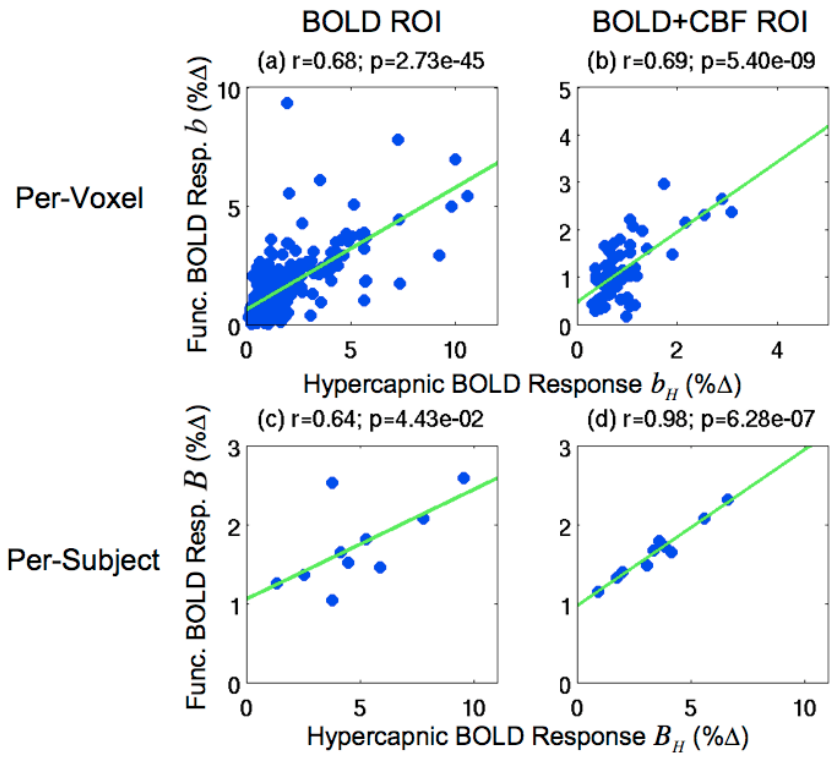

Figure 2.1: Scatter plots of the per-voxel functional BOLD responses b versus the hypercapnic BOLD responses b_H in Subject 1 (top row) and the per-subject functional BOLD responses B versus hypercapnic BOLD responses B_H (bottom row). Responses are from the BOLD ROI (left column) and the BOLD+CBF ROI (right column). Green lines indicate linear fits.

B.1, we make use of the fact that the mean intercept g is approximately equal to 1 in establishing the relationship between the per-subject normalized responses $\hat{B}$ and the per-voxel normalized responses B''.

In the Theory section, we showed that a non-zero intercept G results in a systematic bias G/B_H in the normalized responses. Here, we test for the presence of a non-zero intercept G in our data. The bottom row of Figure 2.1 shows the per-subject functional BOLD responses B versus hypercapnic BOLD responses B_H in the BOLD ROI (left column) and BOLD+CBF ROI (right column) for all subjects. In agreement with (Handwerker et al. 2007; Thomason et al. 2007), we found a significant linear relationship between the functional and hypercapnic BOLD responses in each ROI (BOLD: r=0.64, p=0.044; BOLD+CBF: r=0.98, p<0.001). Also consistent with (Handwerker et al. 2007; Thomason et al. 2007), we found significant positive intercepts G and slopes A in the linear relationship between the functional BOLD responses B and the hypercapnic BOLD responses B_H in the BOLD ROI (G=1.06%, t=3.57, p=0.004; A=0.14, t=2.53, p=0.018) and in the BOLD+CBF ROI (G=0.97%, t=18.87, p<0.001; A=0.20, t=14.94, p<0.001).

While most prior work with hypercapnic normalization have used per-voxel normalized responses B'' (Bandettini and Wong 1997), we based our theoretical development on per-subject normalized responses $\hat{B}$ in order to simplify the mathematical derivations. To demonstrate that the two responses are closely related, Figure 2.2 shows scatter plots of the subject averaged per-voxel normalized responses B'' versus per-subject normalized responses $\hat{B}$ in (a) the BOLD ROI and (b) the BOLD+CBF ROI. Black diagonal lines are lines of equality, and green lines are linear

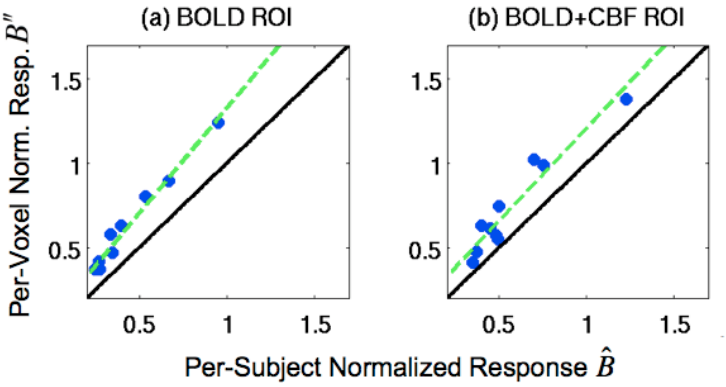

Figure 2.2: Scatter plots of the per-voxel normalized responses B'' versus the per-subject normalized responses $\hat{B}$ in (a) the BOLD ROI and (b) the BOLD+CBF ROI. Black diagonal lines are the lines of equality, and the green lines are linear fits. The location of data points above the lines of equality (black lines) are consistent with the finding that the per-voxel normalized responses B'' were significantly larger than the per-subject normalized responses $\hat{B}$ ($p<0.001$). The significant correlations between the per-voxel normalized responses B'' and the per-subject normalized responses $\hat{B}$ ($p<0.001$) are demonstrated by the overlap of the linear fits (green lines) with the data points.

fits. As shown by the location of data points above the lines of equality (black lines), the per-voxel normalized responses B'' were significantly larger than the per-subject normalized responses $\hat{B}$ in the BOLD ROI ($\overline{B''}$=0.616±0.288, $\overline{\hat{B}}$=0.431±0.228, t=8.02, p<0.001) and in the BOLD+CBF ROI ($\overline{B''}$=0.738±0.303, $\overline{\hat{B}}$=0.572±0.265, t=5.77, p<0.001). We also found significant correlations between the per-voxel normalized responses B'' and the per-subject normalized responses $\hat{B}$ values in each ROI (BOLD: r=0.99, p<0.001; BOLD+CBF: r=0.96, p<0.001).

Figure 2.3 shows scatter plots of functional BOLD responses and normalized responses versus hypercapnic BOLD responses in the BOLD ROI (top row) and BOLD+CBF ROI (bottom row). The first column shows scatter plots of the functional BOLD responses B versus the hypercapnic BOLD responses B_H – these data were also presented in Figure 2.1 and are repeated here for comparison with the normalized results. The remaining columns show scatter plots of the normalized responses (second column: the per-subject normalized responses $\hat{B}$; third column: the per-voxel normalized responses B''; fourth column: the covariate normalized responses B_{cov}) versus the hypercapnic BOLD responses B_H. Green lines indicate linear fits. The per-subject normalized responses $\hat{B}$ had significant negative correlations to the hypercapnic BOLD responses B_H in each ROI (BOLD: r=-0.72, p=0.019; BOLD+CBF: r=-0.83, p=0.003). The per-voxel normalized responses B'' also had significant negative correlations to the hypercapnic BOLD responses B_H in each ROI (BOLD: r=-0.75, p=0.013; BOLD+CBF: r=-0.88, p<0.001). By construction, the covariate normalized responses $\hat{B}_{\text{cov}}$ obtained by projecting out the linear contribution

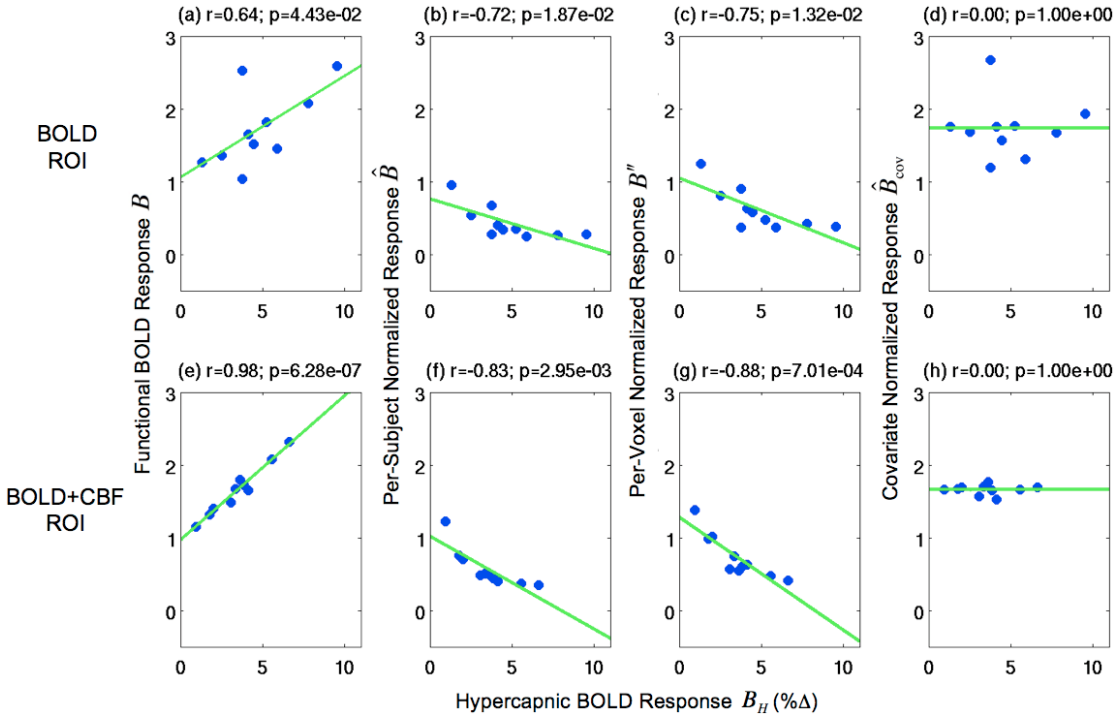

Figure 2.3: Scatter plots of the functional BOLD responses and the normalized responses versus the hypercapnic BOLD responses. The first column shows scatter plots of the functional BOLD responses B vs. the hypercapnic BOLD responses B_H. The remaining columns show scatter plots of the normalized responses ($\hat{B}$, B'', and $\hat{B}_{cov}$) versus the hypercapnic BOLD responses B_H. Second column: the per-subject normalized responses $\hat{B}$. Third column: the per-voxel normalized responses B''. Fourth column: the covariate normalized responses $\hat{B}_{cov}$. Values are shown for the BOLD ROI (top row) and BOLD+CBF ROI (bottom row). Green lines indicate linear fits.

Table 2.1: Coefficient of variation of the functional BOLD responses and the normalized responses in the BOLD ROI and BOLD+CBF ROI.

ROI	Coefficient of variation			
	Functional BOLD responses B	Per-subject normalized responses $\hat{B}$	Per-voxel normalized responses B''	Covariate normalized responses $\hat{B}_{cov}$
BOLD	0.30	0.53	0.47	0.23
BOLD+CBF	0.21	0.46	0.41	0.04

of the hypercapnic BOLD responses B_H were not significantly correlated to the hypercapnic BOLD responses B_H in either ROI (both: r=0.00, p=1.00).

In addition to the lack of correlation between the covariate normalized responses $\hat{B}_{\text{cov}}$ and the hypercapnic BOLD responses B_H, visual comparison of the per-subject values reveals a clear reduction in the inter-subject variability of the covariate normalized responses $\hat{B}_{\text{cov}}$ (fourth column), as compared to the functional BOLD responses B (first column). Visual comparison of the inter-subject variability between the functional BOLD responses B and the normalized responses produced by division ($\hat{B}$ and B'') is less straightforward due to the reduction in mean by division. A quantitative assessment of the inter-subject variability of the functional BOLD responses and the normalized responses is provided in Table 2.1, which lists measures of the coefficient of variation for the functional BOLD responses B, the per-subject normalized responses $\hat{B}$, the per-voxel normalized responses B'', and the covariate normalized responses $\hat{B}_{\text{cov}}$ over the BOLD and BOLD+CBF ROIs. The variability of the per-subject normalized responses $\hat{B}$ was greater than that of the functional BOLD responses B in each ROI (BOLD ROI: +76.7%; BOLD+CBF ROI: +119.1%), as was the variability of the per-voxel normalized responses B'' (BOLD ROI: +56.7%; BOLD+CBF ROI: +95.2%). In contrast, the variability of the covariate normalized responses $\hat{B}_{\text{cov}}$ was smaller than that of the functional BOLD responses B in each ROI (BOLD ROI: -23.3%; BOLD+CBF ROI: -81.0%).

We also assessed whether the baseline CBF was an important source of variability in the BOLD and CBF responses in the BOLD+CBF ROI, where measures

for both responses were obtained. The top row of Figure 2.4 shows the BOLD responses ((a) functional and (b) hypercapnic) versus baseline CBF. Both the functional BOLD responses B (r=-0.68, p=0.031) and the hypercapnic BOLD responses B_H (r=-0.68, p=0.031) exhibited a significant inverse dependence on baseline CBF, indicating that variations in baseline CBF contributed to a large portion of the BOLD response variability. The second row of Figure 2.4 shows the CBF responses ((c) functional and (d) hypercapnic) versus the baseline CBF. Both the functional CBF responses F (r=-0.74, p=0.015) and the hypercapnic CBF responses F_H (r=-0.79, p=0.006) showed a significant inverse dependence on baseline CBF. Although both responses had an inverse dependence, the hypercapnic CBF response F_H was higher than the functional CBF response F at low baseline CBF values and decreased more quickly with increasing baseline CBF.

Further insight into the differences between the functional and hypercapnic CBF can be obtained from the plots in the third row of Figure 2.4, which show (e) the functional CBF responses F versus the hypercapnic CBF responses F_H and (f) the ratio of the functional and hypercapnic CBF responses F/F_H versus the baseline CBF. Consistent with the inverse dependence of both the functional and hypercapnic CBF responses to the baseline CBF, we found that the functional CBF responses F were significantly correlated to the hypercapnic CBF responses F_H (r=0.74, p=0.014). Since the hypercapnic CBF responses F_H decreased more quickly than the functional CBF responses F with increasing baseline CBF, the linear relationship between the two responses had a significant positive slope c_1 (c_1=0.279, t=3.30, p=0.005) and a significant positive intercept c_2 (c_2=36.70%, t=7.80, p<0.001). As discussed in the

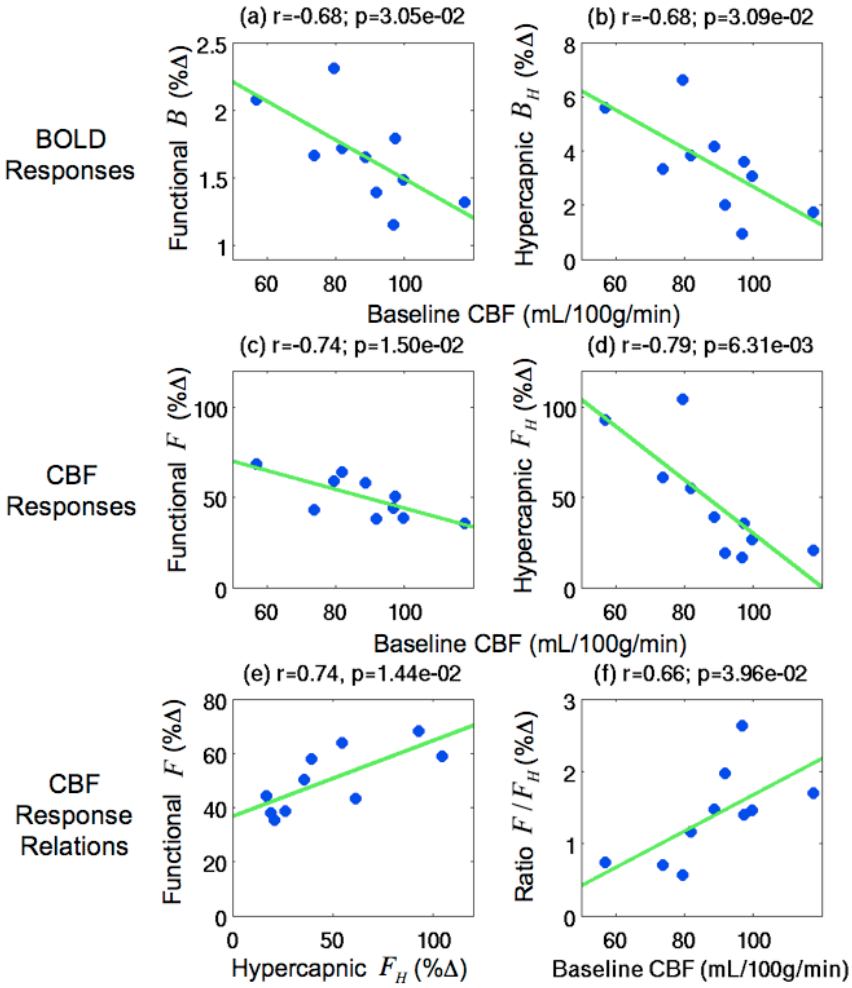

Figure 2.4: Scatter plots showing the dependence of the BOLD and CBF responses on baseline CBF in the BOLD+CBF ROI. Top row: Scatter plots of a) the functional BOLD responses B and (b) the hypercapnic BOLD responses B_H versus baseline CBF. Second row: Scatter plots of (c) the functional CBF responses F and (d) the hypercapnic CBF responses F_H versus baseline CBF. Third row: (e) the functional CBF responses F versus the hypercapnic CBF responses F_H and (f) ratio of the functional and hypercapnic CBF responses F/F_H versus baseline CBF. Green lines indicate linear fits. Baseline CBF values were significantly correlated ($p<0.04$) to the BOLD responses (B and B_H), the CBF responses (F and F_H), and the ratio of the functional and hypercapnic CBF responses F/F_H. Also, the functional CBF responses F were significantly correlated to the hypercapnic CBF responses F_H ($p=0.014$) .

Theory section, the non-zero intercept c_2 in the linear relationship between the functional and hypercapnic CBF responses is predicted to produce a non-zero intercept G in the linear relationship between the functional and hypercapnic BOLD responses (Eqn. 2.8). Consistent with the non-zero intercept c_2 (see Appendix B.2), functional and hypercapnic CBF response ratios F/F_H had a significant positive correlation to the baseline CBF (r=0.66, p=0.040).

In Figure 2.5, we assessed whether the baseline CBF was an important source of variability in the following estimated BOLD model parameters: (a) the cerebral oxygen metabolism ($CMRO_2$) response m, (b) the CBF/$CMRO_2$ coupling ratio n, and (c) the maximum BOLD responses M. The baseline CBF was not significantly correlated to the maximum BOLD response parameter M (r=-0.02, p=0.966), a component of the BOLD signal model for both the functional BOLD responses B and the hypercapnic BOLD responses B_H (Eqns. 2.6 and 2.7). The lack of correlation the maximum BOLD responses M and baseline CBF indicates that M is unlikely to be a major contributor to BOLD inter-subject variability in this study. In addition, baseline CBF was not significantly correlated to either the $CMRO_2$ response m (r=-0.49, p=0.154) or the CBF/$CMRO_2$ coupling ratio n (r=-0.12, p=0.731), which are components of the signal model only for the functional BOLD response B (Eqn. B.2.1). The lack of correlations between either the $CMRO_2$ response m or the CBF/$CMRO_2$ coupling ratio n and the baseline CBF suggests that variations in m nor n were not major contributors to BOLD inter-subject variability in this study. In the theoretical modeling sections of this paper (Theory, Appendix B.2), the lack of significant correlations between baseline CBF and either the maximum BOLD

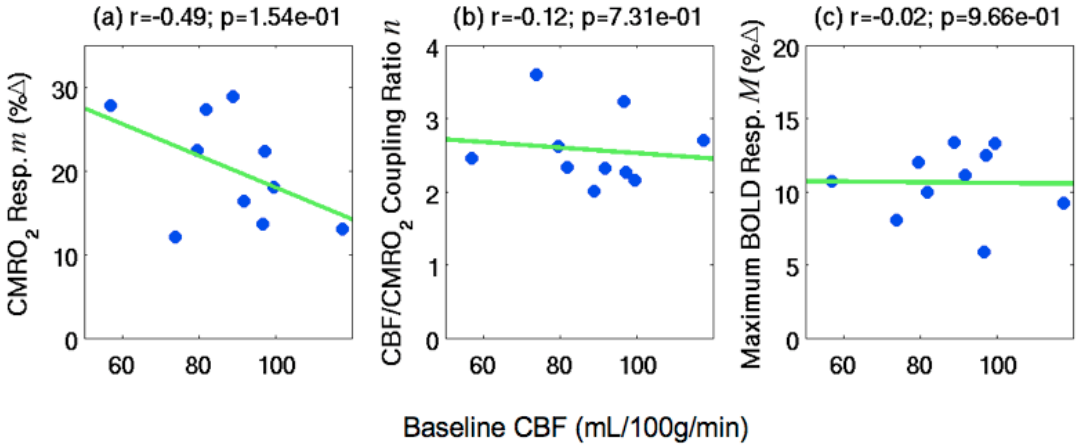

Figure 2.5: Scatter plots of estimated BOLD signal model parameters versus baseline CBF in the BOLD+CBF ROI: (a) the cerebral oxygen metabolism ($CMRO_2$) responses m, (b) the CBF/$CMRO_2$ coupling ratios n, and (c) the maximum BOLD responses M. None of the BOLD model parameters shown were significantly correlated to baseline CBF.

response M or the CBF/$CMRO_2$ coupling ratios n were used in the derivation of the physical meanings of the slope and intercept terms in Eqn. 2.1.

We also tested whether the linear approximations developed in the Theory section and Appendix B.2 provide a good description of the nonlinear relation between the functional and hypercapnic BOLD responses. Panel (a) of Figure 2.6 shows the functional BOLD response B (Eqn. B.2.1) versus the hypercapnic BOLD response B_H (Eqn. 2.7) (solid blue line) computed using the Davis signal model with experimental and published values of the BOLD signal components and the CBF slope c_1 and intercept c_2 parameters described above (see also Methods and Appendix B.2). To assess the sensitivity of the responses, the slope c_1 was increased by 20% (solid red line) or decreased by 20% (solid black line). Panel (b) of Figure 2.6 shows the functional BOLD response B versus the hypercapnic BOLD response B_H (solid blue line, same as (a)), but with the intercept c_2 increased by 20% (solid red line) or decreased by 20% (solid black line). The dashed lines in both panels are the linear approximations, computed using the intercept G (Eqn. 2.8) and slope A (Eqn. 2.9). Linear approximations were used instead of linear fits to provide a straightforward interpretation of the intercept and slope in the linear relationship between the functional and hypercapnic BOLD responses. Although the relations between the functional BOLD response B and the hypercapnic BOLD responses B_H are nonlinear, they are well fit by the linear approximations in the physiological range.

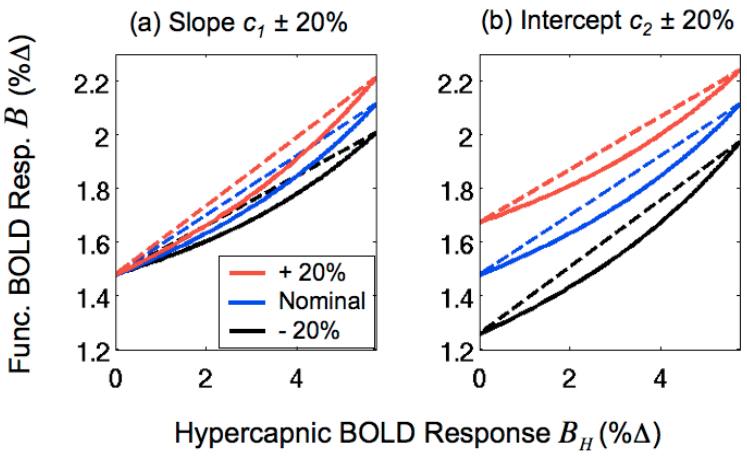

Figure 2.6: Predicted functional BOLD responses B versus hypercapnic BOLD responses B_H. Responses were computed using a BOLD signal model (Eqns. B.2.1 and 2.7) with experimental and published values (solid blue line in both panels). The CBF slope c_1 and intercept c_2 parameter values estimated from the sample were used for the blue lines. In panel (a), the slope c_1 was increased or decreased by 20% for the solid red and black lines, respectively. In panel (b) the intercept c_2 was increased or decreased by 20% for the solid red and black lines, respectively. Dashed lines are linear approximations of the solid lines obtained using the intercept and slope expressions derived in Appendix B.2.

2.6 DISCUSSION

We found that hypercapnic normalization, based on division of the functional BOLD response by the hypercapnic BOLD response $B_{H,}$ increased inter-subject variability. The increase in inter-subject variability was due to a systematic bias term G/B_H (Eqn. 2.2) in the normalized response, where G is the positive intercept found in the linear relationship between the functional and hypercapnic BOLD responses (Eqn. 2.1). The positive G results from a positive intercept c_2 in the linear relationship between the functional CBF response and the hypercapnic CBF response (Eqn. 2.8). In contrast to the increased inter-subject variability found with hypercapnic normalization, we found that the use of the hypercapnic BOLD response as a covariate for the functional BOLD response generated normalized responses with reduced inter-subject variability. Since the use of the hypercapnic BOLD response as a covariate is conceptually similar to estimating the intercept G and removing it as a confound, it is expected to consistently perform better than division by the hypercapnic BOLD response as a method of reducing inter-subject variability.

Our finding of increased inter-subject variability with hypercapnic normalization of a visual task agrees with some previous studies of hypercapnic normalization but not others. Consistent with our findings, the results from (Cohen et al. 2004) showed that hypercapnic normalization (5% CO_2) of a motor task increased inter-subject variability in healthy young subjects. In (Handwerker et al. 2007) hypercapnic normalization of a visuomotor saccade task by a breath-hold task increased inter-subject variability in responses obtained in the front and supplementary

eye fields of older subjects. In contrast, reductions in inter-subject variability were found by two studies that utilized breath-hold based hypercapnic normalization of a motor task (Biswal et al. 2007) and a working memory task (Thomason et al. 2007). These differences in the effect of hypercapnic normalization on inter-subject variability may be related to the different experimental paradigms used in the studies, specifically the type of hypercapnic task (breath-hold vs. 5% CO_2), the brain region, and the composition of the study group.

The positive intercept *G* in the linear relationship between the functional and hypercapnic BOLD responses found in our study was a significant contributor to the increased inter-subject variability observed in the hypercapnia normalized responses. Positive intercept *G* values were also found in (Handwerker et al. 2007). Although that study did not specifically report values of inter-subject variability, the results (Figure 2 in (Handwerker et al. 2007)) showed clear increases in the inter-subject variability of the older subject group in the front and supplementary eye fields, suggesting that the positive intercept *G* was also an important factor in their study. (Thomason et al. 2007)'s data also showed a positive intercept *G*, but they found that hypercapnic normalization decreased inter-subject variability. Several aspects of (Thomason et al. 2007)'s experimental design may have reduced the effect of the systematic bias G/B_H in their study. First, their results (computed from Table 1 in (Thomason et al. 2007)) showed a smaller intercept *G* (0.28%) than those found in our study (BOLD ROI: *G*=1.06%, BOLD+CBF ROI: *G*=0.97%). This may be due to the different functional tasks (working memory vs. visual) used in the two studies. Also, the range of the hypercapnic BOLD values in (Thomason et al. 2007)'s study (0.5% to

3.5%) was much smaller than the values found in our study (16.8% to 104.5%, Figure 2.4) due to the different hypercapnic tasks (breath-hold vs. 5% CO_2). Since the range of the functional BOLD responses were comparable in both studies, the slope A (Eqn. 2.1) of the linear relationship between the functional and hypercapnic BOLD responses in (Thomason et al. 2007)'s work (A=0.41) was larger than those found in our study (BOLD ROI: A=0.14, BOLD+CBF ROI: A=0.20). The increased slope A in (Thomason et al. 2007)'s work caused the systematic bias G/B_H to be a relatively smaller component of the normalized response (Eqn. 2.2). Therefore while a systematic bias G/B_H may have been present in (Thomason et al. 2007)'s data, the experimental protocol (breath-hold and working memory tasks) may have reduced the contribution of the systematic bias to the normalized responses.

While a positive intercept G has been found in previous work (Handwerker et al. 2007; Thomason et al. 2007), its physical meaning has not been explored prior to our study. Using the framework of the Davis model, we have shown that the positive intercept term G is related to the intercept term c_2 (Eqn. 2.8) in the linear relationship between the functional and hypercapnic CBF responses. The presence of the positive intercept c_2 indicates that as the functional CBF response F approaches c_2, the hypercapnic CBF response F_H approaches zero. Another interpretation of the positive intercept c_2 can be made by relating the CBF responses to the baseline CBF. Both the functional and hypercapnic CBF responses had an inverse relationship with baseline CBF (Figures 2.4d and 2.4c). However, the hypercapnic CBF response was higher than the functional CBF response at low CBF_0 and decreased more rapidly and approached zero with increasing CBF_0.

To our knowledge, the difference in the dependence of the functional and hypercapnic CBF responses on baseline CBF has not received significant prior attention, and the mechanisms underlying the difference are not known. One possibility is that variations in baseline CBF may cause vascular endothelial cells to react differently to functional and hypercapnic stimuli. Shear stress and stretch on vascular endothelial cells are known to modify intracellular signaling and gene expression (Chien 2007; White and Frangos 2007). In addition, the functional and hypercapnic CBF responses are most likely driven by different pathways, with the functional CBF responses driven by neurotransmitter signaling (Fergus and Lee 1997; Attwell and Iadecola 2002) and the hypercapnic CBF responses reflecting decreases in pH level (Madden 1993; Okamoto et al. 1997). At low baseline CBF levels, our results show a greater vascular responsiveness to hypercapnia versus functional stimuli. But this responsiveness decreases more rapidly for the hypercapnic response, as compared to the functional response. Increased shear stress and stretch at higher CBF levels may produce cellular changes that selectively reduce vascular responsiveness to decreased pH level as compared to neurotransmitter signaling. However, this proposed mechanism is highly speculative, and further work on how baseline CBF affects the functional and hypercapnic CBF responses is clearly needed.

In this study, we measured the maximum BOLD response M and found that it was relatively constant across subjects, as shown by its lack of correlation with baseline CBF (CBF_0) (Results, Figure 2.5). By using Fick's principle, assuming a steady-state relation between baseline CBF and cerebral blood volume (Grubb et al. 1974), and assuming that the arterial oxygen concentration is relatively constant across

the sample of healthy, young subjects, the relation between the maximum BOLD response M and the oxygen extraction fraction OEF may be written as $M \propto (\mathrm{CBF}_0)^{\alpha} \cdot (\mathrm{OEF})^{\beta}$. The constancy of the maximum BOLD response M across baseline CBF values implies an inverse relationship between the oxygen extraction fraction and baseline CBF. An inverse relationship between the oxygen extraction fraction and baseline CBF is consistent with the direct relationship between the venous oxygenation and baseline CBF found by (Lu et al. 2008b). In addition, the inverse relationship is in agreement with (Buxton and Frank 1997)'s mathematical model, which proposed that the combination of shortened capillary transit times from increased CBF and the limited rate of oxygen extraction across the capillary wall produces a decrease in the oxygen extraction fraction.

Consistent with a prior study (Kastrup et al. 1999), we found that the functional CBF response F was inversely proportional to baseline CBF. Because the functional BOLD response B is tightly coupled to the functional CBF response (see BOLD signal model in Eqn. 2.6), the dependence of F on baseline CBF contributes to the dependence of the BOLD response on baseline CBF. A study by (Lu et al. 2008b) also reported a negative correlation between inter-subject functional BOLD responses and baseline CBF, although the correlation was not significant. In (Lu et al. 2008b)'s study, the functional BOLD response was better explained by measures of venous oxygenation, which may reflect both the maximum BOLD response M and baseline CBF.

In summary, we found that hypercapnic normalization can increase the inter-subject variability of the BOLD response. The increased variability reflects a

systematic bias term, resulting from a positive intercept *G* in the relation between the functional and hypercapnic BOLD responses. The systematic bias resulted from the steeper dependence of the hypercapnic CBF response than the functional CBF response on baseline CBF. These findings suggest a cautious interpretation of prior studies using hypercapnic normalization. In particular, the presence of a positive intercept in the relation between the functional and hypercapnic BOLD responses needs to considered in the analysis of hypercapnia normalized responses. As an alternative, the systematic bias can be avoided by using the hypercapnic BOLD response as a covariate to normalize the functional BOLD response. The effect of the systematic bias may depend on the experimental paradigm, including the type of hypercapnic challenge, brain region, and subject group. Further work elucidating the dependence of the systematic bias on the experimental protocol would aid comparison of results between studies.

2.7 APPENDIX B.1

In this appendix, we derive the relation between the hypercapnic normalized BOLD responses ascertained when the normalization is performed on a per-voxel basis (B_i'') versus a per-subject basis ($\hat{B}_i$). For the i^{th} subject, the average functional BOLD response is defined as:

$$B_i = \frac{1}{N_i}\sum_{j=1}^{N_i} b_{i,j} \qquad \text{[B.1.1]}$$

and the average hypercapnic BOLD response is defined as:

$$B_{H,i} = \frac{1}{N_i}\sum_{j=1}^{N_i} b_{H,i,j} \qquad \text{[B.1.2]}$$

where $b_{i,j}$ and $b_{H,i,j}$ are the per-voxel functional and hypercapnic BOLD responses, respectively, for the i^{th} subject and the j^{th} voxel, and N_i is the number of active voxels.

When hypercapnic normalization is performed on a per-voxel basis, the average normalized response for the i^{th} subject is:

$$B_i'' = \frac{1}{N_i}\sum_{j=1}^{N_i} \frac{b_{i,j}}{b_{H,i,j}} \qquad \text{[B.1.3]}$$

$$= a_i + \frac{1}{N_i}\sum_{j=1}^{N_i}\left(\frac{g_i + e_{i,j}}{b_{H,i,j}}\right) \qquad \text{[B.1.4]}$$

$$= a_i + \frac{g_i}{N_i}\sum_{j=1}^{N_i}\frac{1}{b_{H,i,j}} \qquad \text{[B.1.5]}$$

where we have used the linear relation $b_{i,j} = a_i \cdot b_{H,i,j} + g_i + e_{i,j}$ (Eqn. 2.4) and assumed that the mean of the residuals is equal to zero and the residuals are uncorrelated with $b_{H,i,j}$.

If instead we perform the normalization on a per-subject basis, the average normalized response for the i^{th} subject can be written as:

$$\hat{B}_i = \frac{B_i}{B_{H,i}} \qquad \text{[B.1.6]}$$

$$= \frac{\frac{1}{N_i}\sum_{j=1}^{N_i}\left(a_i \cdot b_{H,i,j} + g_i + e_{i,j}\right)}{\frac{1}{N_i}\sum_{j=1}^{N_i} b_{H,i,j}} \qquad \text{[B.1.7]}$$

$$= a_i + g_i \cdot \frac{1}{\frac{1}{N_i}\sum_{j=1}^{N_i} b_{H,i,j}} \qquad \text{[B.1.8]}$$

Note that Eqns. B.1.5 and B.1.8 implies that the per-voxel (B_i'') and per-subject ($\hat{B}_i$) normalized responses have the following relation:

$$B_i'' = \hat{B}_i + g_i\left(\frac{1}{N_i}\sum_{j=1}^{N_i}\frac{1}{b_{H,i,j}} - \left(\frac{1}{N_i}\sum_{j=1}^{N_i} b_{H,i,j}\right)^{-1}\right) \qquad \text{[B.1.9]}$$

Eqn. B.1.9 indicates that when viewed across the sample, B_i'' and $\hat{B}_i$ are equivalent except for a subject dependent term $g_i\left(\frac{1}{N_i}\sum_{j=1}^{N_i}\frac{1}{b_{H,i,j}} - \left(\frac{1}{N_i}\sum_{j=1}^{N_i} b_{H,i,j}\right)^{-1}\right)$. Empirically (Results and Figure 2.2), we find that this additional term is positive and is around 25% of the average per-voxel normalized response B'' and 33% of the average per-subject normalized response $\hat{B}$. This reflects the empirical findings that the intercept g_i is

approximately equal to 1 across subjects (see Results) and the difference between summation terms is less than one and positive, with $\frac{1}{N_i}\sum_{j=1}^{N_i}\frac{1}{b_{H,i,j}}$ about twice as large as $\left(\frac{1}{N_i}\sum_{j=1}^{N_i}b_{H,i,j}\right)^{-1}$.

2.8 APPENDIX B.2

In this appendix, we derive a linear approximation for the nonlinear relation between the functional BOLD response B_i and the hypercapnic BOLD response $B_{H,i}$ across a sample of subjects (indexed by *i*). Recall that prior work (Handwerker et al. 2007; Thomason et al. 2007) has demonstrated an empirical linear relation (Eqn. 2.1) of the form $B_i = A \cdot B_{H,i} + G + E_i$. Here we use the framework of the Davis Model (Equation 2.6) to derive expressions for *A* and *G*. We also make use of the following empirical observations (see Results and Figure 2.4): (1) the maximum BOLD response *M* is relatively constant across subjects, (2) the CBF/$CMRO_2$ coupling ratio $n = F_i / m_i$ is relatively constant across subjects, and (3) the functional CBF response F_i is linearly related to the hypercapnic CBF response $F_{H,i}$, i.e. $F_i = c_1 \cdot F_{H,i} + c_2$, where c_1 is the group slope and c_2 is the group intercept. With these observations, we obtain:

$$B_i = M\left(1 - \left(\frac{F_i}{100} + 1\right)^{\alpha-\beta}\left(\frac{m_i}{100} + 1\right)^{\beta}\right)$$

$$= M\left(1 - \left(\frac{c_1 \cdot F_{H,i} + c_2}{100} + 1\right)^{\alpha-\beta}\left(\frac{c_1 \cdot F_{H,i} + c_2}{n \cdot 100} + 1\right)^{\beta}\right) \quad \text{[B.2.1]}$$

From Eqn. 2.1, the functional BOLD response B_i is equal to the intercept *G* when the hypercapnic BOLD response $B_{H,i} = 0$ (for these derivations, we assume the residual term $E_i = 0$). From the Davis Model with hypercapnia (Eqn. 2.7), we can see that the hypercapnic BOLD response $B_{H,i} = 0$ when the hypercapnic CBF response $F_{H,i} = 0$. Therefore, the intercept is:

$$G = B_i \mid_{F_{H,i}=0}$$

$$= M\left(1-\left(\frac{c_2}{100}+1\right)^{\alpha-\beta}\left(\frac{c_2}{n\cdot 100}+1\right)^{\beta}\right) \quad \text{[B.2.2]}$$

To derive an approximation for the slope, *A*, we compute the slope between the intercept point ($B_{H,i}=0, B_i=G$) and the point when the hypercapnic CBF response is maximum (F_{HM}):

$$B_H = M\left(1-\left(\frac{F_{HM}}{100}+1\right)^{\alpha-\beta}\right) \quad \text{[B.2.3]}$$

$$B = M\left(1-\left(\frac{c_1\cdot F_{HM}+c_2}{100}+1\right)^{\alpha-\beta}\left(\frac{c_1\cdot F_{HM}+c_2}{n\cdot 100}+1\right)^{\beta}\right) \quad \text{[B.2.4]}$$

A is then:

$$A = \frac{M\left(1-\left(\frac{c_1\cdot F_{HM}+c_2}{100}+1\right)^{\alpha-\beta}\left(\frac{c_1\cdot F_{HM}+c_2}{n\cdot 100}+1\right)^{\beta}\right)-M\left(1-\left(\frac{c_2}{100}+1\right)^{\alpha-\beta}\left(\frac{c_2}{n\cdot 100}+1\right)^{\beta}\right)}{M\left(1-\left(\frac{F_{HM}}{100}+1\right)^{\alpha-\beta}\right)-0}$$

$$= \frac{\left(\frac{c_2}{100}+1\right)^{\alpha-\beta}\left(\frac{c_2}{n\cdot 100}+1\right)^{\beta}-\left(\frac{c_1\cdot F_{HM}+c_2}{100}+1\right)^{\alpha-\beta}\left(\frac{c_1\cdot F_{HM}+c_2}{n\cdot 100}+1\right)^{\beta}}{1-\left(\frac{F_{HM}}{100}+1\right)^{\alpha-\beta}} \quad \text{[B.2.5]}$$

The positive c_2 found in this study (Results and Figure 2.4) indicates that when the functional flow response approaches c_2, the hypercapnic flow response approaches zero. Another interpretation of the positive term c_2 may be obtained by examining the ratio $F_i / F_{H,i}$ of the functional and hypercapnic CBF responses:

$$F_i / F_{H,i} = c_1 + c_2 / F_{H,i} \quad \text{[B.2.6]}$$

Because $F_{H,i}$ exhibits an inverse dependence on baseline CBF (Results and Figure 2.4), the term $c_2/F_{H,i}$ will increase with baseline CBF, as will the ratio $F_i/F_{H,i}$. In this interpretation, c_2 is a component of the slope of the linear relationship between $F_i/F_{H,i}$ and baseline CBF.

To evaluate the linearity of the relation between the functional BOLD response B and the hypercapnic BOLD response B_H, we derive theoretical values of the two responses using experimental and published values of the BOLD signal components (M = 10.62%, n = 2.57, c_1 = 0.28, c_2 = 36.70% (Results and Figure 2.4); α = 0.38 (Grubb et al. 1974); β = 1.5 (Davis et al. 1998)) and the Davis Model equations (Eqns. 1.7 and B.2.1). Also, we vary the slope c_1 and the intercept c_2 by ±20% to assess the robustness of the relation. As shown in Figure 2.6 and discussed in the Results section, the theoretical functional BOLD responses B and hypercapnic BOLD responses B_H are well described by the linear approximations over the range of parameters that are applicable to the sample in this study.

Acknowledgements

This work was supported in part by a grant from the National Institutes of Health (ROINS051661). The authors thank Richard Buxton, Joanna Perthen, and Amy Lansing for their assistance and for kindly sharing the experimental data used for this study.

Chapter 2, in full, has been submitted for publication of the material as it may appear in Neuroimage 2008. Liau, Joy; Liu Thomas T. The dissertation author was the primary investigator and author of this paper.

CHAPTER 3:

BASELINE BLOOD OXYGENATION AND CEREBRAL BLOOD FLOW ACCOUNT FOR INTER-SUBJECT VARIABILITY IN THE BOLD FMRI RESPONSE

3.1 ABSTRACT

Although the blood oxygenation level dependent (BOLD) signal in functional MRI studies is widely interpreted as a measure of neural activity, it has a complex dependence on several physiological variables. As a result, differences in factors unrelated to neural activity can lead to significant variability in the BOLD response. Methods to reduce inter-subject BOLD variability due to non-neural factors are highly desirable to the fMRI community. In this study, we used measures of baseline cerebral blood flow (CBF), venous oxygenation, and the BOLD and CBF responses to both visual stimulus and hypercapnia to assess the use of venous oxygenation and baseline CBF to account for BOLD inter-subject variability. We found that both venous oxygenation and baseline CBF had a significant ($p<0.05$) inverse dependence on the BOLD response in a region of interest based on both BOLD and CBF activation. Furthermore, venous oxygenation was significantly correlated to baseline CBF. However, baseline CBF measures in a region of interest based on BOLD activation only were uncorrelated to either venous oxygenation or the BOLD response. In this region of interest, use of anatomical measures to exclude voxels containing cerebrospinal fluid and include voxels with a high fraction of gray matter produced significant correlations between the resulting baseline CBF and both venous oxygenation and the BOLD response. The findings of this study indicate that both venous oxygenation and baseline CBF may be used to reduce BOLD inter-subject variability provided that anatomical measures are incorporated into the computation of baseline CBF.

3.2 INTRODUCTION

The blood oxygenation level dependent (BOLD) functional MRI signal is widely interpreted as a measure of neural activity. However, it reflects changes in a host of physiological variables, namely cerebral blood volume, cerebral blood flow (CBF), and cerebral oxygen metabolism (Buxton 2002). As a result, differences in factors unrelated to neural activity can lead to significant variability in the BOLD response (D'Esposito et al. 2003; Gustard et al. 2003). The increased variability due to non-neural factors decreases the statistical power of fMRI studies. Also, group differences in the non-neural factors may be misinterpreted as true differences in neural activity. Therefore, a method that reduces BOLD inter-subject variability due to non-neural factors would be useful to the fMRI community.

There is growing evidence that the baseline CBF is one non-neural factor that contributes to BOLD variability. Prior work has found that increased baseline CBF from inhalation of carbon dioxide caused decreases in the BOLD response amplitude (Bandettini and Wong 1997; Cohen et al. 2002; Stefanovic et al. 2006). Also, (Cohen et al. 2002) found that decreased baseline CBF from hyperventilation-induced hypocapnia increased the BOLD response amplitude. These findings suggest that inter-subject variations in baseline CBF may contribute to inter-subject variability in the BOLD response. If so, measures of baseline CBF may be used as a method to reduce BOLD inter-subject variability.

A recent study by (Lu et al. 2008) found that measures of venous oxygenation were inversely correlated with the BOLD response and may be used as a method to reduce BOLD inter-subject variability. In addition, they found that venous oxygenation was directly dependent on baseline CBF, suggesting that the measures are related. However, the baseline CBF measures were not significantly correlated to the BOLD response. These findings suggest that baseline CBF and venous oxygenation have important differences in their relation to the BOLD response.

In this study, we use measures of the baseline CBF, venous oxygenation, and the BOLD and CBF responses to both visual stimulus and hypercapnia to better understand the relation between both baseline CBF and venous oxygenation and the BOLD response. We show that baseline CBF is well correlated with both venous oxygenation and the BOLD response when measured in a region of interest based on both BOLD and CBF activation. We then show that baseline CBF measured in a region of interest based only on BOLD activation is complicated by the presence of draining veins.

3.3 METHODS

Experimental Protocol

Nine young, healthy subjects (age = 31±7 years, 4 female) participated in this study after giving informed consent. During the study, the subjects were presented with a visual stimulus consisting of an "on" condition of a full-contrast full-field 8Hz flickering checkerboard pattern with a small white square in the center. The stimulus also had an "off" condition of a gray background with a small white square in the center and the same average luminance as the "on" condition. The subjects were instructed to fixate on the white square during both conditions.

Each study consisted of the following resting and task-related scans: (1) two hypercapnia scans where subjects inhaled a 5% CO_2 gas mixture through a non-rebreathing face mask (off condition for scan, 2 min room air/ 3 min 5% CO_2/ 2 min room air), (2) one resting-state cerebral blood flow (CBF) scan (4 min 10s of off condition), (3) two block design scans (60 s off, 4 cycles of 20 s on/ 60 s off, 30 s off), and (5) two venous oxygenation scans (4 min 16s of off condition). The scans were performed in the order stated except the block design and venous oxygenation scans were interleaved. In addition, a whole brain resting-state CBF scan was acquired after the hypercapnia scans for analysis of whole brain cerebral oxygen metabolism, which is not presented here. After the hypercapnia scans, the facemask was removed for subject comfort, and a high-resolution anatomical image was acquired. Also, calibration scans were acquired after each resting-state CBF scan to facilitate CBF

quantification, and field maps were acquired after the whole brain resting-state CBF calibration scans.

Imaging Protocol

Imaging data were acquired on a GE Signa Excite 3 Tesla whole body system with a body transmit coil and an eight channel receive head coil. The hypercapnia, block design, and resting-state CBF scans were acquired with a PICORE QUIPSS II (Wong et al. 1998) ASL sequence (TR=2.5 s, TI1/TI2=600/1500 ms) with a spiral readout (TE1/TE2=2.9/24ms, FOV=24cm, 64x64 matrix, 90^{o} flip angle). Six oblique axial 5 mm slices were prescribed about the calcarine sulcus for the ASL scans. The venous oxygenation scans were acquired using a TRUST (Lu and Ge 2008) sequence with a single-shot echo planar readout (TR=8 s, TI=1200 ms, TE=26 ms, FOV=23cm, tag thickness=80 mm, gap between tag and imaging slice=25 mm, 64x64 matrix, 90^{o} flip angle, effective TEs=0 ms, 40 ms, 80 ms, and 160 ms, τ_{CPMG}=10 ms, 4 reps for each effective TE). One oblique axial 5 mm slice was prescribed at the level of the lateral ventricles for the venous oxygenation scans.

The calibration scans for CBF quantification used the same in-plane parameters as the ASL scans, but the number of slices was increased to ensure coverage of the lateral ventricles. The calibration scans consisted of a cerebrospinal fluid (CSF) reference scan acquired at full relaxation (TE=2.9 ms) and a minimum contrast scan (TR=2 s, TE=11 ms). The field maps contained the same slices as the ASL scans, but the number of slices was increased to allow coverage of the whole brain. The field maps were acquired at two echo times (TE1=3.1 ms, TE2=5.5 ms).

The high-resolution anatomical scan was acquired with a magnetization prepared 3D fast spoiled gradient echo (FSPGR) sequence (TI=300 ms, TR=9.8 ms, TE=4.0 ms, 15^{o} flip angle, FOV 25 cm, matrix 256x256x192).

Cardiac pulse and respiratory effort data were monitored using a pulse oximeter (InVivo) and a respiratory effort transducer (BIOPAC), respectively. The pulse oximeter was placed on the subject's right index finger, and the respiratory effort belt was placed around the subject's abdomen. Physiological data were sampled at 40 samples per second using a multi-channel data acquisition board (National Instruments).

Data Preprocessing and General Linear Model Analysis

All images except the venous oxygenation data were coregistered using AFNI software (Cox 1996). Data from the first 10 s of each ASL scan were discarded to allow magnetization to reach a steady state.

General linear model (GLM) analyses were used to determine the statistical significance of the block design and hypercapnia responses. Pre-whitening was performed using an autoregressive AR(1) model (Woolrich et al. 2001). Data from the two block design runs were concatenated, measured cardiac and respiratory data were included as regressors, and a reference function based on the block design task was used in an unfiltered GLM (Mumford et al. 2006; Restom et al. 2006). GLM analysis of the first echo data produced p-value maps indicating the statistical significance of the functional CBF response, and analysis of the second echo data produced statistical maps of the functional BOLD response. This process was repeated with the first echo

hypercapnia data and a reference function based on the CO_2 administration to produce r-value maps of the hypercapnic CBF response. Also, analysis of the second echo hypercapnia data produced statistical maps of the hypercapnic BOLD response.

Regions-of-Interest Definitions

Two regions-of-interest (ROIs) were used for data analyses: 1) a BOLD ROI based on functional BOLD activation, and 2) a BOLD+CBF ROI that had additional inclusion criteria based on hypercapnic BOLD activation and functional and hypercapnic CBF activation. As analyses using the Davis Model require reliable CBF and BOLD measures from both functional and hypercapnic tasks, these analyses used the BOLD+CBF ROI. The BOLD ROI was formed by the intersection of: 1) voxels containing significant functional BOLD responses ($p<0.01$) and 2) a visual cortex anatomical mask defined as the posterior half of the brain to localize visual areas. The BOLD+CBF ROI was formed by the intersection of: 1) the BOLD ROI, 2) voxels containing positive BOLD responses ($r>0$), 2) voxels containing significant functional CBF responses ($p<0.01$), and 3) voxels containing positive hypercapnic CBF responses ($r>0$).

Functional and Hypercapnic Response Amplitudes

The functional response amplitude was defined as the percent increase of the block design response, using the mean signal from both runs in the active state (last 10 s of each on condition) and the mean signal from both runs in the baseline state (initial off condition). The functional BOLD response amplitudes (%ΔBOLD) were

computed from the second echo block design data after taking the running average (Liu and Wong 2005) and averaging over voxels in each ROI. The functional CBF response amplitudes (%ΔCBF) were computed from the first echo block design data after taking the running difference (Liu and Wong 2005) and averaging over voxels in each ROI.

For computation of the hypercapnic response amplitudes, data were averaged over runs, and the hypercapnic response amplitude was defined as the percent increase of the response, using the mean signal in the active state (last 1.5 min of the 5% CO_2 condition) and the mean signal in the baseline state (first air condition and last 30 s of the second air condition). The hypercapnic BOLD response amplitudes ($\%\Delta BOLD_H$) were computed from the second echo hypercapnia data after taking the running average (Liu and Wong 2005) and averaging over runs and voxels in the BOLD+CBF ROI. The hypercapnic CBF response amplitudes ($\%\Delta CBF_H$) were computed from the first echo hypercapnic data after taking the running difference (Liu and Wong 2005) and averaging over runs and voxels in the BOLD+CBF ROI.

Davis Model Calculations

The Davis model signal components of the functional BOLD response were estimated using data from the BOLD+CBF ROI. The percent maximum BOLD responses M were computed from $\%\Delta BOLD_H$ and $\%\Delta CBF_H$ using the relation:

$$M = \frac{\%\Delta BOLD_H}{1 - \left(\%\Delta CBF_H/100 + 1\right)^{\alpha-\beta}} \quad (3.1)$$

where α=0.38 (Grubb et al. 1974) and β=1.5 (Davis et al. 1998). The percent cerebral oxygen metabolism responses ($\%\Delta CMRO_2$) were then computed from M, %ΔBOLD, and %ΔCBF by (Davis et al. 1998):

$$\%\Delta CMRO_2 = \left[\left(1 - \frac{\%\Delta BOLD}{M}\right)^{1/\beta} \cdot \left(\frac{\%\Delta CBF}{100} + 1\right)^{\alpha-\beta} - 1\right] \cdot 100 \quad (3.2)$$

Baseline CBF

For each subject, a mean ASL image was formed from the average difference of the control and tag images from the first echo of the resting-state CBF data (Liu and Wong 2005). This mean ASL image was corrected for coil inhomogeneities using the minimum contrast image (Wang et al. 2005) and converted to physiological units using the CSF image as a reference signal (Chalela et al. 2000) to produce per-voxel baseline CBF values. The per-voxel baseline CBF values were averaged over the ROIs to form per-subject baseline CBF values.

Baseline CBF values were also computed in the BOLD ROI using exclusion criteria based on anatomical tissue types. Using the high-resolution anatomical data and the FSL Automated Segmentation Tool (FAST), we estimated the fractions of gray matter, white matter, and CSF in each voxel (Smith et al. 2004). To allow better alignment between the resting-state CBF data and the anatomical image, the field maps were used to correct for image artifacts in the resting-state CBF data introduced by magnetic field inhomogeneties (Sutton et al. 2003). Using a similar procedure to the previous computation of per-voxel baseline CBF values, the field map corrected

per-voxel baseline CBF values were computed from the first echo of the field map corrected resting-state CBF data. Per-subject baseline CBF values were then calculated by averaging the field map corrected per-voxel baseline CBF values over the voxels in the BOLD ROI that exceeded a gray matter threshold (1% to 99% gray matter). Also, per-subject baseline CBF values were computed by averaging the field map corrected per-voxel baseline CBF values over voxels in the BOLD ROI that contained both greater than 99% gray matter and less than 0.1% CSF.

Venous Oxygenation

Measures of the whole brain venous oxygenation were computed from the transverse relaxation time constant (T_2) in the sagittal sinus. First, the average difference of the control and tag images were computed for each effective TE of the venous oxygenation scan. The four voxels with the highest difference signals were selected from a region of interest liberally drawn around the sagittal sinus. Signals were averaged over voxels, and the T_2 and percent venous oxygenation ($\%O_{2,v}$) of the blood in the sagittal sinus was estimated in a method described by (Lu and Ge 2008).

Statistical Tests

Relations between measured values were assessed by correlation analyses and linear fits. For example, the relation between the %ΔBOLD and baseline CBF in each ROI were determined by correlation analyses and linear fits. The correlation analyses produced r and p values indicating the significance of the relation, and the linear fit provided a visual assessment of the relation.

3.4 RESULTS

In Figure 3.1, we assessed whether the baseline CBF or the venous oxygenation ($\%O_{2,v}$) accounted for inter-subject variability in %ΔBOLD (first column) and in the following estimated BOLD model parameters: (second column) %ΔCBF, (third column) the maximum BOLD response (M), and (fourth column) cerebral oxygen metabolism response ($\%\Delta CMRO_2$). These comparisons were done in the BOLD+CBF ROI, where both BOLD and CBF responses were reliably measured, allowing use of the Davis Model to estimate BOLD model parameters (Davis et al. 1998). Both the baseline CBF (r=-0.74, p=0.023) and $\%O_{2,v}$ (r=-0.80, p=0.00) exhibited a significant inverse dependence on %ΔBOLD, indicating that both the baseline CBF and $\%O_{2,v}$ accounted for a large portion of %ΔBOLD variability. In addition, both the baseline CBF (r=-0.80, p=0.009) and $\%O_{2,v}$ (r=-0.87, p=0.002) had a significant inverse dependence on %ΔCBF. In contrast, a significant positive correlation was found between baseline CBF and M (r=0.71, p=0.031), and an insignificant positive trend was found between $\%O_{2,v}$ and M (r=0.62, p=0.072). Neither the baseline CBF (r=0.46, p=0.218) nor the $\%O_{2,v}$ (r=0.51, p=0.166) were significantly correlated to $\%\Delta CMRO_2$. From these results, the %ΔCBF is the only BOLD model parameter that contributed to the observed inverse dependence of %ΔBOLD on baseline CBF and $\%O_{2,v}$ (Davis et al. 1998).

We also assessed the relation between baseline CBF and $\%O_{2,v}$. Figure 3.2 shows the linear relations between $\%O_{2,v}$ and the per-subject baseline CBF computed

over voxels in (a) the BOLD+CBF ROI, (b) the BOLD ROI, and (c) the BOLD ROI with field map correction and greater than 99% gray matter. The $\%O_{2,v}$ had a significant positive dependence on the baseline CBF computed in the BOLD+CBF ROI (r=0.73, p=0.026) and in the BOLD ROI with field map correction and greater than 99% gray matter (r=0.78, p=0.014) but not in the BOLD ROI (r=0.49, p=0.181).

To determine whether the relation between $\%O_{2,v}$ and baseline CBF depended on the gray matter fraction, correlation analyses were performed between $\%O_{2,v}$ and the baseline CBF computed with field map correction and with the gray matter fraction varied from 1% to 99%. Figure 3.3 shows the (left column) r-values and (right column) p-values of the correlation results for the (top row) baseline CBF and (bottom row) field map corrected baseline CBF. For both the baseline CBF and field map corrected baseline CBF, the r-values increased and the p-values decreased with greater gray matter fraction. The improved correlation between the baseline CBF and $\%O_{2,v}$ with increasing gray matter fraction indicates that the baseline CBF values in the capillaries, which comprise gray matter, may be a better reflection of the baseline state than the baseline CBF in white matter. Also, the correlation between the baseline CBF and $\%O_{2,v}$ improves more quickly with increasing gray matter fraction in the field map corrected baseline CBF than the raw baseline CBF. This suggests that field map correction provided better alignment between the anatomical data and the resting-state CBF data.

It is desirable to apply measures of the baseline state to $\%\Delta$BOLD in the BOLD ROI since $\%\Delta$CBF is not available in most studies. Figure 3.4 shows the relation between $\%\Delta$BOLD in the BOLD ROI and the different baseline state

measures: (a) $\%O_{2,v}$, (b) baseline CBF in the BOLD ROI, (c) field map corrected baseline CBF in the BOLD ROI with >99% gray matter, and (d) field map corrected baseline CBF in the BOLD ROI with >99% gray matter and <0.1% CSF. The %ΔBOLD had a significant inverse dependence on $\%O_{2,v}$ (r=-0.67, p=0.050) and the field map corrected baseline CBF in the BOLD ROI with >99% gray matter and <0.1% CSF (r=-0.73, p=0.025). A negative trend was found between the %ΔBOLD and the field map corrected baseline CBF with >99% gray matter, but the trend was not significant (r=-0.59, p=0.094). The %ΔBOLD was not significantly correlated to the baseline CBF in the BOLD ROI (r=-0.05, p=0.897).

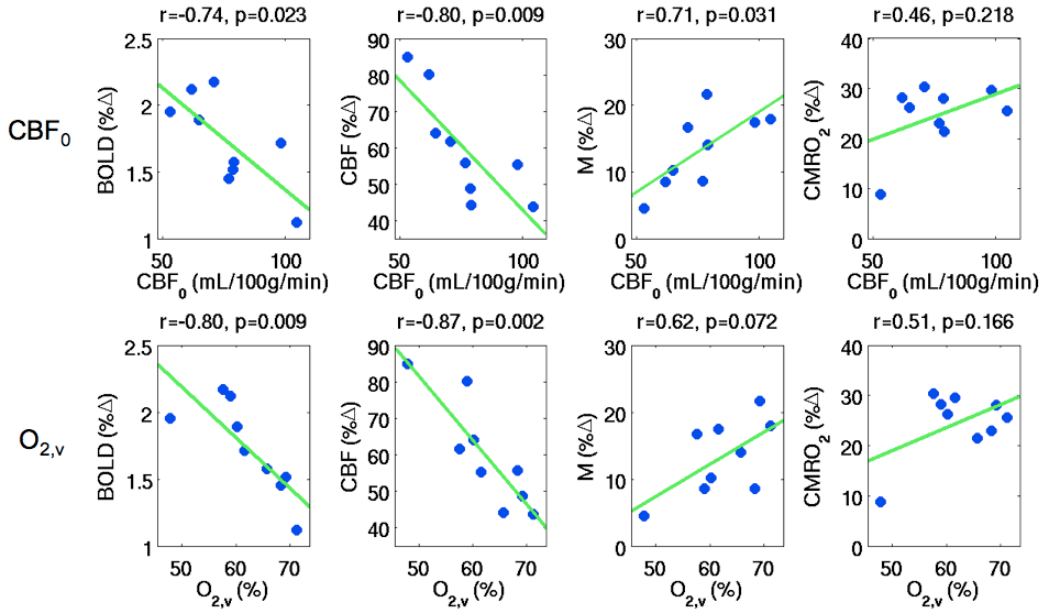

Figure 3.1: Scatter plots showing the dependence of the BOLD responses and the estimated BOLD signal parameters on baseline CBF and venous oxygenation in the BOLD+CBF ROI: (first column) %ΔBOLD, (second column) %ΔCBF, (third column) M, (fourth column) $\%\Delta CMRO_2$. The top row shows comparisons with baseline CBF (CBF_0), and the bottom row shows comparisons with the venous oxygenation ($\%O_{2,v}$). Green lines indicate linear fits.

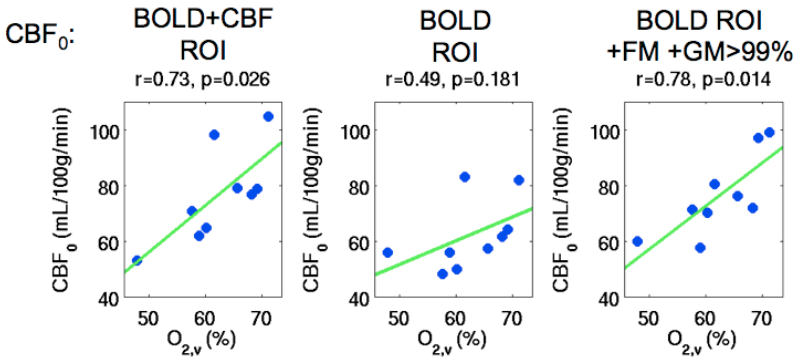

Figure 3.2: Scatter plots showing the relation between the venous oxygenation ($\%O_{2,v}$) and baseline CBF measured in the: (left panel) BOLD+CBF ROI, (middle panel) BOLD ROI, and (right panel) BOLD ROI with field map (FM) correction and greater than 99% gray matter. Green lines indicate linear fits.

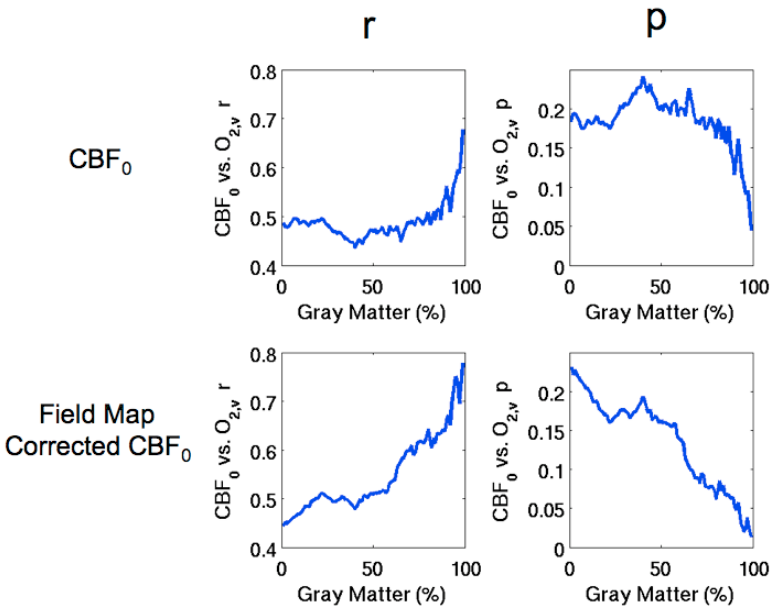

Figure 3.3: Plots of r-value and p-value results from correlation analyses between venous oxygenation ($\%O_{2,v}$) and baseline CBF (CBF_0) computed with different gray matter fractions (1% to 99%). The left column shows the r-values and the right column shows the p-values for the (top row) baseline CBF and (bottom row) field map corrected baseline CBF.

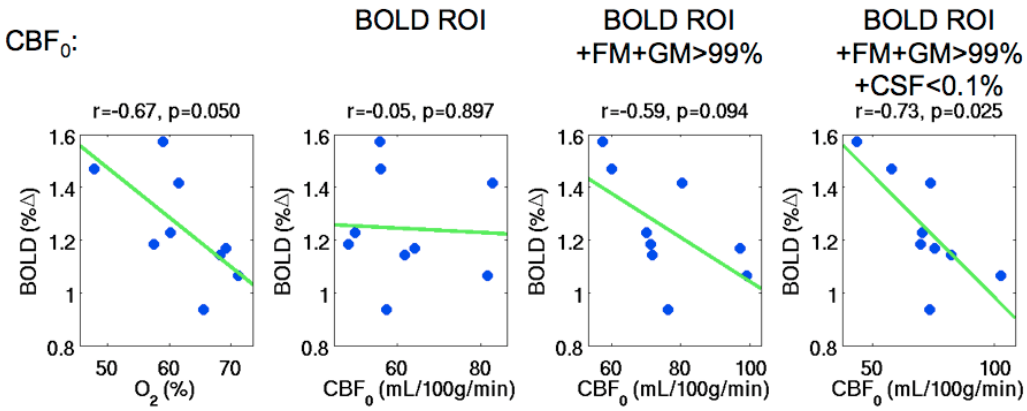

Figure 3.4: Scatter plots of the BOLD responses in the BOLD ROI versus the measures of the baseline state: (first panel) venous oxygenation ($\%O_{2,v}$), (second panel) baseline CBF (CBF_0) in the BOLD ROI, (third panel) field map corrected CBF_0 in the BOLD ROI with greater than 99% gray matter, and (fourth panel) field map corrected CBF_0 in the BOLD ROI with greater than 99% gray matter and less than 0.1% CSF. Green lines indicate linear fits.

3.5 DISCUSSION

We found that measures of both venous oxygenation and baseline CBF accounted for a significant portion of BOLD inter-subject variability in the BOLD+CBF ROI, suggesting that the two measures are closely related. These findings were consistent with the significant correlation between venous oxygenation and baseline CBF computed in the BOLD+CBF ROI. However, the baseline CBF computed in the BOLD ROI was not significantly correlated with either the BOLD response or venous oxygenation. Addition of a strict gray matter threshold (>99%) in calculation of the baseline CBF in the BOLD ROI produced a significant correlation between baseline CBF and venous oxygenation and a near significant inverse correlation between baseline CBF and the BOLD response. Further addition of a strict CSF threshold (<0.1%) in the baseline CBF calculation produced a significant inverse correlation between baseline CBF and the BOLD response.

We found an empirical direct relation between venous oxygenation and baseline CBF. This relationship was also observed in a study by (Lu et al. 2008). In addition, the direct relation venous oxygenation and baseline CBF is in agreement with (Buxton and Frank 1997)'s mathematical model. This model proposed that the combination of shortened capillary transit times from increased CBF and the limited rate of oxygen extraction across the capillary wall produces a decrease in the oxygen extraction fraction. A decrease in the oxygen extraction fraction corresponds to an increase in venous oxygenation.

Although both venous oxygenation and the BOLD response were significantly correlated with baseline CBF measured in the BOLD+CBF ROI, they were not significantly correlated to measures of baseline CBF in the BOLD ROI. These differences may be explained by the possible localization of ASL CBF measurements to capillaries (Luh et al. 2000). Since the BOLD signal relies on deoxyhemoglobin, the BOLD ROI is dominated by draining veins, where ASL CBF is not reliably measured. This hypothesis suggests that exclusion of draining vein regions would improve baseline CBF measures in the BOLD ROI. Consistent with this idea, measurements of baseline CBF in the BOLD ROI with a high gray matter fraction (>99%) to select for capillaries produced a significant correlation between baseline CBF and venous oxygenation and a negative trend between baseline CBF and the BOLD response. In addition, draining veins are located on the exterior cortex in close proximity to CSF. Further exclusion of voxels containing CSF (>0.1%) produced a significant correlation between baseline CBF measured in the BOLD ROI and the BOLD response. These findings indicate that baseline CBF is a robust measure of the baseline state when anatomical data is used to exclude regions of draining veins.

In summary, we found that measures of both venous oxygenation and baseline CBF account for inter-subject BOLD variability in the BOLD+CBF ROI. However, baseline CBF is not correlated with venous oxygenation or the BOLD response in the BOLD ROI due to the inability to measure CBF in draining vein regions. Exclusion of draining vein regions from the BOLD ROI by use of anatomical measures improves the correlation between baseline CBF and both venous oxygenation and the BOLD

response. Therefore, baseline CBF after correction by anatomical measures reflects the baseline state and may be used to account for inter-subject BOLD variability.

CONCLUSION

The indirect relation of functional MRI (fMRI) signals to neural activity has limited the clinical application of fMRI. Methods to obtain more direct measures of neural activity from fMRI signals are of great interest to the fMRI community. However, the effect of non-neural factors on fMRI signals are not well understood, and results from normalization methods have been inconsistent. Here, we developed a better understanding of how non-neural factors influence the blood oxygenation level dependent (BOLD) and cerebral blood flow (CBF) signals. We also used that information to validate and improve an existing normalization method (hypercapnic normalization) that allows a more direct interpretation of fMRI responses as neural activity. Finally, we assessed the use of measures of baseline blood oxygenation and cerebral blood flow as normalization methods to reduce BOLD inter-subject variability.

Original Contributions of Thesis Work

In the first part of this work, we assessed how differences in the baseline CBF affected the contrast-to-noise ratio and measurements of activation extent in the BOLD and CBF responses. We used a 200 mg caffeine dose to decrease baseline CBF and found significant reductions in both the CBF activation extent and contrast-to-noise ratio (CNR) but no significant change in the BOLD activation extent and CNR. The decreases in the CBF activation extent and CNR were consistent with a significant caffeine-induced decrease in the absolute CBF change accompanied by no

significant change in the residual noise. Alternatively, we could also view the drop in CBF CNR as due to a significant drop in the CBF signal-to-noise ratio that is partially offset by an increase in the percent CBF response. Measures of the baseline CBF also accounted for a significant portion of the inter-subject variability in the CBF activation map area and CNR. The tendency of the number of active CBF voxels to increase with higher baseline CBF reduced the ability to distinguish absolute CBF change between subjects with different baseline CBF values. Our results emphasized that factors that modulate baseline CBF, such as age, medication, and disease, should therefore be carefully considered in the interpretation of studies that use functional CBF activation maps.

In the second portion of this work, we used measures of the baseline CBF and the BOLD and CBF responses to both visual stimuli and hypercapnia to assess the effect of hypercapnic normalization on inter-subject variability. We found that the functional and hypercapnic BOLD responses and the functional and hypercapnic CBF responses had significant inverse dependencies on the baseline CBF. In contrast, the maximum BOLD response was independent of the baseline CBF and was not a major source of inter-subject BOLD variability. Division of the functional BOLD response by the hypercapnic BOLD response increased inter-subject variability in the normalized responses as compared to the original responses, reflecting the presence of a systematic bias term that was inversely dependent on the hypercapnic BOLD response. This systematic bias results from a positive intercept term in the linear relationship between the functional and hypercapnic BOLD responses. The positive intercept term was in turn due to the steeper dependence of the hypercapnic CBF

response than the functional CBF response on the baseline CBF. Normalized responses produced by use of the hypercapnic BOLD response as a covariate for the functional BOLD response were unaffected by the systematic bias and exhibited reduced inter-subject variability. These findings suggest a cautious interpretation of prior studies using hypercapnic normalization. In particular, the presence of a positive intercept in the relation between the functional and hypercapnic BOLD responses needs to considered in the analysis of hypercapnia normalized responses. As an alternative, the systematic bias can be avoided by using the hypercapnic BOLD response as a covariate to normalize the functional BOLD response.

In the third part of this work, we used measures of baseline cerebral blood flow (CBF), venous oxygenation, and the BOLD and CBF responses to both visual stimulus and hypercapnia to assess the use of venous oxygenation and baseline CBF to account for BOLD inter-subject variability. We found that both venous oxygenation and baseline CBF had a significant inverse dependence on the BOLD response in a region of interest based on both BOLD and CBF activation. Furthermore, venous oxygenation was significantly correlated to baseline CBF. However, baseline CBF measures in a region of interest based on BOLD activation only were uncorrelated to either venous oxygenation or the BOLD response. In this region of interest, use of anatomical measures to exclude voxels containing cerebrospinal fluid and include voxels with a high fraction of gray matter produced significant correlations between the resulting baseline CBF and both venous oxygenation and the BOLD response. The findings of this study indicate that both venous oxygenation and baseline CBF

may be used to reduce BOLD inter-subject variability provided that anatomical measures are incorporated into the computation of baseline CBF.

Future Work

This work has improved the understanding of how non-neural factors affect fMRI signals. Also, we show that use of the hypercapnic BOLD response a covariate for the functional BOLD response performs better than hypercapnic normalization by division in reducing inter-subject variability. The results of this work suggest several avenues of future research to further facilitate the interpretation of fMRI signals as neural activity. In particular, future work is necessary to: 1) evaluate the effect of non-neural factors on fMRI signals in additional subject groups (children and older subjects), 2) extend the TRUST method using velocity selective tagging to obtain measures of baseline and dynamic $CMRO_2$ in brain voxels, and 3) evaluate the effect of non-neural factors on measures of absolute and percent cerebral blood volume (CBV).

The first area of future work is to evaluate the effect of non-neural factors on fMRI signals in additional subjects groups, specifically in children and older subjects. Our results have shown how non-neural factors contribute to inter-subject fMRI signal variability in young, healthy subjects. While prior work have compared differences in fMRI signals across age groups (Dowker 2006; Handwerker et al. 2007; Restom et al. 2007; Ances et al. 2008), to our knowledge no studies to date have compared inter-subject differences in children and older subject groups. Extending our studies of the effect of non-neural factors on the inter-subject variability of fMRI signals to

additional age groups would aid interpretation of fMRI signals and normalized responses in the general population.

The second area of future work is extend the TRUST method using velocity selective tagging to obtain baseline and dynamic cerebral oxygen metabolism ($CMRO_2$) measures in brain voxels. The current TRUST implementation estimates the venous oxygenation of the whole brain by measuring the transverse relaxation time constant of blood in the sagittal sinus (Lu and Ge 2008). By substituting the slab selective tag of the current implementation with a velocity selective tag to excite blood located in venules (Wong and Cronin 2003), measures of baseline venous oxygenation may be obtained in voxels. Venous oxygenation measurements may be combined with per voxel baseline CBF measurements from ASL fMRI to estimate the per voxel baseline $CMRO_2$. In addition, dynamic measures of the transverse relaxation time constant of blood in voxels using TRUST may be converted to dynamic $CMRO_2$ measures. This method would be limited by the flow of venous blood during the preparation portion of the TRUST sequence, resulting in venous oxygenation measures that are displaced from the sites of origin. If the problem of displacement is not large, velocity selective tagging TRUST would offer a useful alternative to calibrated BOLD.

The third area of future work is to evaluate the effect of non-neural factors on measures of absolute and percent cerebral blood volume (CBV). In our work, we assumed a steady-state relation between cerebral blood volume and CBF, as found by (Grubb et al. 1974). This relation may not be applicable in disease states or with dynamic functional changes. Resting CBV in brain voxels may be measured using

dynamic susceptibility contrast (DSC) MRI (Engvall et al. 2008). Using the resting CBV measures from DSC MRI as a calibration factor, vascular space occupancy MRI (Lu et al. 2003) may then be used to obtain quantitative and percent CBV changes with functional activation. Direct measurements of CBV would be useful to studies using calibrated BOLD, which currently utilizes Grubb's relation.

REFERENCES

Aguirre, G. K., Detre, J. A., Zarahn, E., Alsop, D. C. 2002. Experimental Design and the Relative Sensitivity of BOLD and Perfusion fMRI. *Neuroimage* **15:**488-500.

Aguirre, G. K., Zarahn, E., D'Esposito, M. 1998. The variability of human, BOLD hemodynamic responses. *Neuroimage* **8:**360-369.

Amedi, A., Raz, N., Pianka, P., Malach, R., Zohary, E. 2003. Early 'visual' cortex activation correlates with superior verbal memory performance in the blind. *Nat Neurosci* **6(7):**758-66.

Ances, B. M., Liang, C. L., Leontiev, O., Perthen, J. E., Fleisher, A. S., Lansing, A. E., Buxton, R. B. 2008. Effects of aging on cerebral blood flow, oxygen metabolism, and blood oxygenation level dependent responses to visual stimulation. *Hum Brain Mapp*.

Attwell, D., Iadecola, C. 2002. The neural basis of functional brain imaging signals. *Trends Neurosci* **25(12):**621-5.

Bandettini, P. A., Wong, E. C. 1997. A hypercapnia-based normalization method for improved spatial localization of human brain activation with fMRI. *NMR Biomed* **10(4-5):**197-203.

Behzadi, Y., Liu, T. T. 2006. Caffeine reduces the initial dip in the visual BOLD response at 3 T. *Neuroimage* **32(1):**9-15.

Biswal, B. B., Kannurpatti, S. S., Rypma, B. 2007. Hemodynamic scaling of fMRI-BOLD signal: validation of low-frequency spectral amplitude as a scalability factor. *Magn Reson Imaging* **25(10):**1358-69.

Boynton, G. M., Engel, S. A., Glover, G. H., Heeger, D. J. 1996. Linear systems analysis of functional magnetic resonance imaging in human V1. *J. Neuroscience* **16:**4207-4221.

Buxton, R. B. 2002. *Introduction to Functional Magnetic Resonance Imaging.* Cambridge University Press, Cambridge.

Buxton, R. B., Frank, L. R. 1997. A model for the coupling between cerebral blood flow and oxygen metabolism during neural stimulation. *J. Cereb. Blood Flow and Metabolism* **17:**64-72.

Buxton, R. B., Uludag, K., Dubowitz, D. J., Liu, T. T. 2004. Modeling the hemodynamic response to brain activation. *Neuroimage* **23 Suppl 1:**S220-33.

Chalela, J. A., Alsop, D. C., Gonzalez-Atavales, J. B., Maldjian, J. A., Kasner, S. E., Detre, J. A. 2000. Magnetic resonance perfusion imaging in acute ischemic stroke using continuous arterial spin labeling. *Stroke* **31(3):**680-7.

Chen, Y., Parrish, T. B. 2007. Activation induced BOLD and CBF responses vary with with caffeine dose. In *Proceedings of the 15th ISMRM Scientific Meeting, Berlin,* pp. 112.

Chen, Y., Parrish, T. B. 2008. Caffeine's effects on neurovascular coupling. In *Proceedings of the 15th ISMRM Scientific Meeting, Toronto,* pp. 44.

Chien, S. 2007. Mechanotransduction and endothelial cell homeostasis: the wisdom of the cell. *Am J Physiol Heart Circ Physiol* **292(3):**H1209-24.

Cohen, E. R., Rostrup, E., Sidaros, K., Lund, T. E., Paulson, O. B., Ugurbil, K., Kim, S. G. 2004. Hypercapnic normalization of BOLD fMRI: comparison across field strengths and pulse sequences. *Neuroimage* **23(2):**613-24.

Cohen, E. R., Ugurbil, K., Kim, S. G. 2002. Effect of basal conditions on the magnitude and dynamics of the blood oxygenation level-dependent fMRI response. *J Cereb Blood Flow Metab* **22(9):**1042-53.

Cox, R. W. 1996. AFNI-software for analysis and visualization of functional magnetic resonance neuroimages. *Comput. Biomed. Res.* **29:**162-173.

D'Esposito, M., Deouell, L. Y., Gazzaley, A. 2003. Alterations in the BOLD fMRI signal with ageing and disease: a challenge for neuroimaging. *Nat Rev Neurosci* **4(11):**863-72.

Dagher, A., Nagano-Saito, A. 2007. Functional and anatomical magnetic resonance imaging in Parkinson's disease. *Mol Imaging Biol* **9(4):**234-42.

Davis, C. E., Jeste, D. V., Eyler, L. T. 2005. Review of longitudinal functional neuroimaging studies of drug treatments in patients with schizophrenia. *Schizophr Res* **78(1):**45-60.

Davis, T. L., Kwong, K. K., Weisskoff, R. M., Rosen, B. R. 1998. Calibrated functional MRI: mapping the dynamics of oxidative metabolism. *Proc. Natl. Acad. Sci. USA* **95:**1834-1839.

Dowker, A. 2006. What can functional brain imaging studies tell us about typical and atypical cognitive development in children? *J Physiol Paris* **99(4-6):**333-41.

Engvall, C., Ryding, E., Wirestam, R., Holtas, S., Ljunggren, K., Ohlsson, T., Reinstrup, P. 2008. Human cerebral blood volume (CBV) measured by dynamic susceptibility contrast MRI and 99mTc-RBC SPECT. *J Neurosurg Anesthesiol* **20(1):**41-4.

Fergus, A., Lee, K. S. 1997. Regulation of cerebral microvessels by glutamatergic mechanisms. *Brain Res* **754(1-2):**35-45.

Fredholm, B. B., Battig, K., Holmen, J., Nehlig, A., Zvartau, E. E. 1999. Actions of caffeine in the brain with special reference to factors that contribute to its widespread use. *Pharmacol Rev* **51(1):**83-133.

Grubb, R. L., Raichle, M. E., Eichling, J. O., Ter-Pogossian, M. M. 1974. The effects of changes in $PaCO_2$ on cerebral blood volume, blood flow, and vascular mean transit time. *Stroke* **5:**630 - 639.

Gustard, S., Williams, E. J., Hall, L. D., Pickard, J. D., Carpenter, T. A. 2003. Influence of baseline hematocrit on between-subject BOLD signal change using gradient echo and asymmetric spin echo EPI. *Magn Reson Imaging* **21(6):**599-607.

Haacke, E. M., Hu, C., Parrish, T. B., Xu, Y. 2003. Whole Brain Stress Test Using Caffeine: Effects on fMRI and SWI at 3T. In *Proceedings of the ISMRM 11th Scientific Meeting,* pp. 1731.

Haberg, A., Kvistad, K. A., Unsgard, G., Haraldseth, O. 2004. Preoperative blood oxygen level-dependent functional magnetic resonance imaging in patients with primary brain tumors: clinical application and outcome. *Neurosurgery* **54(4):**902-14; discussion 914-5.

Handwerker, D. A., Gazzaley, A., Inglis, B. A., D'Esposito, M. 2007. Reducing vascular variability of fMRI data across aging populations using a breathholding task. *Hum Brain Mapp* **28(9):**846-59.

Hoge, R. D., Atkinson, J., Gill, B., Crelier, G. R., Marrett, S., Pike, G. B. 1999. Investigation of BOLD signal dependence on cerebral blood flow and oxygen consumption: the deoxyhemoglobin dilution model. *Magn Reson Med* **42(5):**849-63.

Jones, M., Berwick, J., Hewson-Stoate, N., Gias, C., Mayhew, J. 2005. The effect of hypercapnia on the neural and hemodynamic responses to somatosensory stimulation. *Neuroimage* **27(3):**609-23.

Kastrup, A., Li, T. Q., Kruger, G., Glover, G. H., Moseley, M. E. 1999. Relationship between cerebral blood flow changes during visual stimulation and baseline flow levels investigated with functional MRI. *Neuroreport* **10(8):**1751-6.

Kemna, L. J., Posse, S., Tellmann, L., Schmitz, T., Herzog, H. 2001. Interdependence of regional and global cerebral blood flow during visual stimulation: an O-15-butanol positron emission tomography study. *J Cereb Blood Flow Metab* **21(6):**664-70.

Lassen, N. A. 1959. Cerebral blood flow and oxygen consumption in man. *Physiol Rev* **39(2):**183-238.

Laurienti, P. J., Field, A. S., Burdette, J. H., Maldjian, J. A., Yen, Y.-F., Moody, D. M. 2002. Dietary Caffeine Consumption Modulates fMRI Measures. *Neuroimage* **17:**751-757.

Li, T. Q., Kastrup, A., Moseley, M. E., Glover, G. H. 2000. Changes in baseline cerebral blood flow in humans do not influence regional cerebral blood flow response to photic stimulation. *J Magn Reson Imaging* **12(5):**757-62.

Liau, J., Perthen, J. E., Liu, T. T. 2008. Caffeine reduces the activation extent and contrast-to-noise ratio of the functional cerebral blood flow response but not the BOLD response. *Neuroimage* **42(1):**296-305.

Liu, T. T., Behzadi, Y., Restom, K., Uludag, K. 2004a. Caffeine Affects the Dynamics of the Visual BOLD Response. *NeuroImage* **22(S1):**TU148.

Liu, T. T., Behzadi, Y., Restom, K., Uludag, K., Lu, K., Buracas, G. T., Dubowitz, D. J., Buxton, R. B. 2004b. Caffeine alters the temporal dynamics of the visual BOLD response. *Neuroimage* **23(4):**1402-13.

Liu, T. T., Frank, L. R., Wong, E. C., Buxton, R. B. 2001. Detection power, estimation efficiency, and predictability in event-related fMRI. *Neuroimage* **13(4):**759-73.

Liu, T. T., Wong, E. C. 2005. A signal processing model for arterial spin labeling functional MRI. *Neuroimage* **24(1):**207-15.

Lu, H., Clingman, C., Golay, X., van Zijl, P. C. 2004. Determining the longitudinal relaxation time (T1) of blood at 3.0 Tesla. *Magn Reson Med* **52(3):**679-82.

Lu, H., Ge, Y. 2008. Quantitative evaluation of oxygenation in venous vessels using T2-Relaxation-Under-Spin-Tagging MRI. *Magn Reson Med* **60(2):**357-63.

Lu, H., Golay, X., Pekar, J. J., Van Zijl, P. C. 2003. Functional magnetic resonance imaging based on changes in vascular space occupancy. *Magn Reson Med* **50(2):**263-74.

Lu, H., U., Y., Lewis-Amezcua, K. 2008a. Normalization of fMRI signal with basal physiological state improves sensitivity in differentiating subject groups. In *Proceedings of the 15th ISMRM Scientific Meeting, Toronto,* pp. 167.

Lu, H., Zhao, C., Ge, Y., Lewis-Amezcua, K. 2008b. Baseline blood oxygenation modulates response amplitude: Physiologic basis for intersubject variations in functional MRI signals. *Magn Reson Med* **60(2):**364-72.

Luh, W. M., Wong, E. C., Bandettini, P. A., Ward, B. D., Hyde, J. S. 2000. Comparison of simultaneously measured perfusion and BOLD signal increases during brain activation with T(1)-based tissue identification. *Magn Reson Med* **44(1):**137-43. Madden, J. A. 1993. The effect of carbon dioxide on cerebral arteries. *Pharmacol Ther* **59(2):**229-50.

McGonigle, D. J., Howseman, A. M., Athwal, B. S., Friston, K. J., Frackowiak, R. S., Holmes, A. P. 2000. Variability in fMRI: an examination of intersession differences. *Neuroimage* **11(6 Pt 1):**708-34.

Melamed, E., Lavy, S., Bentin, S., Cooper, G., Rinot, Y. 1980. Reduction in regional cerebral blood flow during normal aging in man. *Stroke* **11(1):**31-5.

Mulderink, T. A., Gitelman, D. R., Mesulam, M.-M., Parrish, T. B. 2002. On the use of caffeine as a contrast booster for BOLD fMRI studies. *Neuroimage* **15:**37-44.

Mumford, J. A., Hernandez-Garcia, L., Lee, G. R., Nichols, T. E. 2006. Estimation efficiency and statistical power in arterial spin labeling fMRI. *Neuroimage* **33(1):**103-14.

Okamoto, H., Hudetz, A. G., Roman, R. J., Bosnjak, Z. J., Kampine, J. P. 1997. Neuronal NOS-derived NO plays permissive role in cerebral blood flow response to hypercapnia. *Am J Physiol* **272(1 Pt 2):**H559-66.

Olson, I. R., Rao, H., Moore, K. S., Wang, J., Detre, J. A., Aguirre, G. K. 2006. Using perfusion fMRI to measure continuous changes in neural activity with learning. *Brain Cogn*.

Perthen, J. E., Lansing, A. E., Liau, J., Liu, T. T., Buxton, R. B. 2008. Caffeine-induced uncoupling of cerebral blood flow and oxygen metabolism: A calibrated BOLD fMRI study. *Neuroimage* **40(1):**237-47.

Ragland, J. D., Yoon, J., Minzenberg, M. J., Carter, C. S. 2007. Neuroimaging of cognitive disability in schizophrenia: search for a pathophysiological mechanism. *Int Rev Psychiatry* **19(4):**417-27.

Restom, K., Bangen, K. J., Bondi, M. W., Perthen, J. E., Liu, T. T. 2007. Cerebral blood flow and BOLD responses to a memory encoding task: a comparison between healthy young and elderly adults. *Neuroimage* **37(2):**430-9.

Restom, K., Behzadi, Y., Liu, T. T. 2006. Physiological noise reduction for arterial spin labeling functional MRI. *Neuroimage* **31(3):**1104-15.

Seber, G. A. F., Lee, A. J. 2003. *Linear Regression Analysis.* John Wiley & Sons, New York.

Shimosegawa, E., et al. 1995. Photic stimulation study of changing the arterial partial pressure level of carbon dioxide. *J Cereb Blood Flow Metab* **15(1):**111-4.

Sicard, K. M., Duong, T. Q. 2005. Effects of hypoxia, hyperoxia, and hypercapnia on baseline and stimulus-evoked BOLD, CBF, and CMRO2 in spontaneously breathing animals. *Neuroimage* **25(3):**850-8.

St Lawrence, K. S., Wang, J. 2005. Effects of the apparent transverse relaxation time on cerebral blood flow measurements obtained by arterial spin labeling. *Magn Reson Med* **53(2):**425-33.

St Lawrence, K. S., Ye, F. Q., Lewis, B. K., Frank, J. A., McLaughlin, A. C. 2003. Measuring the effects of indomethacin on changes in cerebral oxidative metabolism and cerebral blood flow during sensorimotor activation. *Magn Reson Med* **50(1):**99-106.

St Lawrence, K. S., Ye, F. Q., Lewis, B. K., Weinberger, D. R., Frank, J. A., McLaughlin, A. C. 2002. Effects of indomethacin on cerebral blood flow at rest and during hypercapnia: an arterial spin tagging study in humans. *J Magn Reson Imaging* **15(6):**628-35.

Stefanovic, B., Warnking, J. M., Rylander, K. M., Pike, G. B. 2006. The effect of global cerebral vasodilation on focal activation hemodynamics. *Neuroimage* **30(3):**726-34.

Thomason, M. E., Foland, L. C., Glover, G. H. 2007. Calibration of BOLD fMRI using breath holding reduces group variance during a cognitive task. *Hum Brain Mapp* **28(1):**59-68.

Tjandra, T., Brooks, J. C., Figueiredo, P., Wise, R., Matthews, P. M., Tracey, I. 2005. Quantitative assessment of the reproducibility of functional activation measured with BOLD and MR perfusion imaging: Implications for clinical trial design. *Neuroimage*.

Wang, J., Aguirre, G. K., Kimberg, D. Y., Roc, A. C., Li, L., Detre, J. A. 2003. Arterial Spin Labeling Perfusion fMRI with Very Low Task Frequency. *Magn. Reson. Med.* **49:**796-802.

Wang, J., Qiu, M., Constable, R. T. 2005. In vivo method for correcting transmit/receive nonuniformities with phased array coils. *Magn Reson Med* **53(3):**666-74.

White, C. R., Frangos, J. A. 2007. The shear stress of it all: the cell membrane and mechanochemical transduction. *Philos Trans R Soc Lond B Biol Sci* **362(1484):**1459-67.

Williams, D. L., Minshew, N. J. 2007. Understanding autism and related disorders: what has imaging taught us? *Neuroimaging Clin N Am* **17(4):**495-509, ix.

Wong, E. C., Buxton, R. B., Frank, L. R. 1998. Quantitative imaging of perfusion using a single subtraction (QUIPSS and QUIPSS II). *Magn. Reson. Med.* **39(5):**702-708.

Wong, E. C., Cronin, M. 2003. Velocity selective arterial spin labeling using and adiabatic hyperecho pulse train. In *Proceedings of the 11th ISMRM Scientific Meeting, Toronto,* pp. 2181.

Woolrich, M. W., Chiarelli, P., Gallichan, D., Perthen, J., Liu, T. T. 2006. Bayesian inference of hemodynamic changes in functional arterial spin labeling data. *Magn Reson Med* **56(4):**891-906.

Woolrich, M. W., Ripley, B. D., Brady, M., Smith, S. M. 2001. Temporal autocorrelation in univariate linear modeling of FMRI data. *Neuroimage* **14(6):**1370-86.

Yang, L. L., Peiffer, A. M., Addicott, M. A., Kraft, R. A., Maldjian, J. A., Burdette, J. H., Burnett, L. R., Chen, M. Y., Laurienti, P. J. 2007. BOLD Signal Decreases Following Caffeine Challenge in Individuals Who Intake High Daily Doses of Caffeine. In *Proceedings of the 13th Human Brain Mapping, Chicago,* pp. 396M.

Zappe, A. C., Uludag, K., Oeltermann, A., Ugurbil, K., Logothetis, N. K. 2008. The Influence of Moderate Hypercapnia on Neural Activity in the Anesthetized Nonhuman Primate. *Cereb Cortex*.